Electroproduction of an isobar as a background from the beam–residual-gas interaction in ϕ factories

M. N. Achasov,[a)] V. B. Golubev, and S. I. Serednyakov
G. I. Budker Institute of Nuclear Physics, Siberian Branch of the Russian Academy of Sciences, 630090 Novosibirsk, Russia

N. N. Achasov
S. L. Sobolev Institute of Mathematics, Siberian Branch of the Russian Academy of Sciences, 630090 Novosibirsk, Russia

(Submitted 5 January 1997)
Pis'ma Zh. Éksp. Teor. Fiz. **65**, No. 4, 295–300 (25 February 1997)

It is shown that the electroproduction of the isobar $\Delta(1232)$ occurs in ϕ factories when the beams interact with the residual gas. In one effective year (10^7 s) the decay of this isobar over an interaction length of one meter gives $\sim 10^7$ pions, moving predominantly in a direction transverse to the axis of the beams, with a resonance energy distribution having a 120-MeV wide peak near 265 MeV. Formulas required for modeling the process under discussion, giving the distributions over the momentum transfer, angles, energies, and momenta of the decay products are presented. © *1997 American Institute of Physics.* [S0021-3640(97)00104-7]

PACS numbers: 14.20.Gk, 13.60.Rj

The goal of ϕ factories — DAPHNE in Frascati, which should start operation in 1997,[1] and the ϕ factory now under construction in Novosibirsk[1,2] — is to perform precision measurements of very important physical quantities, primarily ϵ'/ϵ (Ref. 3).

In order to implement this program it is necessary to have a thorough knowledge of the installation and the most important backgrounds. One source of background is the interaction of the beams with the residual gas.

In this letter we show that the cross section for the electroproduction of the isobar $\Delta(1232)$ with $I(J^P)=\frac{3}{2}(\frac{3}{2}^+)$ (Ref. 1) on a nucleon at an electron (positron) energy of 509.5 MeV (energy of ϕ factories) equals 3 μb, which at a total beam current of 1.3→5.2 A and a residual-gas pressure of ~1 nTorr (which is planned for DAPHNE[4]) leads to the production of $\sim 10^7$ isobars in the residual gas in the course of one effective year (10^7 s). The decay of the isobar ($\Delta(1232)\to\pi N$ and γN) produces π mesons with a resonance energy distribution near 265 MeV and a peak width of 120 MeV, which emerge predominantly transverse to the beam axis, and photons with a resonance energy distribution near 257 MeV and a peak width of 120 MeV, which disperse more isotropically.

A characteristic feature of the process under discussion are the protons and neutrons produced in the decay of the isobar, which have a very narrow (peak width 30 MeV) resonance energy distribution near 970 MeV and emerge predominantly transverse to the beam axis.

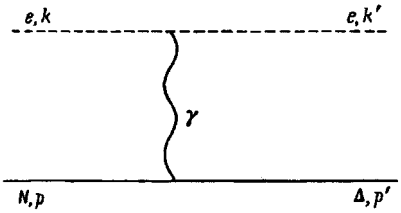

FIG. 1. Diagram describing electroproduction.

We present all the distributions required for modeling and distinguishing the background under discussion — the distributions over the momentum transfer from the electron (positron), over the angles of emergence of the decay pions (nucleons) and photons (nucleons) in the rest frame of the isobar, over the energies of the pions, nucleons, and photons in the rest frame of the isobar, and over the momentum of the pion (nucleon) in the rest frame of the isobar.

The phenomenological Lagrangian describing the interaction of an isobar with a nucleon and photon (magnetic dipole transition) is[5]

$$L_{em}=e\frac{\mu}{m_N}F^{\nu\rho}(x)(\overline{\psi_{\nu(x)}}\gamma_\rho\gamma_5\psi(x)+\text{h.c.}), \tag{1}$$

where e is the electron charge, $\alpha=e^2/4\pi=1/137$, $m_N=0.94$ GeV is the nucleon mass, $F^{\nu\rho}(x)=\partial^\nu A^\rho(x)-\partial^\rho A^\nu(x)$ is the electromagnetic field, $\psi_\nu(x)$ is the spinor–vector field of the isobar, and $\psi(x)$ is the spinor field of the nucleon.

The width of the radiative decay $\Delta\to\gamma N$ is

$$\Gamma(\Delta\to\gamma N,m_\Delta)=\alpha\left(\frac{\mu}{m_N}\right)^2\omega^3(m_\Delta)\left(1+\frac{1}{3}\left(\frac{m_N}{m_\Delta}\right)^2\right), \tag{2}$$

where $\omega(m_\Delta)=m_\Delta(1-m_N^2/m_\Delta^2)/2=0.257$ GeV is the photon energy, and $m_\Delta=1.232$ GeV.

Using the experimental data[1] $\Gamma(\Delta\to\gamma N,\ m_\Delta)=BR(\Delta\to\gamma N,\ m_\Delta)\cdot\Gamma_\Delta(m_\Delta)$ $=0.58\cdot10^{-2}\cdot0.12$ GeV $=0.7\cdot10^{-3}$ GeV, we obtain $\mu^2/m_N^2=4.7$ GeV^{-2}.

Now we can calculate the amplitude for the electroproduction of the isobar $(e^-N\to e^-\Delta)$; see Fig. 1. It is convenient to employ the helicity amplitudes $A^{\lambda_e'\lambda_e}_{\lambda_\Delta\lambda_N}$ in the center-of-mass frame of the reaction, where λ_N, λ_Δ, λ_e, and λ_e' are the helicities of the nucleon, isobar, and initial and scattered electrons, respectively. The amplitudes for the production of an isobar by a positron differ from the corresponding electroproduction amplitudes only in sign.

We now write out the amplitudes which are important for our analysis:

$$A^{-1/2\,-1/2}_{3/2\quad 1/2}=A^{1/2\quad 1/2}_{-3/2\,-1/2}=e^2\frac{\mu}{m_N}\sqrt{2(t-t_{\min}(m))}(s-m_N^2)\frac{f(t)}{t},$$

$$A^{1/2\,1/2}_{3/2\,1/2}=A^{-1/2-1/2}_{-3/2-1/2}=e^2\frac{\mu}{m_N}\sqrt{2(t-t_{\min}(m))}(s-m_N^2)\left(1-\frac{m^2-m_N^2}{s-m_N^2}\right)\frac{f(t)}{t}, \tag{3}$$

and

$$A^{-1/2-1/2}_{1/2-1/2}=A^{1/2\,1/2}_{-1/2\,1/2}=e^2\frac{\mu}{m}\sqrt{\tfrac{2}{3}(t-t_{\min}(m))}(s-m_N^2)\frac{f(t)}{t},$$

$$A^{1/2\;\;1/2}_{1/2-1/2}=A^{-1/2-1/2}_{-1/2\;\;1/2}=e^2\frac{\mu}{m}\sqrt{\tfrac{2}{3}(t-t_{\min}(m))}(s-m_N^2)\left(1-\frac{m^2-m_N^2}{s-m_N^2}\right)\frac{f(t)}{t}, \tag{4}$$

where m is the mass of the isobar (invariant mass of the πN or γN states into which the isobar decays), $t=-(k-k')^2=-(p'-p)^2$, $s=(k+p)^2=(k'+p')^2$, p, p', and k' are the four-momenta of the nucleon, isobar, and the initial and final electrons (positrons), respectively (see Fig. 1); $f(t)=1/(1+2t)^2$ is the ''dipole'' form factor of the electromagnetic transition $N\to\Delta$ (see, for example, Refs. 6 and 7 and the literature cited therein). Here and below t is expressed in GeV^2.

We have neglected the amplitudes $A^{\lambda\lambda}_{1/2\,1/2}$, $A^{\lambda\lambda}_{-1/2-1/2}$, $A^{\lambda\lambda}_{3/2-1/2}$, and $A^{\lambda\lambda}_{-3/2\,1/2}$ which are proportional to t, and the contributions, proportional to t, to the amplitudes (3) and (4). The magnitude of all omitted contributions to the total cross section of the process is of the order of 1%.

The m,t differential cross section of the process $e^{\mp}N\to e^{\mp}\Delta\to e^{\mp}\pi N$ is

$$\frac{d^2\sigma}{dmdt}=4\alpha^2\left(\frac{\mu}{m_N}\right)^2\frac{t-t_{\min}(m)}{t^2}(f(t))^2$$
$$\times\left(1+\frac{m_N^2}{3m^2}\right)\left[1-\frac{m^2-m_N^2}{s-m_N^2}+\frac{(m^2-m_N^2)^2}{2(s-m_N^2)^2}\right]\frac{m^2\Gamma(\Delta\to\pi N,m)}{|D_\Delta(m)|^2}, \tag{5}$$

where the isobar propagator and its mass-dependent width have the form

$$D_\Delta(m)=m^2-m_\Delta^2+im\Gamma(\Delta\to\pi N,m),$$

$$\Gamma(\Delta\to\pi N,m)=\Gamma(\Delta\to\pi N,m_\Delta)\frac{m_\Delta}{m}\left(\frac{1+m_N/m}{1+m_N/m_\Delta}\right)^2\frac{2(q(m)/q(m_\Delta))^3}{1+(q(m)/q(m_\Delta))^2},$$

$$q(m)=\frac{1}{2m}\sqrt{(m^2-(m_N+m_\pi)^2)(m^2-(m_N-m_\pi)^2)}, \tag{6}$$

$m_\pi=0.14$ GeV is the pion mass and $q(m_\Delta)=0.225$ GeV. In Eq. (6) we set $\Gamma_\Delta(m)=\Gamma(\Delta\to\pi N,\ m)$, $\Gamma(\Delta\to\pi N,\ m_\Delta)=0.12$ GeV. The m distribution integrated over the entire interval $t_{\min}(m)\leqslant t\leqslant t_{\max}(m)$ has the form

$$\frac{d\sigma}{dm}=\sigma(m)=4\alpha^2\left(\frac{\mu}{m_N}\right)^2\left(\ln\frac{t_{\max}(m)(1+2t_{\min}(m))}{t_{\min}(m)(1+2t_{\max}(m))}-1+\frac{t_{\min}(m)}{t_{\max}(m)}\right.$$
$$\left.-\frac{11+24t_{\min}(m)+24t_{\min}^2(m)}{6(1+2t_{\min}(m))^3}+\frac{11+24t_{\max}(m)+24t_{\max}^2(m)}{6(1+2t_{\max}(m))^3}\right)$$

$$\times\left(1+\frac{m_N^2}{3m^2}\right)\left[1-\frac{m^2-m_N^2}{s-m_N^2}+\frac{(m^2-m_N^2)^2}{2(s-m_N^2)^2}\right]\frac{m^2\Gamma(\Delta\to\pi N,m)}{|D_\Delta(m)|^2}, \tag{7}$$

where

$$t_{\max}(m)=-2m_e+\frac{1}{2s}\{(s-m^2+m_e^2)(s-m_N^2+m_e^2)$$
$$+\sqrt{(s-(m-m_e)^2)(s-(m+m_e)^2)(s-(m_N-m_e)^2)(s-(m_N+m_e)^2)}\},$$
$$t_{\min}(m)=-2m_e+\frac{1}{2s}\{(s-m^2+m_e^2)(s-m_N^2+m_e^2)$$
$$-\sqrt{(s-(m-m_e)^2)(s-(m+m_e)^2)(s-(m_N-m_e)^2)(s-(m_N+m_e)^2)}\}, \tag{8}$$

$m_e=0.51\cdot10^{-3}$ GeV is the electron mass for $s=1.842$ GeV^2 (the electron energy equals $m_\phi/2$). The total cross section integrated over the entire interval $m_\pi+m_N\leqslant m\leqslant\sqrt{s}-m_e$ is $\sigma=2.95$ μb.[b)] Such a large value of this cross section is due to the ''large'' logarithm in Eq. (8): $\ln(t_{\max}(m_\Delta)/t_{\min}(m_\Delta))=13.11$, where $t_{\max}(m_\Delta)=0.169$, $t_{\min}(m_\Delta)=1.29\cdot m_e^2=0.336\cdot10^{-6}$. The isobar $\Delta(1.232)$ has no competitors in this energy range.

The distributions over the pion energy E_π, nucleon energy E_N, and pion (nucleon) momentum q in the rest frame of the isobar have the form

$$\frac{d\sigma}{dE_\pi}=\sigma(E_\pi)=\frac{m(E_\pi)}{\sqrt{m_N^2+E_\pi^2-m_\pi^2}}\sigma(m(E_\pi)),$$
$$\frac{d\sigma}{dE_N}=\sigma(E_N)=\frac{m(E_N)}{\sqrt{m_\pi^2+E_N^2-m_N^2}}\sigma(m(E_N)) \tag{9}$$
$$\frac{d\sigma}{dq}=\sigma(q)=\frac{qm(q)}{\sqrt{(m_N^2+q^2)(m_\pi^2+q^2)}}\sigma(m(q)),$$

where

$$m(E_\pi)=E_\pi+\sqrt{m_N^2+E_\pi^2-m_\pi^2},\quad m(E_N)=E_N+\sqrt{m_\pi^2+E_N^2-m_N^2},$$
$$m(q)=\sqrt{m_\pi^2+q^2}+\sqrt{m_N^2+q^2},\quad q(m(q))=q.$$

The distribution $\sigma(E_\pi)$ is presented in Fig. 2.

The amplitudes (3) and (4) can be used to construct the spin density matrix of the isobar and the angular distributions of the decay products in the helicity frame, i.e., in the rest frame of the isobar with the axis of quantization directed along the 3-momentum of the isobar in the center-of-mass frame of the reaction.

For the decay $\Delta\to\pi N$, the angular distribution integrated over the azimuthal angle is

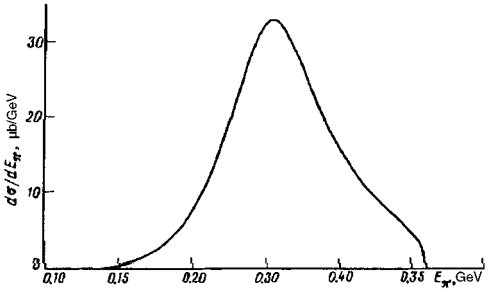

FIG. 2. Pion energy distribution in the rest frame of the isobar.

$$\frac{dW^{\pi(N)}}{d\cos\,\theta}=\frac{1}{1+\dfrac{m_N^2}{3m^2}}\left\{\frac{3}{4}\left(1+\frac{m_N^2}{9m^2}\right)\sin^2\theta+\frac{m_N^2}{3m^2}\cos^2\theta\right\}, \tag{10}$$

where θ is the angle between the direction of the 3-momentum of the pion (nucleon) and the quantization axis. For $m=m_\Delta$

$$\frac{dW^{\pi(N)}}{d\,\cos\,\theta}=0.67\,\sin^2\theta+0.16\,\cos^2\theta. \tag{11}$$

We note that averaging the distribution (10) over m changes the coefficients in Eq. (11) by less than 1%.

In deriving the distribution (10) we employed the phenomenological Lagrangian describing the interaction of an isobar with a nucleon and pion,[5]

$$L=\frac{G}{m_N}(\overline{\psi_\nu}(x)\psi(x)\partial^\nu\phi(x)+\text{h.c.}), \tag{12}$$

where $\phi(x)$ is the pion field.

In the center-of-mass frame of the reaction, 64% of the isobars emerge at an angle of not more than 10° with respect to the beam axis. Therefore, the axis of quantization is close to the beam axis. Since the momentum of the isobars is small (of the order of 100 MeV), it is obvious that because the pions (nucleons) emerge predominantly perpendicular to the quantization axis in the rest frame of isobar (see Eq. (10)), the pions (nucleons) will emerge predominantly transverse to the beam axis.

Twice as many π^0 mesons as π^+ (π^-) mesons are produced in the decay of $\Delta^+(1.232)$ ($\Delta^0(1.232)$). This property can be used to analyze the composition of the residual gas.

For the decay $\Delta\to\gamma N$, the angular distribution integrated over the azimuthal angle is given by

$$\frac{dW^{\gamma(N)}}{d\cos\vartheta}=\frac{1}{\left(1+\frac{m_N^2}{3m^2}\right)^2}\left\{\frac{1}{4}\left(1+\frac{2m_N^2}{m^2}+\frac{m_N^4}{9m^4}\right)\sin^2\vartheta+\left(1+\frac{m_N^4}{9m^4}\right)\cos^2\vartheta\right\}$$

$$=0.386\,\sin^2\vartheta+0.728\,\cos^2\vartheta, \tag{13}$$

where ϑ is the angle between the direction of the 3-momentum of the photon (nucleon) and the quantization axis.

To obtain the energy and momentum distributions for the process $e^{\mp}N\to e^{\mp}\Delta\to e^{\mp}\gamma N$ it is necessary to make the following substitution in Eqs. (5) and (7):

$$\Gamma(\Delta\to\pi N,m)\to\Gamma(\Delta\to\gamma N,m)$$

$$=BR(\Delta\to\gamma N,m_\Delta)\cdot\Gamma_\Delta(m_\Delta)\frac{m_\Delta}{m}\left(\frac{1+m_N^2/3m^2}{1+m_N^2/3m_\Delta^2}\right)\frac{2\,\omega(m)^3/\omega(m_\Delta)^3}{1+\omega(m)^2/\omega(m_\Delta)^2}, \tag{14}$$

and the substitutions $E_\pi\to\omega$, $q\to\omega$, and $m_\pi\to 0$ in Eq. (9), where ω is the photon energy in the rest frame of the isobar, and $\omega(m)=m(1-m_N^2/m^2)/2$.

The expected number of Δ isobars produced per unit time per length of the vacuum chamber of the accelerator is

$$N=\frac{2I}{e}n\sigma\left[\frac{1}{\mathrm{m}\cdot\mathrm{s}}\right],$$

where n is the density of interacting nucleons in the vacuum chamber and I is the current in one beam.

The nucleon density n is determined by the pressure and partial composition of the gas. The residual gas pressure is $p\simeq 3\cdot 10^{-9}$ Torr.[8] The gas contains mainly H_2 — 50%, CO — 30%, and CO_2 — 20%.[8] The density of molecules can be estimated from the formula

$$p=n_M kT,$$

where k is Boltzmann's constant and $T=300$ K is the gas temperature (determined by the temperature of the accelerator walls). Then we obtain $n_M\simeq 10^{14}$ m^{-3}. The effective number of nucleons in the nuclei with which the electrons interact in this process equals $A^{2/3}$, where A is the number of nucleons in the nucleus. Taking account of the partial composition of the gas, the effective nucleon density is $n=7\cdot 10^{14}$ nucleons/m^3.

So, for a current $I=1$ A and cross section $\sigma=3$ μb the number of isobars produced per unit time per unit length is $N=2$ events/m·s. Although this counting rate is low compared with the counting rate from the ϕ meson resonance ~ 1 kHz, the events of this process can nonetheless make it difficult to distinguish rare decays in the ϕ factory, and for this reason it must be taken into account when processing the experimental data.

A study of the process of electroproduction of the Δ isobar in experiments with the SND detector in the VÉPP-2M accelerator complex in Novosibirsk has now begun.

This work is partially supported by the Russian Fund for Fundamental Research, Grants 94-02-05188 and 96-02-00548) and INTAS, Grant 94-3986.

[a)]e-mail: achasov@math.nsc.ru

[b)]We note that the cross section under discussion equals 7.74 μb in the c-τ factories ($s=4.644$ GeV^2) and 11.63 μb in the b factories ($s=17.8$ GeV^2).

[1] Particle Data Group, Phys. Rev. D **54**, 129, 600 (1996).
[2] A. N. Skrinsky, in *Proceedings of Workshop on Physics and Detectors for DAPHNE*, edited by R. Baldini *et al.*, LNF, Frascati, Italy, April 7–14, 1995, p. 3.
[3] L. Maiani in *The Second DAPHNE Physics Handbook*, Vol. I, edited by L. Maiani, G. Pancheri, and N. Paver, LNF, Frascati, Italy, 1995, p. 3.
[4] J. Lee-Franzini in *The Second DAPHNE Physics Handbook*, Vol. II, edited by L. Maiani, G. Pancheri, and N. Paver, LNF, Frascati, Italy, 1995. p. 761.
[5] S. Gasiorowicz, *Elementary Particle Physics*, Wiley, New York (1966), Chapters 25 and 26 [Russian translation, Nauka, Moscow (1969), pp. 482, 465].
[6] A. S. Omeleanko, Yad. Fiz. **30**, 1504 (1979) [Sov. J. Nucl. Phys. **30**, 779 (1979)].
[7] I. G. Aznauryan and I. A. Troshenkova, Yad. Fiz. **43**, 342 (1986) [Sov. J. Nucl. Phys. **43**, 219 (1986)].
[8] *Physical Design of the VEPP-5 Complex* [in Russian], Main Science Center of the Russian Federation, G. I. Budker Institute of Nuclear Physics, Novosibirsk (1995).

Translated by M. E. Alferieff

Anomalous reflection of light in novel distributed-feedback structures

S. M. Loktev, V. A. Sychugov, and B. A. Usievich
Institute of General Physics, Russian Academy of Sciences, 117942 Moscow, Russia

O. Parriaux
Friedrich-Schiller-Universität, 07743 Jena, Germany

(Submitted 5 December 1996)
Pis'ma Zh. Éksp. Teor. Fiz. **65**, No. 4, 301–305 (25 February 1997)

The possibility that lasing can occur in a rippled waveguide structure containing a high-reflectivity layer is studied. Lasing is achieved experimentally in a waveguide structure with an active buffer layer. Different mechanisms of distributed feedback in the structure are examined. © *1997 American Institute of Physics.*
[S0021-3640(97)00204-1]

PACS numbers: 42.79.Gn, 78.20.Ci, 42.25.Fx, 42.72.Bj

Investigations of the radiation of light in rippled (corrugated) waveguides containing high-reflectivity layers[1,2] have revealed the possibility of practically loss-free propagation of light along such structures (see Fig. 1). The point is that under the condition

$$2kb\sqrt{n_b^2-(n^*-\lambda/\Lambda)^2}=2\pi m, \tag{1}$$

$$\alpha_{\rm rad} l \gg 1, \tag{2}$$

where $k=2\pi/\lambda$, $\alpha_{\rm rad}$ is the radiative loss of light in the rippled waveguide and n^* is the effective refractive index of the mode, the so-called ''total'' external (anomalous) reflection of light from the surface of the rippled waveguide plays the main role in the propagation of light.[3,4] The essence of this effect is that the light incident on the waveguide from the buffer layer at the angle of excitation of the waveguide mode undergoes 100% reflection from the surface of the rippled waveguide. Since the reflection of light from an ideally reflecting metal (or multilayer dielectric) mirror is also 100%, a mode of the structure can propagate along the structure without loss. The field distribution of the mode under the conditions (1) and (2) is also shown in Fig. 1. The presence of the electromagnetic field of this mode inside the buffer layer indicates that there is a possibility of achieving amplification of this mode if the buffer layer is an active medium. This condition will be realized at wavelengths determined by the dispersion relation

$$2kb\sqrt{n_b^2-n_b^{*2}}=2m\pi \tag{3}$$

for buffer-layer modes with effective refractive index n_b^*. In our experiments on lasing in the waveguide structure under study, a Ta_2O_5 ($n_f=2.02$) film, deposited on a glass substrate ($n_s=1.51$), was used as the waveguide. The top boundary of the Ta_2O_5 film was rippled. The period of the ripple was equal to $\Lambda_c=0.33$ μm and the depth of the ripple reached $2\sigma=300$ Å. Ethylene glycol with rhodamine 6G ($C\approx 10^{-3}$ mol.%) served

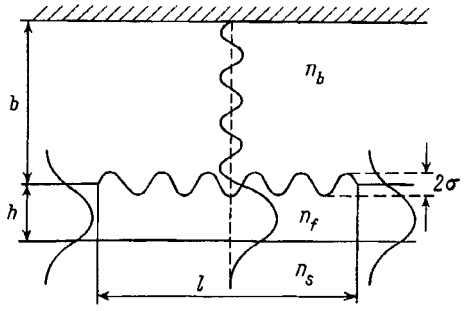

FIG. 1. Transverse cross section of a waveguide structure with a grating. The field distributions of the modes are shown.

as the buffer layer. The buffer layer was ~ 100 μm thick. The dye was pumped with the second harmonic of a Nd^{3+}:YAG laser ($\lambda_p = 0.53$ μm). In our experiments the thickness h_w of the waveguide film was 1650 Å, and it was therefore impossible to polish the end faces and to produce mirrors on them. For this reason, other approaches were used to produce feedback. One approach is to deposit an additional grating, operating in the autocollimation regime (Fig. 2a), on the metallic mirror. The period of this grating must equal

$$\Lambda_a = \frac{\lambda_{\text{gen}}}{2 n_b \sin \theta_b}. \tag{4}$$

The lasing wavelength λ_{gen} will then be determined by the expression

$$\lambda_{\text{gen}} = \frac{2 n^* \Lambda_a \Lambda_c}{2\Lambda_a + \Lambda_c}. \tag{5}$$

The practical implementation of such a feedback system requires that the lines of the grating on the waveguide and the grating on the metallic mirror must be strictly parallel

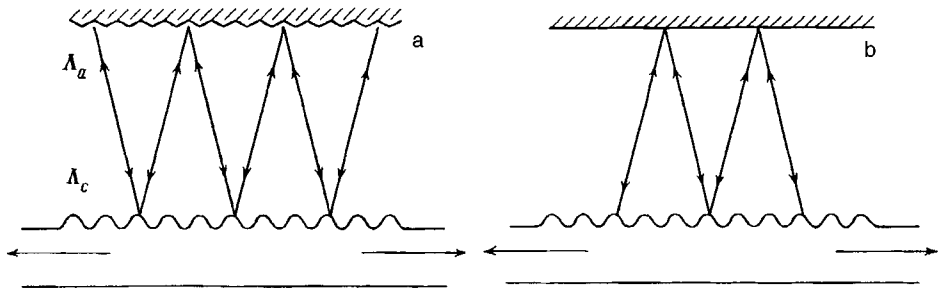

FIG. 2. a — Waveguide structure with two gratings. The grating on the waveguide provides coupling with the thick active layer. A second grating is deposited on a metal surface and operates in the autocollimation regime. It provides the distributed feedback. b — Waveguide structure with one grating. Experimental arrangement.

to each other; this makes it much more difficult to align this scheme. However, this difficulty can be eliminated if a single grating on the waveguide performs the functions of both gratings (Fig. 2b). This is achieved in this case when $\Lambda_a = \Lambda_c$. For this choice of the period of the waveguide grating, two waveguide modes propagating in the Ta_2O_5 film in opposite directions turn out to be coupled. In our experiment the period of the grating was taken to be 0.472 μm, which gave a lasing wavelength at the maximum of the gain band $\lambda_{gen} = 0.56$ μm, since the effective index of the waveguide mode was $n^* = 1.788$, and $\lambda_{gen} = 2n^*\Lambda/3$. The lasing spectrum in this situation consisted of two narrow lines, displaced from each other by $\Delta\lambda = 16$ Å. It is well known[5] that the spectral separation of two laser lines of a distributed-feedback laser is determined by the relation $\Delta\lambda = \lambda^2 k/n\pi$, where k is the coupling constant of the counterpropagating waves in the active medium and n is the index of refraction of these waves. This relation was obtained for distributed feedback acting in the -1-st order of diffraction. To estimate k in our structure it is necessary to find the corresponding value of n and be confident that in our case feedback is realized in the -1-st order of diffraction. The latter condition, incidentally, is obvious, since on a grating with $\Lambda = 0.472$ μm the autocollimation reflection of light in the active layer does indeed occur in the -1-st order of diffraction. In our case n must equal the effective index of refraction n^*_{str} for a mode of the structure shown in Fig. 1. This quantity can be found from the condition $\Lambda_a = \Lambda_c$, and is found to be $n^*_{str} = n_b \sin\theta_b = n^*/3$. Substituting the value obtained for n^*_{str} into the formula for $\Delta\lambda$ makes it possible to find k, which is found to be 96 cm^{-1}. Why is this value so high in our structure? The point is that the feedback in the structure under study is due to two processes: reflection of the mode of the rippled waveguide in the -3-rd order of diffraction of light and autocollimation reflection of light in the buffer layer. It should be noted that here this autocollimation reflection is of an anomalous character (similar to the anomalous specular reflection of light, mentioned above), since it occurs with the participation of waveguide modes excited in the $+1$-st and -2-nd order of diffraction of light by the grating.

Our estimates of the coefficient of autocollimation reflection of light from the rippled interface of two media — a liquid ($n_b = 1.43$) and tantalum oxide ($n_f = 2.02$) — and from the rippled surface of the waveguide in our structure reveal a substantial difference: $R_L = 0.27\%$ and $R_{L\ abnormal} = 6.8\%$. This confirms the fact that the waveguide modes play a large role in the anomalous autocollimation reflection of light. We note here that if the autocollimation reflection of light is realized not in the -1-st but rather in some other order of diffraction of light, then the period of the grating must be chosen from the condition

$$\lambda_{gen} = \frac{2n^*\Lambda}{|K| + 2}, \tag{6}$$

where K is the order of the autocollimation diffraction. The case $K = 0$ is of special interest, since in this case the specularly reflected and autocollimation waves propagate in the same direction.[6] We shall present the case $K = 0$ in subsequent papers.

Let us return once again to the beginning of this letter and turn to Fig. 1, which shows the field distribution of a mode of the combined waveguide structure. We call attention to the fact that the angle θ_b characterizing this mode can be positive or negative.

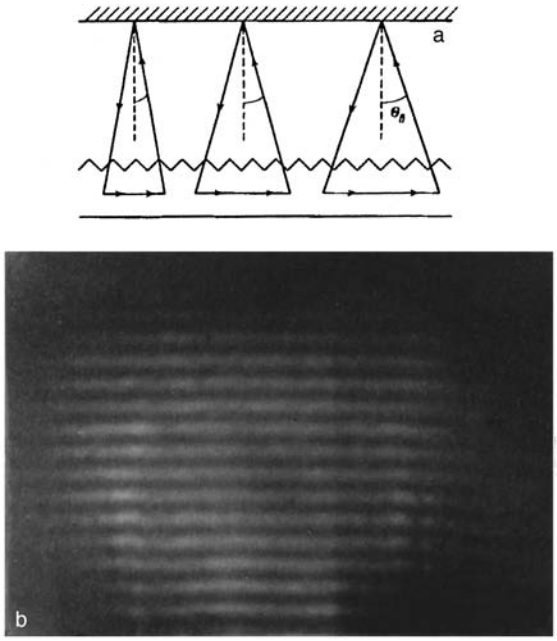

FIG. 3. a — Possible modes of oscillation in a structure with $\Lambda < \lambda/n^*$, b — radiation spectrum of the second mode.

In the latter case the mode of the structure transfers energy along the waveguide in a direction opposite to the direction of propagation of the waveguide mode in the rippled waveguide. Since the mode of the combined waveguide structure is essentially a superposition of a mode of the buffer layer and a mode of a conventional waveguide (Ta_2O_5), the resulting energy flux is determined by the difference of the energy fluxes transferred by the buffer-layer mode and the waveguide-layer mode. In the presence of gain in the buffer layer and resonant coupling of the modes indicated above, the losses of the waveguide mode in the Ta_2O_5 film and the losses of the buffer-layer mode can be compensated by the gain of the buffer-layer mode, and this will result in lasing in the combined waveguide structure at a wavelength determined by the condition

$$\lambda_{\text{gen}} = \frac{\Lambda}{n^* - n_b^*}. \tag{7}$$

The quantity n_b^* is determined by the dispersion relation (3).

The possible modes of oscillation in the experimental structure are shown in Fig. 3a for the case $\theta_b < 0$. The existence of the modes of oscillation indicated in Fig. 3a essentially means that for $\theta_b < 0$ our structure is in itself a structure with distributed feedback, and lasing can be achieved in it without any mirrors. The difference of our distributed feedback structure from the standard structures lies in the fact that it is a quite wide-band structure, and all buffer-layer modes for which the gain exceeds the loss will lase in this structure. To demonstrate this possibility experimentally, we employed a two-mode

waveguide (Ta_2O_5 film on glass $h_w = 0.32$ μm) with ripple period $\Lambda = 0.33$ μm and length of the rippled section $l \sim 2$ mm. In the experiment we achieved lasing at the wavelength $\lambda = 0.56$ μm on the second mode of the rippled waveguide, for which the angle $\theta_b = -3.1°$, which corresponds to $n^* = 1.564$. The width of the lasing spectrum equalled 170 Å, and the spectrum consisted of a set of 16 lines corresponding to the modes of the buffer layer (see Fig. 3b).

In summary, our investigations show the following:

1) A waveguide layer with an active zone of quite large volume can be obtained by using the medium adjoining the rippled waveguide layer as the active material;

2) the autocollimation anomalous reflection of light from the surface of the rippled waveguide makes a large contribution to the intermode coupling constant; and,

3) a waveguide structure containing a high-reflectivity mirror is in itself a distributed-feedback structure if the ripple period is such as to permit extraction of light into the buffer layer at an angle $\theta_b < 0$.

This work was supported by the Russian Fund for Fundamental Research (Grant No. 95-02-06173).

[1] B. A. Ataya and A. N. Osovitskiĭ, Opt. Spektrosk. **66**, 879 (1989) [Opt. Spectrosc. **66**, 514 (1989)].
[2] O. Par'e, V. A. Sychugov, A.E. Tikhomirov *et al.*, Kvantovaya Elektron. (Moscow) **21**, 1090 (1994).
[3] G. A. Golubenko, A. S. Svakhin, V. A. Sychugov *et al.*, Kvantovaya Elektron. (Moscow) **12**, 1334 (1985) [Sov. J. Quantum Electron. **15**, 886 (1985)].
[4] I. A. Avrutsky and V. A. Sychugov, J. Mod. Optics **36**, 1527 (1989).
[5] H. Kogelnick and C. V. Shank, J. Appl. Phys. **43**, 2327 (1972).
[6] O. Par'e, V. A. Sychugov, and A. V. Tishchenko, Kvantovaya Elektron. (Moscow) **22**, 608 (1995).

Translated by M. E. Alferieff

Vibrational transitions in experiments with a scanning tunneling microscope

F. I. Dalidchik, M. V. Grishin, S. A. Kovalevskiĭ, and N. N. Kolchenko
N. N. Semenov Institute of Chemical Physics, Russian Academy of Sciences, 117977 Moscow, Russia

(Submitted 27 December 1996; resubmitted 29 January 1997)
Pis'ma Zh. Éksp. Teor. Fiz. **65**, No. 4, 306–310 (25 February 1997)

A method of in-cavity scanning tunneling spectroscopy is proposed by which one can observe distinct spectra of electronic–vibrational field-emission resonances. © *1997 American Institute of Physics.* [S0021-3640(97)00304-6]

PACS numbers: 61.16.Ch, 73.20.Hb

Scanning tunneling (ST) microscopy and spectroscopy are the only modern methods by which one can study the electronic structure of the surfaces of conducting materials at atomic resolution.[1] There are many known applications of the scanning tunneling microscope (STM) for topographic and spectroscopic measurements of the structure and properties of the most diverse systems (see, for example, Refs. 2 and 3). These measurements are usually conducted for $eV<\phi$, where $\phi\approx 5$ eV is the electronic work function.

Topographic measurements yield direct information about the geometry of surface structures. Spectroscopic measurements make it possible to reconstruct the electron density distribution near the surfaces being studied, but information about the dynamics of surface complexes cannot be obtained by the conventional methods of scanning tunneling microscopy. Many attempts to observe vibrational transitions in adsorbed atoms by the methods of scanning tunneling microscopy, which repeat the scheme of macroscopic tunneling inelastic spectroscopy[4] have been unsuccessful.[5]

There are two reasons for these failures. First, the probability of excitation of the vibrational degrees of freedom of molecules and adatoms under nonresonance conditions of interaction of the particles with electrons is small. (The probability does not exceed $\sim(a_0/R_0)^{\delta u}\leqslant 10^{-2}$, where a_0 is the amplitude of the zero-point vibrations, R_0 is the equilibrium value of the vibrational coordinate, and δu is the change in the vibrational quantum number.) The second reason is the difficulty of finding systems that meet the conditions for a strong resonance interaction,[6] viz., $E^0\approx E_F$, $\Gamma\leqslant\omega$, and $\alpha\geqslant 1$, which are necessary in order for sufficiently intense vibrational transitions to be excited (E^0 is the energy of the resonance level, E_F is the Fermi energy, Γ is the reciprocal of the lifetime of the resonances, ω is the vibrational frequency, and α is the electron–vibrational interaction constant in the resonance complex).

These difficulties can be overcome by using a STM operating in the field-emission mode, i.e., for voltages $V>\phi\approx 5$ V.[7] Under these conditions the path of an electron from the tip to the surface contains a segment of classically allowed motion, $l_c\sim(1-\phi/V)d$ (d is the tip–surface distance, and the voltage on the sample is positive). When the

condition $l_c \sim n\lambda/2$, $n=1,2,3,\ldots$, where λ is the electron wavelength, is met in the three-dimensional cavity formed by the potential barrier and the surface being studied, a standing wave — a field-emission resonance (FER) — is formed; n is the number of resonance.[8,9] The probability of a tunneling transition is maximum for voltages

$$V_n = E_n + \phi, \quad E_n > 0, \tag{1}$$

where E_n is the energy level of the nth FER, measured from the vacuum level of the surface. Under these conditions the transition of an electron through the vacuum gap includes a stage where an intermediate short-lived state is formed, whose lifetime τ_n is determined by the period of the motion of the electron in the STM cavity, $T_n \approx (\partial E_n/\partial n)^{-1}$, and by the electron reflection coefficient of the surface $K(E_n)$:

$$\tau_n \sim T_n/(1-K), \quad e=\hbar=m=1. \tag{2}$$

When an adsorbed particle or local surface vibrations are present in the cavity, electronic transitions (from the tip into the ''cavity'' and from the ''cavity'' into the sample) will shake the vibrational subsystem, inducing (for $\Gamma \leqslant \omega$, $\alpha > 1$[6]) intense multiple-quantum transitions. In experiments with a STM this should be manifested in the characteristic features of tunneling currents, similar to those which are observed in transmission measurements in experiments on electron scattering by gaseous targets.[10,11] Indeed, let the voltage applied to the STM be close to the value determined by formula (1). Let

$$\Gamma \left. \frac{\partial \rho^{t,s}}{\partial E} \right|_{E_F} \ll 1, \tag{3}$$

$$\alpha\omega \ll V, \tag{4}$$

i.e., the characteristic features of the currents which are of interest to us are not related with either the changes in the electron density of states of the tip (ρ^t) or sample (ρ^s) or with threshold defects, which are important only for $V \sim \alpha\omega < \phi$. For simplicity, we neglect nonresonant tunneling transitions and write out the expression for the STM current in which averaging over the vibrational distribution $f(u_i)$ is performed. (For sufficiently strong currents and sufficiently slow relaxation of the vibrational excitation, this distribution can differ from the equilibrium distribution.) According to Eqs. (22)–(25) of Ref. 6, we have

$$J(V,d) = \text{const} \int^{E_F} \sum_{u_i} f(u_i) \sum_{u} \frac{\Gamma_n^t(u_i,u,V,d)\Gamma_n^s(u,V,d)}{(E+\omega_0(u_i+1/2)-E_n(u,V,d))^2+\Gamma_n^2(u,V,d)} dE. \tag{5}$$

Here E_F is the Fermi level of the tip, ω_0 is the frequency of the vibrational subsystem of the STM cavity (local surface vibration or adsorbed particle),

$$E_n(u,V,d) = E_n(V,d) + \omega_n(V,d)(u+1/2), \quad u=0,\ 1,\ 2,\ldots, \tag{6}$$

are the energy levels of the complex formed by an electron trapped by the cavity and the vibrational degrees of freedom of the cavity, $\omega_n(V,d)$ is the corresponding vibrational frequency of the complex, $\Gamma_n^t(u_i,u,V,d)$ is the probability of a transition of an electron from the tip into the cavity, $\Gamma_n^s(u,V,d)$ is the probability of a transition of an electron into the sample ($\Gamma_n^s(u,V,d) = \Sigma_{u_f} \Gamma_n^s(u,u_f,V,d)$, $\Gamma_n^s(u,u_f,V,d)$ is the partial decay prob-

ability of the complex $(n,\ u)$, corresponding to a transition of the vibrational subsystem into the state u_f, $\Gamma_n(u,V,d)=\Gamma_n^s(u,V,d)+\Gamma_n^t(u,V,d)$is the reciprocal of the sojourn time of an electron in the cavity, and $\Gamma_n^t(u,V,d)=\Sigma_{u_i}\Gamma_n^t(u_i,u,V,d))$.

The energy parameters of the complex evidently depend on V and d. These dependences lead to the appearance in the STM currents, $J(V,d)$, of resonance features whose spectra are determined by the roots of the equation

$$V=\phi-\omega_0(u_i+1/2)-E_n(u,V,d), \tag{7}$$

which corresponds to the condition that the level of the complex equals the Fermi level in the tip.

The vibrational frequencies in the complex must be close to the frequencies of local vibrations of an isolated sample ($\omega_0\approx\omega_n(V,d)$), since the field in the STM is usually much weaker than the atomic field (for $V\leqslant 10$ V, $d\geqslant 10$ Å, $F\approx V/d\leqslant 10^{-2}$ a.u.). The functions $E_n(V,d)$ and $\Gamma_n^{s,t}(V,d)$ are most important for the formation of the characteristic features of the functions $J(V,d)$. The functions $E_n(V,d)$ and $\Gamma_n^{s,t}(V,d)$ are determined by the geometry of the STM cavity and the electron reflection coefficient of the surface. In the simplest 1D model of a triangular potential well

$$E_n(V)\approx\left(\frac{cVn}{d}\right)^{2/3},\quad c\sim 1. \tag{8}$$

The functions $\Gamma_n^t(V,d)$ are determined by the penetrability of the field barrier separating the STM cavity from the tip

$$\Gamma_n^t(V,d)\sim\exp\left(-\frac{4E_F^{3/2}d}{3V}\right).$$

The functions $\Gamma_n^s(V,d)$ are determined by the electronic transmission coefficient of the surface layers of the sample.

We assume below for definiteness that $d=$ const. Then, according to Eqs. (7) and (8), the spectrum of the resonance values of the voltages has the form

$$V_n(u,u_i)=\phi+\alpha n^{2/3}+\omega_0(u-u_i),$$

$$V_n(u,u_i)-\phi\ll\phi(n=1,2,\ldots;u,u_i=0,\ 1,\ 2,\ldots), \tag{9}$$

$$\alpha\approx\left(c\frac{\phi}{d}\right)^{2/3}. \tag{10}$$

The surface vibrational frequencies ω_0 correspond to values $\sim 0.05-0.5$ eV and the electronic transition frequencies for characteristic values of ϕ and d (~ 5 eV and 10 Å, respectively) are 1–2 eV according to the estimate (10) with $n\sim 1$, i.e., the spectra of the resonance features of the currents of STMs operating in the field-emission regime must have the form of electronic–vibrational bands in which both ''Stokes'' ($u>u_i$) and ''anti-Stokes'' ($u<u_i$) lines can be observed.

Analysis of expression (5) shows that the form of the resonance feature can be different. It is determined by the ratios of the six energy parameters

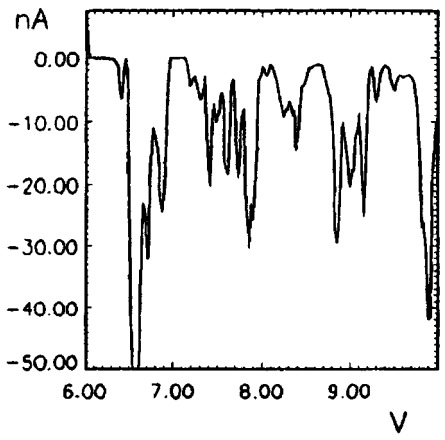

FIG. 1. Electronic–vibrational series of field-emission resonances.

$$\Gamma_n^{s,t}, \left(\frac{\partial}{\partial E}\ln\Gamma_n^{s,t}\right)^{-1}, \quad \omega_0 \quad \text{and} \quad \alpha\omega_0. \tag{11}$$

Analysis of the line shapes of the resonance features of a STM operating in the field-emission regime falls outside the scope of this letter. We shall merely indicate the conditions under which these features have the form of resonance peaks. For this, the necessary conditions are

$$\Gamma_n < \omega_0, \tag{12}$$

$$\omega_0\tau_m \geqslant 1\left(\tau_m = \max\left(\frac{\partial \ln\Gamma_n^{s,t}}{\partial E}\right)_{E_F}\right). \tag{13}$$

It is natural to conjecture that the condition for the formation of long-lived complexes, i.e., the inequality (12), can be satisfied for metal surfaces coated with a thin dielectric layer, for example, an appropriate oxide. For pure metals containing isolated adsorbed particles, $\Gamma \geqslant \omega_0$.[8,9] Analysis of expression (5) shows that under these conditions resonance features can be observed in the conductivity of the STM, which should have bands of broadened (up to $\alpha\Gamma$) maxima with fine-scale oscillatory structure on both shoulders. An example of such features can be found in Ref. 8, where the conductivity of a STM scanning the Ni (100) surface containing isolated oxygen atoms was measured (see Fig. 2 of Ref. 8, curve *C*).

To observe the electronic–vibrational field-emission resonance bands we performed systematic measurements of the functions $J(V)$ in a Omicron STM with a platinum tip scanning a titanium surface in air. The spectra $J(V)$ were measured at 10^4 different points of the 10×10^2 nm surface for V ranging from -10 to 10 eV. The step in V was of the order of 0.01 V, which was necessary to resolve the fine (vibrational) structure of the bands (in the latter case, averaging over 2–4 neighboring values of V was performed in order to eliminate the fine-scale current fluctuations). Different values of d, for which

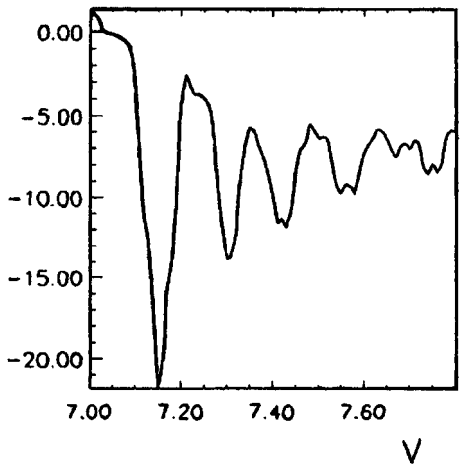

FIG. 2. Fine structure of the electronic–vibrational series corresponding to $V_n(u_i=u_f=0)\simeq 7.2$ V ($\omega_0\simeq 0.1$ eV).

$J(V)$ were measured, were fixed by setting the current J_0 with the maximum voltage $V_{\max}$. The electronic–vibrational bands, examples of which are displayed in Figs. 1 and 2, were measured for $J_0(10\text{ V})=10$ nA. In the overwhelming majority of the cases the distances in energy between the neighboring vibrational lines were close to 0.1 eV, which corresponds to the frequency of local vibrations of titanium oxide ($\omega_0=0.09$ eV).[12] Ordinarily, three or four equidistant vibrational lines, corresponding to one- and multiple-quantum ''Stokes'' transitions, can be distinguished in each band (see Fig. 2). Lines of one-quantum ''anti-Stokes'' transitions were also visible in the vibrational bands at separate points on the surface. An example of such spectra is given in Fig. 1. Besides the series with $\omega_0\approx 0.1$ eV, we also obtained spectra with frequencies ω_0 close to the frequencies of the chemically adsorbed molecules CO (2185 cm^{-1}), OH (3650 cm^{-1}), and O_2 (1680 cm^{-1}).[13] Data from these measurements will be published separately.

In summary, this letter has demonstrated the observation of electronic–vibrational interactions in experiments in STMs. These effects can be used to study the dynamics of the motion of individual adsorbed particles occupying on the surface different but strictly determined (according to topographic measurements) positions.

This work was supported by the Russian Fund for Fundamental Research (Project 96-03-34129).

[1] G. Binning, H. Rohrer, Ch. Gerber, Phys. Rev. Lett. **49**, 57 (1982).
[2] H.-J. Günterrodt and R.Wiesendanger [Eds.], *Scanning Tunnelling Microscopy I*, Springer Series in Surface Science, Vol. 20, Springer-Verlag, Berlin, 1992.
[3] H.-J.Günterrodt and R.Wiesendanger, *Scanning Tunnelling Microscopy II*, Springer Series in Surface Science, Vol. 28, Springer-Verlag, Berlin, 1992.
[4] J. Lambe, R. C. Jaklevic, *Tunnelling Phenomena in Solids*, Plenum Press, New York (1969), p. 243.
[5] Ph. Avoris, J. Chem. Phys. **94**, 2246 (1990).
[6] F. I. Dalidchik, Zh. Éksp. Teor. Fiz. **87**, 1384 (1984) [Sov. Phys. JETP **60**, 795 (1984)].

[7] F. I. Dalidchik, M. V. Grishin, N. N. Kolchenko, and S. A. Kovalevskii, in *Abstracts of the 43rd International Field Emission Symposium*, Moscow, Russia, July 14–19, 1996, Abstract p. 25.
[8] G. Binning, K. H. Frank, and H. Fuchs, Phys. Rev. Lett. **55**, 991 (1985).
[9] R. C. Becker, I. A. Golovchenko, B. S. Swartzentruller, Phys. Rev. Lett. **55**, 987 (1985).
[10] G. Schultz, Rev. Mod. Phys. **45**, 378 (1973).
[11] R. E. Kennerly, Phys. Rev. A **21**, 1876 (1980).
[12] S. Eriksen and R. G. Egdell, Surf. Sci. **180**, 263 (1987).
[13] A. A. Davydov, Adsorbtsiya i Adsorbenty **5**, 83 (1977).

Translated by M. E. Alferieff

Linear response of layered superconductors with *d* pairing to a longitudinal electric field

S. N. Artemenko[a)] and A. G. Kobel'kov
Institute of Radio Engineering and Electronics, Russian Academy of Sciences, 103907 Moscow, Russia

(Submitted 24 December 1996)
Pis'ma Zh. Éksp. Teor. Fiz. **65**, No. 4, 311–316 (25 February 1997)

Simple expressions are obtained for the current and charge densities in layered superconductors with *d* pairing. The conductivities describing the response to solenoidal and potential electric fields are determined by the momentum relaxation time and the imbalance time of the populations of the branches of the quasiparticle spectrum and exhibit a different frequency dependence. The collective modes associated with the oscillations of the potential electric field are investigated. © *1997 American Institute of Physics.* [S0021-3640(97)00404-0]

PACS numbers: 74.72.−h, 74.80.Dm, 74.20.Mn, 74.25.Fg

A great deal of experimental evidence supporting *d* pairing in high-T_c superconductors has been obtained recently with the aid of Josephson experiments,[1] angle-resolved photoemission measurements,[2] and a number of other methods. At the same time, it has been possible to describe many properties of high-T_c superconductors on the basis of a model with *d* pairing (see, for example, Ref. 3 and the references cited therein). The presence of nodes of a superconducting gap in the *d*-superconductors means that effects due to quasiparticles and their relaxation should play a much larger role in them than in superconductors with isotropic pairing. Specifically, the behavior of the potential electric field, associated with the relaxation of the population difference of the branches of the quasiparticle spectrum, should differ substantially.[4–6] Our objective in the present work is to calculate the linear response of a layered superconductor with *d* pairing and to investigate the collective oscillations associated with the potential electric field.

The linear response of a superconductor is ordinarily taken to be the response to a transverse (solenoidal) electric field determined by the time derivative of the vector potential. This is how the response was calculated in, for example, Ref. 7 for the case of *d* pairing. However, in inhomogeneous and anisotropic systems a longitudinal field can appear even when a purely transverse external electromagnetic field is applied. We shall show that the quasiparticle currents arising under the action of potential and solenoidal fields are characterized by different electrical conductivities. Moreover, it turns out that in the case of *d* pairing the decrease in the number of quasiparticles in a quite wide temperature range is compensated by an increase in the scattering time, as a result of which the normal-electron current and the associated dissipation processes can be substantial even at low temperatures. To study these effects, we derive simple expressions for the current and charge densities produced by gradient-invariant vector and scalar potentials, and we use the obtained expressions to investigate collective oscillations. Our calcula-

tions are based on the kinetic equations for the Green's functions, which are a modification of the classical equations of superconductivity.[8] We will not be interested in the nature of the interaction leading to *d* pairing; we assume that the symmetry of the order parameter is determined by the symmetry of the interaction potential in the self-consistency condition. This semiphenomenological approach is used to describe *d* pairing in many works on high-T_c superconductors (see, for example, Refs. 3, 7, and 9).

We are studying a layered superconductor in two limits. In the first limit, using a continuous representation we study the motion of a band nature (itinerant motion) of electrons between layers, which is valid for $t_\perp \gg \nu$, where $t_\perp$ is the overlap integral describing the electron spectrum in a perpendicular direction, $\epsilon_\perp = 2t_\perp \cos dp_\perp$, d is the lattice constant in the perpendicular direction, and ν is the reciprocal of the mean free time in a direction parallel to the layers. In the second limit, we employ the equations of Refs. 10 and 11 in Wannier's discrete representation, studying the opposite case, $t_\perp \ll \nu$, corresponding to incoherent transitions between the layers (this approach is close to the model of Ref. 12, where electron transitions between layers occur only as a result of scattering, and the overlap integral $t_\perp$ is neglected). The results obtained in both cases are virtually identical, and for this reason we shall study mainly the band-type motion and then we shall note how the results differ in the case of hopping conductivity between the layers.

To derive the equations, in contrast to Ref. 8, we integrate Green's functions with respect to $\xi = p_\parallel^2/2m - \epsilon_F$, where $\mathbf{p}_\parallel$ is the component of the momentum parallel to the layers. As a result, we obtain an equation for the retarded (advanced) Green's function $g^{R(A)}$ and for the function g^K related with the quasiparticle distribution function, which depend on the perpendicular component of the momentum $p_\perp$ and on the angle ϕ determining the direction of $\mathbf{p}_\parallel$. Each function is a matrix with respect to the spin indices.

The unperturbed retarded and advance functions can be represented in an explicit form as $g^{R(A)} = \sigma_z a^{R(A)} + i\sigma_y b^{R(A)}$, where $a^{R(A)} = (\epsilon + i\nu\langle a^{R(A)}\rangle_\phi/2)/\xi^{R(A)}$ and $b^{R(A)} = \Delta(\phi)/\xi^{R(A)}$. The brackets $\langle \ldots \rangle$ denote averaging with respect to the variable indicated in the subscript, $\xi^{R(A)} = \pm\sqrt{(\epsilon + i\nu\langle a^{(RA)}\rangle_\phi/2)^2 - \Delta(\phi)^2}$.

We shall solve the equation for the anomalous function determined in the standard manner as $g^K = g^R(\epsilon,\epsilon')\tanh(\epsilon'/2T) - g^A(\epsilon,\epsilon')\tanh(\epsilon/2T) + g^{(a)}(\epsilon,\epsilon')$:

$$\mathbf{v}\cdot\nabla g^{(a)} - [\epsilon_+\sigma_z + \Delta(\phi) i\sigma_y]g^{(a)} + g^{(a)}[\epsilon_-\sigma_z + \Delta(\phi) i\sigma_y] - (\Sigma^R g^{(a)} - g^R\Sigma^{(a)} + \Sigma^{(a)}g^A - g^{(a)}\Sigma^A) = \alpha[(\mathbf{v}\cdot\mathbf{P}_s\sigma_z + \mu)g^A - g^R(\mathbf{v}\cdot\mathbf{P}_s\sigma_z + \mu)]. \quad (1)$$

Here $\Delta(\phi)$ and χ are the amplitude and phase of the order parameter, $\mathbf{v}$ is the velocity at the Fermi surface, $\mathbf{P}_s = (1/2)\nabla\chi - \mathbf{A}$ is the superconducting momentum, $\mu = (1/2) \times (\partial\chi/\partial t) + \Phi$, $\mathbf{A}$ and Φ are the vector and scalar electromagnetic potentials, $\alpha = \tanh \epsilon_+/2T - \tanh \epsilon_-/2T$, and $\sigma_{y,z}$ are Pauli matrices. The quantities $\mathbf{P}_s$ and μ play the role of gradient-invariant potentials. The functions $g^{R(A)}$ in Eq. (1) depend on the energies $\epsilon_\pm = \epsilon \pm \omega/2$, respectively. The mass operators in the collision integral have the form

$$\hat{\Sigma}^{\iota}=\int_{-\pi/d}^{\pi/d}\frac{dp_{\perp}'}{2\pi/d}\int_{0}^{2\pi}\frac{d\phi'}{2\pi}\,\nu(p_{\perp},\phi;p_{\perp}',\phi')\hat{g}^{\iota}(p_{\perp}',\phi'),\tag{2}$$

where $\iota=R$, A, and K; ν is the elastic scattering rate in the normal state. Strictly speaking, Eq. (2) describes impurity scattering in the Born approximation, but it can also be used to describe scattering by phonons in neglect of the inelasticity of the scattering. Confining ourselves to the Born approximation, we shall neglect the localized states produced by impurities at the Fermi surface (see Ref. 13 and the references cited therein). Therefore our results are valid when the characteristic quasiparticle energy is greater than the width of the band of impurity states, $T>\sqrt{\Delta\nu}$.

We shall simplify the momentum dependence of ν, neglecting the dependence of the scattering on the angle in the plane of the layers. Since in-layer scattering suppresses the order parameter and scattering between the layers does not and in order to take account of the possibility of a different temperature dependence of in-layer and between-layer scattering, we retain the difference between scatterings in the parallel and perpendicular directions, distinguishing components corresponding to the isotropic scattering, ν, and scattering in the perpendicular direction, $\nu_{\perp}$:

$$\nu(p_{\perp},\phi;p_{\perp}',\phi')=\nu+\nu_{\perp}\delta(\phi-\phi').$$

We solve Eq. (1) for continuously varying perturbations $|\mathbf{q}\cdot\mathbf{v}|\ll\nu$, when the changes in all quantities in the plane of the layers are smaller than the mean free path length. This condition is satisfied in the most interesting frequency range, since the characteristic values of $1/q$ are determined either by the magnetic field penetration depth (at low frequencies) or the skin depth (at high frequencies). These lengths are greater than the mean free path length, if the frequency of the oscillations lies below the frequency range of the anomalous skin effect. Then the solution for the components $g^{(a)}$ determining the quasiparticle charge and current densities have the form

$$(1/2)\mathrm{Tr}\langle g^{(a)}\rangle=-\frac{\alpha\mu}{A}\left(h+\frac{(1/2)q^2v^2h_1+k^2\langle v_z^2\rangle_{p_\perp}h_2}{A}\right)$$
$$-\frac{\alpha}{A}\langle v^2\mathbf{q}\cdot\mathbf{P}_{\|}a/\xi_s^2+k\langle v_z^2\rangle_{p_\perp}P_{\perp}a/(\xi_s\zeta)\rangle_{\phi},\tag{3}$$

$$(1/2)\mathrm{Tr}\;\sigma_z\langle\mathbf{v}g^{(a)}\rangle=-\alpha\left\langle\mathbf{v}(\mathbf{v}\cdot\mathbf{P}_{\|})\frac{1-a^Ra^A-b^Rb^A}{\xi_s}\right\rangle_{\phi}-\frac{\alpha\mu}{A}\langle\mathbf{v}(\mathbf{v}\cdot\mathbf{q})a/\xi_s^2\rangle_{\phi},\tag{4}$$

$$(1/2)\mathrm{Tr}\;\sigma_z\langle v_zg^{(a)}\rangle=-\alpha\langle v_z^2\rangle_{p_\perp}P_{\perp}\left\langle\frac{1-a^Ra^A-b^Rb^A}{\zeta}\right\rangle_{\phi}-\frac{\alpha\mu}{A}k\langle v_z^2\rangle_{p_\perp}\langle a/(\xi_s\zeta)\rangle_{\phi}.\tag{5}$$

Here $h=\langle(1-a^Ra^A+b^Rb^A)/\xi_s\rangle_{\phi}$, $h_1=\langle(1-a^Ra^A+b^Rb^A)/\xi_s^3\rangle_{\phi}$, $h_2=\langle(1-a^Ra^A+b^Rb^A)/(\xi_s^2\zeta)\rangle_{\phi}$, and $A=1-(i/2)\nu h$, and the components of the retarded and advanced functions once again depend on the energies $\epsilon\pm\omega/2$, respectively. Next, $a=(a^R-a^A)/2$, $\mathbf{P}_{\|}$ and $P_{\perp}$ are the components of $\mathbf{P}_s$ parallel and perpendicular to the layers, $\mathbf{q}$ and k are the components of the wave vector parallel and perpendicular to the layers, $\xi_s=\xi^R(\epsilon+\omega/2)+\xi^A(\epsilon-\omega/2)$, and $\zeta=\xi_s+i\nu_{\perp}$.

The solutions of the equations for the perturbations of the retarded (advanced) Green's function, similar to Eq. (1), are obtained by replacing α by 1 and interchanging all superscripts $R(A)$. The current and charge densities are calculated by integrating Eqs. (3)–(5) over energy together with solutions for the retarded and advanced Green's functions, which, being substituted into g^K, determine the superconducting current. We shall integrate in the limit of low frequencies, $\omega \ll \Delta$, where Δ is the maximum value of the superconducting gap, having in mind in so doing a pure superconductor, $\Delta, T_c \gg \nu$ (the opposite limit corresponds to a zero-gap state). In this case the linear response can be represented in a simple form, admitting a clear interpretation in the spirit of a two-fluid model:

$$-i\omega\rho = -i\omega\gamma\frac{\kappa^2}{4\pi}\mu + (\sigma_{2\|}q^2 + \sigma_{2\perp}k^2)\mu + \omega(\sigma_{1\|}\mathbf{q}\cdot\mathbf{P}_\| + \sigma_{1\perp}kP_\perp), \tag{6}$$

$$\mathbf{j}_\| = \frac{c^2}{4\pi\lambda_\|^2}\mathbf{P}_\| - i(\omega\sigma_{0\|}\mathbf{P}_\| + \sigma_{1\|}\mathbf{q}\mu), \tag{7}$$

$$j_\perp = \frac{c^2}{4\pi\lambda_\perp^2}P_\perp - i(\omega\sigma_{0\perp}P_\perp + \sigma_{1\perp}k\mu), \tag{8}$$

where κ^{-1} is the Thomas–Fermi screening length, $\lambda_{\|(\perp)}$ is the penetration depth of the magnetic field for currents parallel (perpendicular) to the layers. The factor γ and the conductivities $\sigma_{n\alpha}$ ($n=0$, 1, 2 and $\alpha = l,t$) depend on the frequency:

$$\gamma = 1 + \int_{-\infty}^{\infty} d\epsilon \frac{\omega\langle a_0\rangle_\phi}{(\omega + i\nu_b)}\frac{dn_F}{d\epsilon}, \tag{9}$$

$$\sigma_{n\alpha} = -\sigma_{N\alpha}\frac{1}{\tau_\alpha}\int_{-\infty}^{\infty} d\epsilon \left\langle \frac{i\theta(|\epsilon| - |\Delta(\phi)|)a_0^{1-2n}\omega^n}{(\omega + i\tilde{\nu}_\alpha)(\omega + i\nu_b)^n}\frac{dn_F}{d\epsilon}\right\rangle_\phi . \tag{10}$$

Here $\sigma_{N\alpha}$ is the normal-state conductivity in the direction α, n_F is the Fermi distribution function, $a_0 = \epsilon/\sqrt{\epsilon^2 - \Delta^2}$; $\tilde{\nu}_\| = \nu\langle a\rangle_\phi$ and $\tilde{\nu}_\perp = \tilde{\nu}_\| + \nu_\perp/a_0$ are the reciprocals of the quasiparticle momentum relaxation times for the corresponding directions. Finally, $\nu_b = \nu\langle \Delta^2(\phi)a_0/\epsilon^2\rangle_\phi$ describes the electron–hole imbalance relaxation rate, which in *d*-superconductors is determined by elastic scattering.

The first terms in Eqs. (7) and (8) describe the superconducting current, and the remaining terms describe the quasiparticle current. It is evident from the definition of the electric field $\mathbf{E} = -\nabla\mu - i\omega\mathbf{P}_s$ that the simple expression $\mathbf{j} = \hat{\sigma}\mathbf{E}$ for the quasiparticle does not hold, since $\sigma_{n\alpha}$ are different for the contributions of the scalar and vector potentials to the electric field. In addition, the frequency dispersion of the electrical conductivities $\sigma_{0\alpha}$, describing the response to a solenoidal field, is determined only by the quasiparticle momentum relaxation time, and the dispersion of $\sigma_{1\alpha}$, which describe the response to a potential field, also depends on the electron–hole imbalance relaxation time.

According to Eq. (6), the changes in the current density are determined by the changes in the potential μ, which is associated with the imbalance of the density of

electron- and hole-like excitations (see Refs. 5 and 6), and by the spatial changes of the quasiparticle currents. The equation (6) plays the role of the continuity equation for quasiparticles.

In the limit of small differences of the order parameter between the layers, the results obtained in a discrete model for the case of incoherent transitions of electrons between layers, $t_\perp \ll \nu$, are similar to the results obtained above for the itinerant motion in the perpendicular direction. They can be obtained from Eqs. (6)–(10) by replacing $P_\perp$ by $(\chi_n - \chi_{n-1})/d$ with $\nu_\perp = 0$, where χ_n is the phase of the order parameter in the layer n.

Let us consider the case of low temperatures $\Delta \gg T$. Let the angular dependence of the gap parameter have the simplest form for d pairing: $\Delta = \Delta_0 \cos 2\phi$. Averaging over angles, we obtain for the characteristic times at low temperatures $\tilde{\tau}_\parallel \equiv 1/\tilde{\nu}_\parallel = \Delta_0/(2T\nu) \approx \tau_b \gg 1/\nu$. Therefore the quasiparticle momentum relaxation time increases as $\propto 1/T$ compared with the electron scattering time in the normal state. We obtain for the response to a solenoidal field

$$\sigma_{0\alpha} = \sigma_{N\alpha} \mathbf{P}_\alpha R_\alpha(\omega), \quad R_\parallel = \int_0^\infty \frac{x\,dx}{(x - i\omega\tilde{\tau}_\parallel)\cosh^2 x},$$

$$R_\perp = \frac{2(\nu + \nu_\perp)}{\pi\nu} \int_0^\infty dx \int_0^1 \frac{x\,dy}{(x - i\omega\tilde{\tau}_\parallel + \nu_\perp \tilde{\tau}_\parallel \sqrt{1-y^2})\cosh^2 x}, \tag{11}$$

where $\tau_\perp = 1/(\nu_i + \nu_\perp)$. Let us consider a current in the plane of the layers. According to Eq. (11), for $\omega\tilde{\tau}_\parallel \ll 1$, when scattering is important, $R_\parallel = 1$, i.e., the decrease in the quasiparticle density with decreasing temperature is compensated by an increase in the mean free time of the quasiparticles. At high frequencies $\omega \gg 1/\tilde{\tau}_\parallel$ we obtain $R_\parallel = i(1 - N_s)/\omega\tau_\parallel$, where $N_s = 1 - (T/\Delta_0)\ln 4 = (\lambda(0)/\lambda(T))^2 \approx 1$ describes the decrease in the density of superconducting electrons. In this case, the scattering can be neglected and the quasiparticle current, which adds with the superconducting current, describes the free motion of all electrons.

Let us now consider the conductivity in a direction perpendicular to the layers. If either $\nu_\perp \ll 1/\tilde{\tau}_\parallel$ or $\nu_\perp \ll \omega$, we obtain $R_\perp = R_\parallel/\nu\tau_\perp$, i.e., the conductivity $\sigma_\perp$ is determined by scattering in the plane of the layers. In the opposite case, $\nu_\perp \gg 1/\tilde{\tau}_\parallel$ and $\nu_\perp \gg \omega$, the contribution of the quasiparticles can be neglected.

We now examine the plasma oscillations of the superconducting electrons. Such oscillations have been observed in high-T_c superconductors[14] and have been investigated theoretically in a number of works (see, for example, Refs. 11, 15, and 16) assuming isotropic pairing. To calculate their spectra, expressions (6)–(8) must be substituted into Maxwell's equations. In the long-wavelength limit we obtain a result which differs from the case of s pairing[11] primarily by the damping:

$$\omega^2 = \omega_0^2 \left(\frac{1 + k^2\lambda_\parallel^2 + q^2\lambda_\perp^2}{1 + k^2\lambda_\parallel^2} - iR_\perp \omega\tau_\perp \right). \tag{12}$$

The last term in Eq. (12) at low frequencies describes damping due to dielectric relaxation. According to Eq. (11), the damping is determined by the large quantity σ_N only at

frequencies less than the reciprocal of the quasiparticle scattering time, $\omega < \nu T/\Delta \ll \nu$. At frequencies of the order ω_0, the damping is small. For this reason, plasma oscillations remain weakly damped.

At high temperatures, $\Delta \ll T$, the effective relaxation time of the imbalance becomes much longer than the momentum relaxation time. In superconductors with isotropic pairing at such temperatures and frequencies $\omega \gg \nu(\Delta/T)^2$, there exist weakly-damped collective oscillations of the electron–hole imbalance (Carlson–Goldman mode). This is expressed mathematically in that in such superconductors the factor γ in Eq. (6), to which the frequency of the oscillations is proportional, is real (see review[6]). In *d*-superconductors $\gamma = (\pi\Delta_0/2T)\sqrt{i\nu/\omega}$ contains a large imaginary part and the oscillations are strongly damped.

In the static limit, our equations determine the penetration depth of the electric field in the superconductor when current flows through the boundary with normal metal. This length for the α direction equals $l_E\sqrt{\pi\Delta_0 D_\alpha/4T\nu}$, which agrees with the result of Ref. 17. Here the diffusion coefficients are related with the conductivities in the corresponding direction by the relation $D_\alpha\kappa^2 = 4\pi\sigma_{N_\alpha}$.

In conclusion we note that, as can be shown, the obtained results largely remain in force also in the case when the symmetry of the order parameter is different from but close to *d* symmetry: $\langle\Delta(\phi)\rangle^2 \ll \langle\Delta(\phi)^2\rangle$. The main changes in this case reduce to a somewhat different angular and energy dependences of the momentum and electron–hole imbalance relaxation times.

[a)]e-mail: Art@mail.cplire.ru

[1] D. A. Wollman, D. J. Von Harlingen, W. C. Lee *et al.*, Phys. Rev. Lett. **71**, 2134 (1993).
[2] Y. Tokoya, T. Takahashi, T. Mochiku *et al.*, Phys. Rev. B **53**, 14 055 (1996).
[3] K. Maki and H. Won, J. Phys. (France) I **6**, No. 12 (1996).
[4] M. Tinkham and J. Clarke, Phys. Rev. Lett. **28**, 1366 (1972).
[5] M. Tinkham, Phys. Rev. B **6**, 1747 (1972).
[6] S. N. Artemenko and A. F. Volkov, Usp. Fiz. Nauk **128**, 3 (1979) [Sov. Phys. Usp. **22**, 295 (1979)].
[7] P. J. Hirschfeld, W. O. Putikka, and D. J. Scalapino, Phys. Rev. Lett. **71**, 3705 (1993); Phys. Rev. B **50**, 10 250 (1996).
[8] A. I. Larkin and Yu. N. Ovchinnikov, Zh. Éksp. Teor. Fiz. **73**, 299 (1977) [Sov. Phys. JETP **46**, 155 (1977)].
[9] S. V. Pokrovsky and V. L. Pokrovsky, Phys. Rev. Lett. **75**, 1150 (1995).
[10] S. N. Artemenko, Zh. Éksp. Teor. Fiz. **79**, 162 (1980) [Sov. Phys. JETP **52**, 81 (1980)].
[11] S. N. Artemenko and A. G. Kobel'kov, JETP Lett. **58**, 445 (1993); Physica C **253**, 373 (1995).
[12] M. J. Graf, D. Rainer, and J. A. Souls, Phys. Rev. B **47**, 12 089 (1993).
[13] M. J. Graf, S-K. Yip, and J. A. Souls, Phys. Rev. B **53**, 15 147 (1996).
[14] K. Tamasaku, Y. Nakomura, and S. Ushida, Phys. Rev. Lett. **69**, 1455 (1992).
[15] T. Mishonov, Phys. Rev. Lett. B **44**, 12033 (1991).
[16] M. Tachiki, T. Koyama, and S. Takahashy, Phys. Rev. **50**, 7065 (1994).
[17] C. H. Choi, Phys. Rev. B **54**, 3044 (1996).

Translated by M. E. Alferieff

Acoustic light diffraction, associated with the modulation of the polarization of the light, in an easy-plane antiferromagnet

E. A. Turov[a)]

Institute of Metal Physics, Urals Branch of the Russian Academy of Sciences, 620219 Ekaterinburg, Russia

(Submitted 27 December, 1996)
Pis'ma Zh. Éksp. Teor. Fiz. **65**, No. 4, 317–321 (25 February 1997)

The intensity of acoustic light diffraction by an easy-plane antiferromagnet in the Raman–Nath regime, due to a photoelastic interaction of antiferromagnetic origin, is calculated in the case when there is no modulation of the refractive index to first order in the acoustic deformations, and the entire effect is due to the linear modulation of the light polarization. Quantitative estimates are made for $FeBO_3$. © *1997 American Institute of Physics.* [S0021-3640(97)00504-5]

PACS numbers: 75.50.Ee, 78.20.Hp, 42.25.Fx, 75.80.+q

Photoelastic interaction (PEI) due to acoustic modulation of the antiferromagnetic part of the permittivity $\epsilon_{\alpha\beta}$ can exist in antiferromagnets of the easy-plane (EP) type (for example, $FeBO_3$).[1] This interaction is characterized by the presence of the so-called exchange enhancement, on account of which the antiferromagnetic contribution to the PEI is comparable in magnitude to the PEI of well-known acoustooptic materials (for example, lithium niobate and sapphire). The advantage of the antiferromagnetic contribution is that it depends strongly on the magnitude and direction of the magnetic field **H**.

In Ref. 1 acoustic diffraction of light was studied in application to the antiferromagnets α-Fe_2O_3 and $FeBO_3$ in the Bragg regime, requiring (at least, for the antiferromagnets indicated) quite high acoustic frequencies ($\Omega/2\pi > 100$ MHz) and comparatively thick samples ($d > 1$ cm). This regime corresponds to the condition[2]

$$Q = \frac{2\pi\lambda d}{n\Lambda^2} \gg 1. \tag{1}$$

Here d is the thickness of the light beam traversed by the light, λ and Λ are, respectively, the wavelengths of the light and the sound, and n is the index of refraction for light.

The Raman–Nath diffraction (RND) regime, which is characteristic for sufficiently thin plates and comparatively low sound frequencies, is apparently more favorable from the standpoint of the experimental possibilities. It is well known[3] that an acoustooptic cell operates in the Raman–Nath regime in practice even for $Q < 10$. However, for values of the parameters appearing in Q given by expression (1), for example, for $FeBO_3$ (Ref. 1) at sound frequency $\Omega/2\pi = 100$ MHz and thickness $d = 1$ mm we find $Q = 0.6$, which decreases rapidly with Ω. In studying RND, my goal in the present letter is to show that

in this case there exists a new RND mechanism associated not with the modulation of the index of refraction, ordinarily considered to be responsible for the RND,[2] but rather with the modulation of the polarization vector of the light. This modulation is due to rotations of the antiferromagnetism vector L which are caused by the elastic (acoustic) deformations on account of the magnetoelastic interaction.[1,4] Under some conditions this channel of the RND may not only be more efficient than the conventional channel via the index of refraction, but it leads to a much different result.

Let us consider an antiferromagnetic with an exchange magnetic structure $\underline{1}(+)3(+)2(-)$ (Refs. 4 and 5) in the orientational state with $L\perp 3 \parallel Z$ (EP). The coordinate axes in the basal plane are directed so that $X \parallel H \parallel M \perp Z$ (M is the total magnetization) and $Y \parallel L$. Let an elastic wave with circular frequency Ω and wave vector $q \parallel x$ propagate along the X axis. It corresponds to transverse deformations with

$$e_{x\alpha}=a_\alpha \sin(qx-\Omega t), \quad \alpha=y,\ z. \tag{2}$$

For $\Omega \ll \omega_{\mathrm{AFMR}}$ of the lower branch of the AFMR, these deformations produce a quasiequilibrium rotation (oscillation) of the L vector in the XY plane by an angle φ determined by the equation[1]

$$\sin\varphi=-L_x/L=-2(U_\alpha e_{x\alpha}). \tag{3}$$

Here U_α are the coefficients of the aforementioned exchange enhancement, which in 50–100 Oe fields reaches values of the order of 10^4.

We shall study scattering of light with frequency ω and wave vector $k \parallel Z$, such that the components of the tensor $\epsilon_{\alpha\beta}$ are in play:[4]

$$\epsilon_{xx}=\epsilon_0+b_2L_y^2+c_1L_yH_x, \quad \epsilon_{yy}=\epsilon_0+b_1L_y^2-c_2L_yH_x, \tag{4}$$

$$\epsilon_{xy}=\epsilon_{yx}=\left[(b_1-b_2)L_y-\frac{1}{2}(c_1+c_2)H_x\right]L_x.$$

Here $L_y \approx L$ and terms of order no higher than linear in L_x (and therefore in $\epsilon_{\alpha\beta}$) are retained. The refractive indices and polarization of the normal light modes are determined by the relations

$$n_{1,2}^2=\frac{\epsilon_{xx}+\epsilon_{yy}}{2}\pm\sqrt{\left(\frac{\epsilon_{xx}-\epsilon_{yy}}{2}\right)^2+\epsilon_{xy}^2}, \tag{5}$$

$$\left(\frac{E_y}{E_x}\right)_1=-\left(\frac{E_x}{E_y}\right)_2\simeq\frac{\epsilon_{xy}}{\epsilon_{xx}-\epsilon_{yy}}\equiv -A(x,t), \tag{6}$$

where, according to Eqs. (3)–(6),

$$A=(1-h)2U_\alpha a_\alpha \sin(qx-\Omega t). \tag{7}$$

Here $h=(c_1+c_2)H_x/2(b_2-b_1)L$ represents the relative field contribution (in order of magnitude) to the polarizability ϵ_{xx} and ϵ_{yy}. For weak fields H_x, in which the coeffi-

cients U_α in Eq. (3) are quite large, it can be assumed that $h \ll 1$. Furthermore, the derivation of Eqs. (5) and (6) takes account of the fact that the light frequency $\omega \gg \Omega$ (in our case $\Omega/\omega < 10^{-7}$).

It is evident from Eq. (5), substituting Eqs. (3) and (4), that the refractive indices $n_{1,2}$ equal, in the approximation linear in the deformations,

$$n_{10} = \sqrt{\epsilon_{xx}}, \quad n_{20} = \sqrt{\epsilon_{yy}}, \tag{8}$$

whence it follows that in this approximation sound has no effect on them. At the same time, the polarization relations (6) are modulated linearly by the deformations (2).

In addition, the boundary conditions for the amplitude of the incident light ($Z=0$) are of the form

$$E_x(0) = E_{x1}(0) + E_{x2}(0) = E_0, \quad E_y(0) = E_{y1}(0) + E_{y2}(0) = 0. \tag{9}$$

Together with Eqs. (6) this gives

$$E_{1x}(0) = \frac{E_0}{1+A^2}, \quad E_{1y}(0) = \frac{E_0 A}{1+A^2},$$

$$E_{2x}(0) = \frac{E_0 A^2}{1+A^2}, \quad E_{2y}(0) = -\frac{E_0 A}{1+A^2}. \tag{10}$$

Taking account of the phase difference between the optical modes 1 and 2 (due to the difference in the refractive indices (8)) and using expression (10) for their amplitudes, we obtain for the field $E(x,z,t)$ at the exit (at $Z=d$)

$$\frac{E_x}{E_0} = \frac{1}{1+A^2}\left[\exp\left(i\frac{\omega}{c}n_{10}d\right) + A^2\exp\left(i\frac{\omega}{c}n_{20}d\right)\right]\exp(-i\omega t),$$

$$\frac{E_y}{E_0} = \frac{A}{1+A^2}\left[\exp\left(i\frac{\omega}{c}n_{20}d\right) - \exp\left(i\frac{\omega}{c}n_{10}d\right)\right]\exp(-i\omega t). \tag{11}$$

The real parts $r_{x,y} \equiv \mathrm{Re}(E_{xy}/E_0)$, substituting expression (7) for A, can be put into the form

$$r_x = \cos\left(\frac{\omega}{c}n_{10}d - \omega t\right), \tag{12}$$

$$r_y = 2(1-h)U_\alpha a_\alpha \sin\left[\frac{\omega}{c}\frac{n_{10}-n_{20}}{2}d\right]$$
$$\times\left\{\cos\left[\frac{\omega}{c}nd + qx - (\omega+\Omega)t\right] - \cos\left[\frac{\omega}{c}nd - qx - (\omega-\Omega)t\right]\right\}, \tag{13}$$

$$n = (n_{10}+n_{20})/2.$$

Remaining in the linear approximation in the amplitudes a_α of the deformations, we assumed here that $A^2 \ll 1$. Retaining in Eq. (13) the frequency Ω in the arguments of the cosines together with ω is, of course, of purely symbolic significance, since the deriva-

tion of Eqs. (5) and (6) neglected terms of order Ω/ω. This notation demonstrates more clearly that here we are talking about light-scattering processes with absorption or emission of one phonon.

Therefore, after the light passes through the light beam, besides the unscattered wave (12), there appear two scattered waves with frequencies $\omega \pm \Omega$ and fronts which are symmetrically deflected from the initial wave by the angles

$$\theta_{1,2} \approx \sin\ \theta_{1,2} = \pm q/k = \pm(\Omega/2\pi)\lambda/vn, \tag{14}$$

where $k = \omega n/c$. The situation is completely analogous to Bragg diffraction, in which, just as here, in contrast to the conventional RND, the entire scattered intensity passes into first-order diffraction. The law of conservation of energy is satisfied here — the total intensity of the transmitted light equals the intensity of the incident light:

$$|r_x(0)|^2 + |r_y(0)|^2 = |r_x(d)|^2 + |r_y(d)|^2 = 1.$$

(This is most easily verified using the exact formulas (11)). It is also important to note that the polarization of the diffracted waves is rotated by $\pi/2$ relative to the incident wave.

Now we shall discuss sound waves on which experiments are convenient to perform. To simplify the interpretation, it is desirable that these be normal acoustic modes. Let us consider two suitable situations.

Variant 1: $\mathbf{H} \parallel 2$ (two-fold symmetry axis), sound is polarized along the Z axis: $u \| Z$. For a trigonal crystal such sound is not a purely acoustic mode, since the mode also contains a component u_y. But the ratio u_y/u_x is quite small (once again we have in mind $FeBO_3$), of the order of 0.1 for fields $H \approx 50-100$ Oe. The velocity of these waves is $v \approx 4 \cdot 10^5$ cm/s.

Variant 2: $\mathbf{H} \perp \mathbf{2}$. In this case sound with polarization $u \| Y \| L$ (for $q \| X \| H$) is a purely acoustic mode. Its velocity is $v \approx 6 \cdot 10^5$ cm/s.

We note that for the weak fields $H \approx 50-100$ Oe considered here we are actually dealing with not the conventional elastic waves but rather magnetoelastic waves, whose velocity v can vary with H by tens of percent.[4,6] This signifies that the deflection angles $\theta_{1,2}$ (14) also depend on H.

In conclusion, I shall present some quantitative estimates for $FeBO_3$. (The numerical values of the required parameters are presented in Ref. 1.) The angle $|\theta_{1,2}|$ for the two situations considered above at sound frequency $\Omega/2\pi = 100$ MHz equals approximately $0°20' - 0°10'$. The scattering intensity as a function of the thickness is determined by the factor $\sin[(n_{10}-n_{20})d\omega/2c]$ in Eq. (13) and therefore has maximum for $d \equiv d_{\max} = (2p+1)\lambda/2(n_{10}-n_{20})$, where p are integers. For $p=0$ we obtain $d_{\max} = 1.75$ mm. For such thicknesses (which can also be changed by a magnetic field) the factor $2U_\alpha a_\alpha$ in Eq. (13) gives the relative amplitude of scattered waves with $\alpha \equiv z$ for the first variant and $\alpha = y$ for the second variant. The quantity r_y depends through a_α (see Eq. (2)) on the power of the sound flux $I_s = 2\rho v_\alpha^3 a_\alpha^2$, so that for $I_s = (1-10)$ W/cm^2 we have, for example,

$$2(U_z a_z) = |\sin\ \varphi|_{\max} = 0.16\text{–}0.52.$$

The second (larger) term, strictly speaking, already falls outside the scope of the approximations made here ($\sin^2\varphi \ll 1$), but it still gives the correct result in order of magnitude. The quantity r_y depends on H through U_α (see Eqs. (25) and (16) in Ref. 1), and therefore not only the angle, but also the intensity of the diffracted light can be controlled (specifically, modulated with a definite frequency) with the aid of a magnetic field.

It is also of interest to examine the case of the field $\mathbf{H} \parallel Z$, when linear acoustic modulation can occur both for the index of refraction and for the light polarization, but this will not be done in this letter.

I thank M. I. Kurkin for a helpful discussion and the Russian Fund for Fundamental Research for support (Grants 96-02-16489 and 95-02-07231).

[a)]e-mail: theormag@ifm.e-burg.su

---

[1] E. A. Turov, Zh. Éksp. Teor. Fiz. **98**, 655 (1990) [Sov. Phys. JETP **71**, 365 (1990)].
[2] A. Yariv and P. Yeh, *Optical Waves in Crystals*, Wiley, N. Y. 919840 [Russian translation, Mir, Moscow (1987)].
[3] J. N. Lee and A. Vanderlugt, Proc. IEEE **77**, 1528 (1989).
[4] E. A. Turov, *Kinetic, Optical, and Acoustic Properties of Antiferromagnets* [in Russian], Ural Branch of the Russian Academy of Sciences Press (1990).
[5] E. A. Turov, Usp. Fiz. Nauk **164**, 325 (1994).
[6] V. I. Ozhogin and V. L. Preobrazhenskiĭ, Usp. Fiz. Nauk **155**, 593 (1988) [Sov. Phys. Usp. **31**, 713 (1988)].

Translated by M. E. Alferieff

Onset of a nonoptimal hopping regime for ac conductivity in amorphous gallium antimonide

S. V. Demishev, A. A. Pronin, N. E. Sluchanko, and N. A. Samarin
Institute of General Physics, Russian Academy of Sciences, 117942 Moscow, Russia

A. G. Lyapin
Institute of High-Pressure Physics, Russian Academy of Sciences, 142092 Troitsk, Moscow District, Russia

(Submitted 30 December 1996)
Pis'ma Zh. Éksp. Teor. Fiz. **65**, No. 4, 322–327 (25 February 1997)

A possible explanation has been found for the typical discrepancy between the parameters of localized states as determined from the static and dynamic hopping conductivities in tetrahedral amorphous semiconductors. It is shown for the example of *a*-GaSb that the Mott hopping length $R_{\rm opt}$, the correlation length for nonoptimal hops L_T, and the ac hopping length R_ω are related as $R_{\rm opt}<L_T<R_\omega$, as a result of which the Mott law holds for the dc conductivity and the Zvyagin regime of nonoptimal hops holds for the ac conductivity $\sigma(\omega)$. The observed value of $\sigma(\omega)$ is two orders of magnitude lower than the conductivity calculated by the Austin–Mott formula for the parameters of localized states found from dc measurements. A model that quantitatively describes the static and dynamic conductivity of *a*-GaSb with the aid of a single set of parameters characterizing the Miller–Abrahams resistor network is proposed. © *1997 American Institute of Physics.* [S0021-3640(97)00604-X]

PACS numbers: 72.80.Ey, 72.20.My, 72.20.Fr, 71.38.+i

1. A classical example of current transport along localized states in disordered-media physics is Mott-type hopping conduction. From the theoretical standpoint, this case has also been investigated in greatest detail and reduces to the problem of $R-\epsilon$ percolation on a Miller–Abrahams random network of resistors.[1,2] If a is the localization radius of the wave function, then for a constant density of states at the Fermi level $g(E_F)\approx$const, the resistivity is given by the formula[1]

$$\rho=\rho_0\,\exp[(T_0/T)^{1/4}],\quad T_0=17.6/g(E_F)a^3k_B. \tag{1}$$

The positive part of the magnetoresistance, due to the compression of the wave function in a magnetic field H, has the form[2]

$$\ln[\rho(H)/\rho(0)]=\frac{5}{2016}a^4H^2(T_0/T)^{3/4}/(c^2\hbar^2). \tag{2}$$

It follows from formulas (1) and (2) that by measuring simultaneously the temperature dependences of the conductivity and magnetoresistance it is possible to find independently the density of states and the localization radius.[3]

It is also known that for the Mott hopping conduction regime the real part σ' of the ac conductivity with frequency ω should be described by the Austin–Mott formula[4]

$$\sigma'(\omega)=\frac{\pi^4}{24}ae^2k_BTg(E_F)^2\omega R_\omega^4, \quad R_\omega=(a/2)\ln(\nu_{\rm ph}/\omega), \tag{3}$$

where $\nu_{\rm ph}$ and R_ω are the characteristic phonon frequency and hopping length, respectively. It is obvious that formula (3) yields independent information about the parameters of the localized states and together with Eqs. (1) and (2) it can also be used to calculate $g(E_F)$ and a.

It is found, however, that attempts of this kind for tetrahedral materials of the type *a*-Ge give densities of states which can differ by more than two orders of magnitude for the static (Eqs. (1) and (2)) and dynamic (Eq. (3)) measurements.[4,5] Moreover, in the experiments a weaker temperature dependence $\sigma'(\omega,T)$[5,6] than the Austin–Mott predictions is often observed.

This problem was posed more than ten years ago[4–6] and has still not been solved satisfactorily. In Refs. 5 and 6, a quite exotic way out of the situation was proposed based on an analysis of polaron hops, which, in the opinion of the authors of Refs. 5 and 6, determine $\sigma'(\omega,T)$ and can actually lead to a weaker temperature dependence. However, this approach cannot be combined with simultaneous observance of the Mott law (1). Therefore, as far as we know, it has still not been possible to describe the static and dynamic hopping conductivity on the basis of a single set of parameters. This casts doubt on the adequacy of the theoretical solutions (1)–(3).

The objective of this work was to investigate experimentally the problem of matching the static and dynamic characteristics. To this end, we studied the temperature dependences of the conductivity and magnetoresistivity $\rho(T,H)$ and the dielectric losses $\sigma'(\omega,T)$ in the region of hopping conductivity with a variable hopping length.

2. As the object of investigation we chose bulk samples of amorphous gallium antimonide, *a*-GaSb, synthesized by the method of thermobaric quenching under high-pressure conditions.[7] It is well known[3] that *a*-GaSb is a convenient object for studying hopping conductivity with a variable hopping length. Figure 1 displays data on $\rho(T)$ and $\rho(H,T=4.2\ \text{K})$. One can see that Mott's law holds for $T<100$ K, and at liquid-helium temperatures there exists an extended section of asymptotic behavior $\ln\rho\propto H^2$. In weak fields a small negative magnetoresistivity due to quantum interference effects is observed.[8,3] A calculation on the basis of Eqs. (1) and (2) gives $g(E_F)=4.2\cdot10^{20}$ cm^{-3}/eV and $a=46$ Å, which agree with the results of Ref. 3.

The measurements of the temperature dependences of the real and imaginary parts of the dynamic conductivity, $\sigma'(\omega,T)$ and $\sigma''(\omega,T)$, respectively, were performed for frequencies $\nu=\omega/2\pi=1-500$ MHz on the same *a*-GaSb samples (Fig. 2). For this, the reflection coefficient of a coaxial line with a characteristic impedance of 50 Ω loaded on the sample was recorded with the aid of an NR-4191 A impedance meter. The sample was placed inside an ampul in a helium cryostat, whose temperature could be varied and

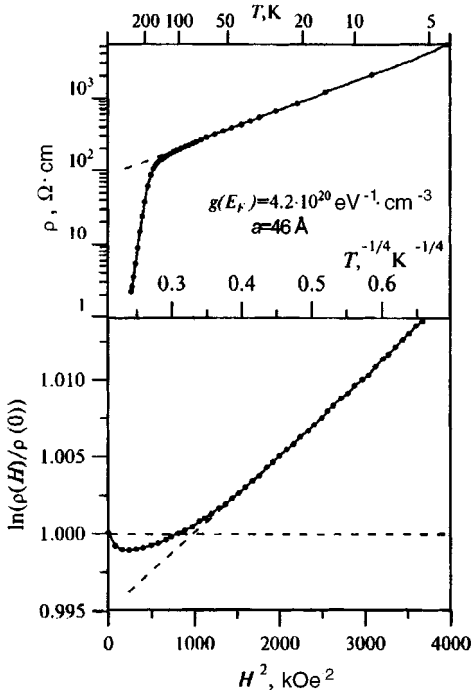

FIG. 1. Temperature dependence of the resistivity and field dependence of the magnetoresistivity at $T=4.2$ K which were used to determine the parameters of localized states in the *a*-GaSb sample.

stabilized in the range 4.2–300 K. The parasitic contribution from the line could be eliminated both by both the built-in compensation system of the impedance meter and by performing calibration measurements of the short-circuited and open-circuit line for each frequency–temperature point. A recording system based on a personal computer made it possible to introduce a correction automatically and to convert the modulus of the reflection coefficient and phase of the signal into the real and imaginary parts of the dynamic conductivity of the sample. The data on $\sigma(\omega,T)$ for disordered media are ordinarily represented in the asymptotically exact form[1,4–6,9]

$$\sigma(\omega,T)\propto T^{\alpha}\omega^{s}. \tag{4}$$

In the Austin–Mott case $\alpha=1$ and $s=1-4/\ln(\nu_{\rm ph}/\omega)$. It follows from Fig. 2 that for *a*-GaSb at $T=300$ K the exponent $s=0.91-0.94$ and in the hopping conduction region it decreases to $s\approx 0.8-0.7$ ($T=77$ K) and $s\approx 0.76-0.64$ ($T=4.2$ K). We note that in our case the relation $\sigma''=\sigma'\tan(\pi s/2)$ (Refs. 1–5) which follows from the Kramers–Krönig relation for power-law dependences, holds to within 5–10%. This agreement is entirely satisfactory, considering the approximate character of formula (4). It is interesting that the empirical value of the exponent α in the hopping conduction region is $\alpha\approx 0.3$ (see inset in Fig. 2), which is substantially different from the theoretical value $\alpha=1$. There-

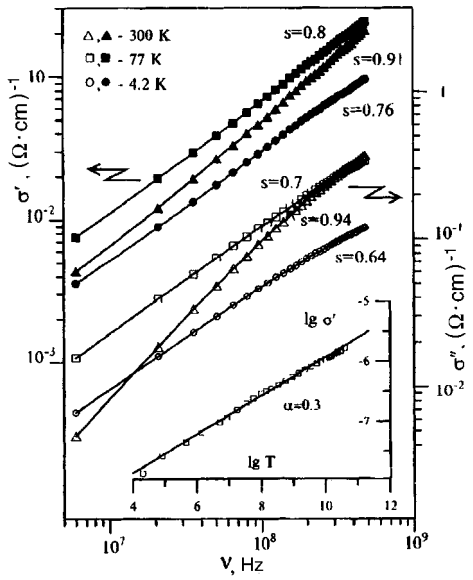

FIG. 2. Real and imaginary parts of the high-frequency conductivity at different temperatures for the *a*-GaSb sample.

fore, just as in the case of *a*-Ge,[6] the temperature dependence of the high-frequency hopping conductivity is found to be weaker than the prediction (3).

Comparing the results in Figs. 1 and 2 with the published data,[4–6,9] it can be concluded that the case of *a*-GaSb is typical for a sample with Mott-type hopping conductivity, and the discrepancy between the static and dynamic data which is described in Sec. 1 is present. Let us compare the experimental data for the static $\sigma'(\omega=0,T)\equiv\rho(T)^{-1}$ and dynamic $\sigma'(\omega,T)$ conductivity at the frequency $\nu=100$ MHz with the results of a model calculation using the Austin–Mott formula with the parameters $g(E_F)$ and a determined from the static measurements and the phonon frequency $\nu_{\rm ph}\sim(4-5)\cdot 10^{13}$ s^{-1}, chosen so as to obtain agreement with the observed exponents s (see Fig. 3, curves *1–3*, respectively). One can see that although $\sigma'(\omega,T)$ is 75–20 times greater for $T<100$ K than the static conductivity (Fig. 3, curves *1* and *2*), it still does not increase as strongly as it should according to Eq. (3), and the discrepancy between the theoretical and experimental values is two orders of magnitude and much larger than the error arising as a result of the experimental error in determining $g(E_F)$ and a.

3. Let us now analyze the possible reasons for the discrepancy between the static and dynamic data. One can imagine *a priori* a situation when the dc conductivity is due to electrons and the ac losses are due to polarons which make a weak contribution to the static conductivity. In this case, it is natural to expect densities of state and localization radii which are in no way related with the results of static measurements and which determine $\sigma'(\omega,T)$ for polaron hops. In addition, according to Ref. 6 the temperature dependence of the high-frequency conductivity could turn out to be weaker. However, the

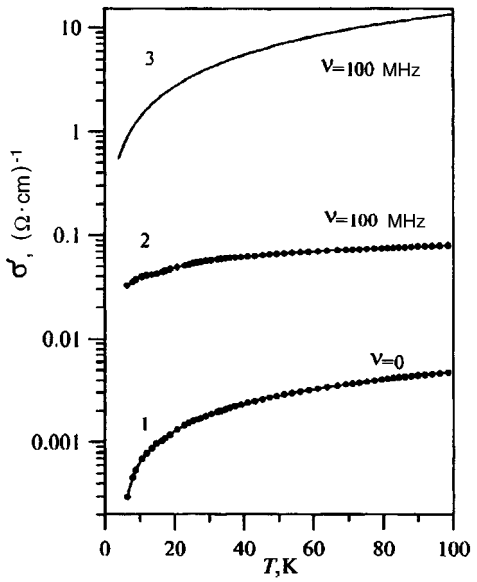

FIG. 3. Comparison of the static (*1*) and dynamic (*2*) hopping conductivity with the calculation according to the Austin–Mott formula (*3*) for the experimental parameters of the localized states (Fig. 1).

data in Ref. 3 practically rule out such an interpretation. Indeed, if polarons do not contribute to dc transport because of their stronger localization, the electrons will contribute to both the static and dynamic conductivity, and the value of $\sigma'(\omega,T)$estimated from the Austin–Mott formula for the experimental parameters of the Miller–Abrahams resistance network (Fig. 3, curve *3*) is much greater than the hypothetical polaron contribution, which should be compared with the experimental data (Fig. 3, curve *2*). Therefore the real problem is not the use of an additional polaron contribution, but rather explaining the fact that the electrons participating in the hops give a value of $\sigma'(\omega,T)$ which is less than expected on the basis of Eq. (3).

In our opinion, a consistent interpretation of the data in Figs. 1–3 can be achieved in a model based on an analysis of nonoptimal hops.[10] According to Ref. 10, at finite temperatures there exists a coherence length L_T of the phase of the wave function that is determined by an inelastic interaction with phonons. As a result, it is incorrect to study the envelope of the wave function $\Psi(R)\propto\exp(-R/a)$ of a localized center at distances $R>L_T$, and the parameter L_T plays the role of the limiting hopping length.[10] Therefore the observation of the Mott law (1) is possible only if $R_{\rm opt}<L_T$, where $R_{\rm opt}=(a/2)\times(T_0/T)^{1/4}$ is the dc hopping length. Using the simplest estimate for $L_T=(g(E_F)k_BT)^{-1/3}$,[10] it is easy to show that for *a*-GaSb in the region 4.2 K $<T<$100 K the characteristic spatial scales fall within the limits 190 Å $>L_T>$65 Å and 130 Å $>R_{\rm opt}>$60 Å, i.e., the condition $R_{\rm opt}<L_T$ holds for $T<$100 K. However, for the dynamic conductivity the hopping length will be $R_\omega=(a/2)\ln(\nu_{\rm ph}/\omega)=(a/2)\times(4/(1-s))\approx$300 Å, and the relation $R_{\rm opt}<L_T<R_\omega$ holds in the case at hand, i.e., the Mott regime is realized for dc hops and a nonoptimal hopping regime obtains for ac hops.

Since $\sigma'(\omega,T)$ increases with the hopping length (Eq. (3)), cutting R_ω off at L_T should appreciably decrease the conductivity compared with the Austin–Mott result, as is in fact observed experimentally (Fig. 3).

Let us now make a quantitative estimate. Following Ref. 9, we write the expression for $\sigma'(\omega,T)$ in the form

$$\sigma' = \left\langle \frac{e^2R^2}{12k_BT} \cosh^{-2}\left(\frac{\Delta}{2k_BT}\right) \frac{\omega\tau}{1+(\omega\tau)^2}\,\omega \right\rangle \approx \left\langle \frac{e^2R^2}{12k_BT} \right\rangle \left\langle \cosh^{-2}\left(\frac{\Delta}{2k_BT}\right) \right\rangle \left\langle \frac{\omega\tau}{1+(\omega\tau)^2} \right\rangle \omega. \tag{5}$$

In this formula it is assumed that in the suboptimal hopping regime, in contrast to the Austin–Mott case, there is no correlation between the dipole moment eR and the Debye factor and these quantities must be averaged independently. Then, to within a numerical factor, the Debye factor is proportional to the number of centers for which $\omega\tau \sim 1$:[9]

$$\langle \omega\tau/(1+(\omega\tau)^2) \rangle \approx \frac{\pi}{4} a^3 \ln^2 \frac{\nu_{\rm ph}}{\omega} g(E_F) k_B T,$$

and the factor accounting for the energy variance of the levels of the centers between which hops occur is estimated in the standard manner to be $\langle \cosh^{-2}(\Delta/2k_BT) \rangle \approx 2g(E_F)k_BT$. For nonoptimal hops $\langle R^2 \rangle = L_T^2$ and the characteristic phonon frequency equals $\nu_{\rm ph} = k_BT/\hbar$.[10] Then

$$\sigma' = \frac{\pi}{24} e^2 L_T^2 g(E_F)^2 k_B T a^3 \omega \ln^2 \frac{k_BT}{\hbar\omega} = \frac{\pi}{24} e^2 \hbar D^* g(E_F)^2 a^3 \omega \ln^2 \frac{k_BT}{\hbar\omega}. \tag{6}$$

In deriving Eq. (6) we took account of the fact that for the nonoptimal hopping regime L_T is given more accurately by the formula $L_T = \sqrt{D^*/\nu_{\rm ph}} \equiv \sqrt{\hbar D^*/k_BT}$, where D^* is the effective diffusion coefficient.[10] It follows from Eq. (6) that the exponents α and s in Eq. (4) are related by the relation $\alpha + s \approx 1$, which holds fairly well for *a*-GaSb (Fig. 2). Moreover, it follows from the explicit expression for $s = 1 - 2/\ln(k_BT/\hbar\omega)$ that in the nonoptimal hopping regime this exponent will decrease with temperature, as is in fact observed experimentally (Fig.2).

The expression for $\sigma'(\omega,T)$ contains one unknown parameter D^*, which can be found by comparing the relation (6) and the experimental data (Fig. 4). One can see that Eq. (6) approximates well both the temperature and frequency dependences of σ for $D^* = 4.9$ cm^2/s. Apparently, it is quite difficult to calculate D^* from first principles,[10] but an independent estimate can be proposed. If $T^* \approx 100$ K corresponds to the start of the section of hopping conductivity (Fig. 1), then the condition $R_{\rm opt} \approx L_T = \sqrt{\hbar D^*/k_BT}$ should hold at this temperature,[10] whence follows the value $D^* = 5$ cm^2/s, which is virtually identical to the estimate based on Eq. (6).

In summary we have shown that the idea of nonoptimal hops makes it possible not only to interpret qualitatively the reason for the discrepancy between the static and dynamic data but also to describe quantitatively the static and dynamic conductivity on the basis of a single set of parameters for localized states. This result can be regarded as independent evidence in support of the possibility of realizing a nonoptimal hopping regime in experimental systems, since the very early attempts to interpret the data for the dc hopping conductivity on the basis of the indicated ideas[11] turned out to be ambiguous,

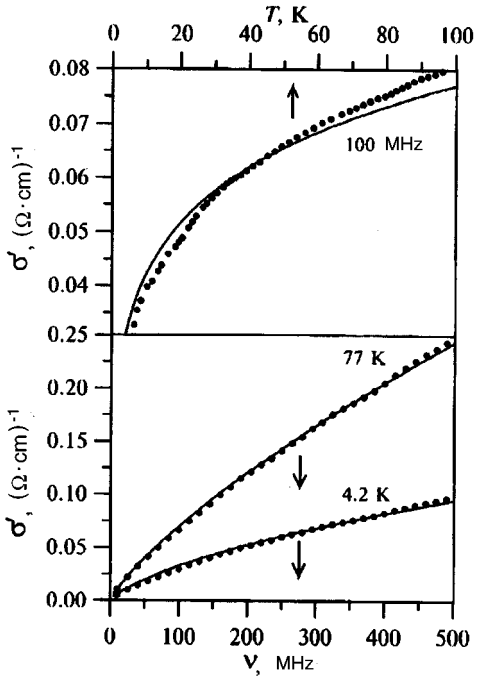

FIG. 4. Comparison of the experimental frequency and temperature dependences of the dynamic hopping conductivity with the model of nonoptimal hops for the experimental values of $g(E_F)$ and a (Fig. 1) and $D^* = 4.9$ cm^2/s.

since such behavior could be expected in a Coulomb-gap model. Since the Mott law is valid for *a*-GaSb, the Coulomb correlations are weak and apparently in the present work we were able to observe effects due to nonoptimal hops.

This work was performed as part of the Russian Fund for Fundamental Research, Project 95-02-03815a and INTAS, Project 94-4435.

[1] I. P. Zvyagin, *Kinetic Phenomena in Disordered Semiconductors* [in Russian], Moscow State University Press, Moscow (1984).
[2] B. I. Shklovskiĭ and A. L. Éfros, *Electronic Properties of Doped Semiconductors*, Springer-Verlag, New York. (1984).
[3] S. V. Demishev, D. G. Lunts, A. G. Lyapin*et al.*, Zh. Éksp. Teor. Fiz. **110,** 334 (1996) [JETP **83**, 180 (1996)].
[4] N. Mott and E. Davis, *Electronic Processes in Non-Crystalline Materials*, Oxford University Press, New York, 1979 [Russian translsation, Mir, Moscow (1982)].
[5] A. R. Long, Adv. Phys. **31**, 553 (1982).
[6] A. R. Long, N. Balkan, W. R. Hogg, and R. P. Ferrier, Philos. Mag. B **45**, 497 (1982).
[7] S. V. Demishev, Yu. V. Kosichkin, N. E. Sluchanko, and A. G. Lyapin, Usp. Fiz. Nauk **164,** 195 (1994).
[8] W. Schirmacher and R. Kempter, in *Hopping and Related Phenomena*, World Scientific, Singapore (1994), p. 31.
[9] S. R. Elliott, Adv. Phys. **36**, 135 (1987).
[10] I. P. Zvyagin, Phys. Status Solidi B **120**, 503 (1983).
[11] N. B. Brandt, S. V. Demishev, A. A. Dmitriev, and V. V. Moshchalkov, JETP Lett. **38**, 386 (1983).

Translated by M. E. Alferieff

Electronic superconductor $Pr_2CuO_{4-x}F_x$: Magnetic correlations at high temperatures ($150 < T < 600$ K) according to ^{19}F NMR data

E. F. Kukovitskiĭ and R. G. Mustafin[a)]

E. K. Zavoĭskiĭ Kazan Physicotechnical Institute, Kazan Science Center of the Russian Academy of Sciences, 420029 Kazan, Russia

(Submitted 5 January 1997)
Pis'ma Zh. Éksp. Teor. Fiz. **65**, No. 4, 328–332 (25 February 1997)

The longitudinal and transverse relaxation rates of ^{19}F nuclei in $Pr_2CuO_{4-x}F_x$ ($x=0.20$) samples are measured at high temperatures ($150\ \text{K} < T < 600\ \text{K}$). A feature is found in the temperature dependence of the relaxation rates at temperature $T' \cong 300$ K. The magnetic properties of the electronic superconductor $Pr_2CuO_{4-x}F_x$ as a possible system with a stripe ordering of carriers and spins are discussed.
 [S0021-3640(97)00704-4]

PACS numbers: 74.72.Jt, 74.25.Ha, 74.25.Nf

Magnetic correlations in high-T_c superconductors are attracting a great deal of attention as an explanation of the mechanism of superconductivity in metal oxides (see, for example, Ref. 1). High-T_c superconducting compounds with electronic-type conductivity[2] exhibit magnetic properties which are different from those of hole systems. For example, the magnetically ordered and superconducting states lie next one another in the phase diagram of electronic high-T_c compounds.[3] A unique magnetic phase transition in the CuO_2 plane has been discovered in the electronic superconductor $Pr_2CuO_{4-x}F_x$ at temperatures $T^* \cong 100$ K (followed by a transition at $T_c \cong 20$ K into the superconducting state).[4] For this reason, new information for understanding the behavior of magnetic correlations in high-T_c superconducting compounds could be obtained by performing measurements on electronic superconductors over a wider temperature range.

The present work is devoted to the study of magnetic correlations at high temperatures ($150\ \text{K} < T < 600\ \text{K}$) in the electronic superconductor $Pr_2CuO_{4-x}F_x$ by the method of NMR on ^{19}F nuclei. The temperature range of the present investigations is limited from below by the onset of the magnetic phase transition[4] at $T < 150$ K and from above by the onset of degradation, irreversible changes in the properties of the sample at temperatures $T > 600$ K. The NMR signals from the superconducting phase and impurity phases are easily distinguished,[4] which enabled us to study the magnetic properties of the superconducting phase of the samples.

The ceramic samples of $Pr_2CuO_{4-x}F_x$ ($x=0.20$) were prepared by the standard technology of three-phase synthesis and annealing (reduction) in an inert-gas medium.[4] The onset temperature of the superconducting transition $T_c = 27$ K was determined from measurements of the rf susceptibility of the samples. The NMR measurements on ^{19}F were performed on a Bruker CXP-100 pulsed spectrometer at frequency $f = 57$ MHz.

Measurements of the longitudinal relaxation rate T_1^{-1} of the fluorine nuclei were

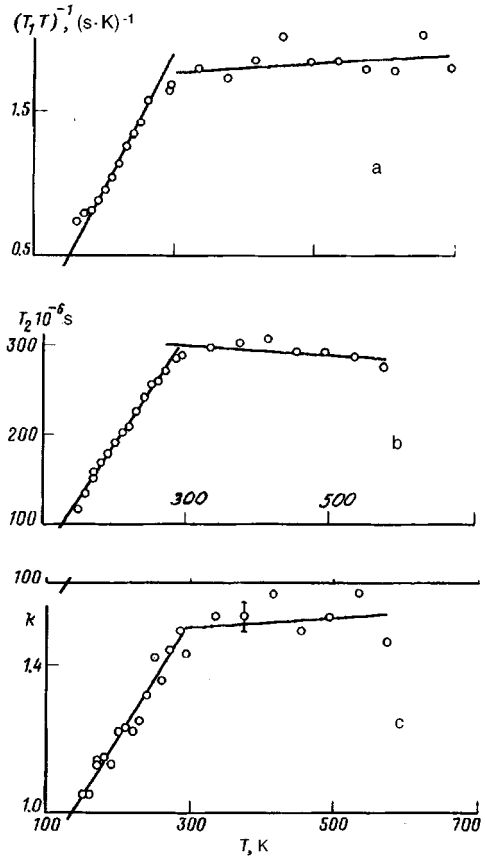

FIG. 1. Temperature dependences observed in the investigation of NMR on ^{19}F nuclei in the sample $Pr_2CuO_{3.8}F_{0.2}$: a) $(T_1T)^{-1}$, where T_1 is the longitudinal relaxation time; b) transverse relaxation time T_2; c) the quantities k are used to describe the decay of the echo amplitude $A(t)=A_0\exp\{-(2t/T_2)^k\}$in measurements of the transverse/relaxation time T_2. (The straight lines in the figures are drawn as visual aids).

performed according to the three-pulse stimulated-echo method (Fig. 1a).[b)] The magnetic moments of the van Vleck praseodymium ions Pr^{3+} do not make an appreciable contribution to the relaxation of the fluorine nuclei, and the magnetic system of the CuO_2 planes of the electronic superconductor makes the main contribution to the nuclear relaxation.[4] Fluorine, replacing oxygen in the structure of the electronic superconductors, mainly occupies the oxygen positions in the Pr_2O_2 planes and has four symmetrially arranged nearest-neighbor copper ions from the CuO_2 planes. This has the effect that the contribution of the antiferromagnetic (AF) fluctuations to the relaxation of the fluorine nuclei is small and the uniform susceptibility of the CuO_2 plane $\chi(0,\omega_n)$, where ω_n is the resonance frequency of the nuclei, makes the main contribution to the relaxation. For this reason, the quantity $(T_1T)^{-1}$ presented in Fig. 1a characterizes the behavior of the imaginary part of the uniform susceptibility of the electronic system of a CuO_2 plane: $(T_1T)^{-1}\sim\chi''(0,\omega_n)/\omega_n$ (see, for example, Ref. 5).

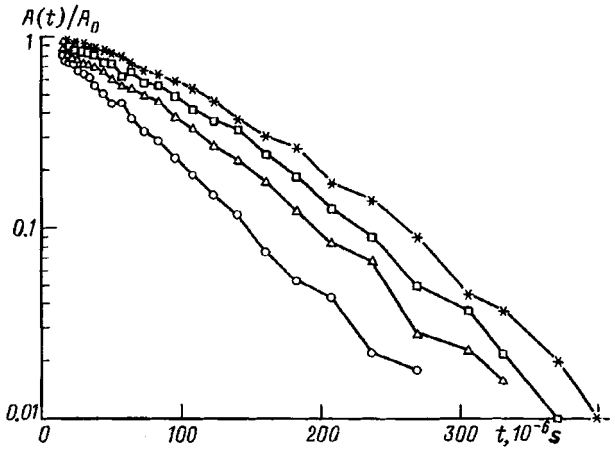

FIG. 2. The decay of the echo amplitude $A(t)$ observed in measurements of the T_2 transverse-relaxation time at temperatures $T=360$ K (asterisks), 240 K (squares), 200 K (triangles), and 160 K (circles).

In the case of measurements of the transverse relaxation time T_2 of the fluorine nuclei, the observed decay of the echo signal $A(t)$, where t is the delay between the two exciting pulses, changed with temperature (see Fig. 2). In the process, the decay of the echo amplitude was described quite well in the entire temperature interval by the function

$$A(t)=A_0 \ \exp\{-(2t/T_2)^k\}. \tag{1}$$

Not only the time T_2 (Fig. 1b) but also the quantity k changed with temperature (Fig. 1c). The transverse-relaxation rate is determined by two mechanisms: a direct dipole–dipole interaction of the nuclei with one another and an indirect interaction of the nuclei via the magnetic system of the CuO_2 plane. The contribution of the dipole–dipole interaction changes very little with temperature. The contribution of the indirect interaction is determined by the real part of the susceptibility of the CuO_2 plane $T_2^{-1}\sim\chi'(0,\omega_n)$ and is related with the magnetic correlation length ζ at zero wave vector as $T_2^{-1}\sim\zeta^2$ (Ref. 6).

The contribution of the indirect interaction of the copper nuclei via the magnetic subsystem of the CuO_2 plane is usually described by a Gaussian decay of the amplitude of a two-pulse echo: $A(t)\sim\exp\{-(t/T_{2g})^2\}$ (Ref. 6). This is connected with the characteristic features of the hyperfine interactions of copper ions in high-T_c superconducting compounds: For an external field H_0 oriented in a direction normal to the CuO_2 planes, the main interaction is the interaction of the longitudinal components of the nuclear spins and flip-flop processes are suppressed. This is what leads to the Gaussian decay of the echo amplitude. Conversely, when the external field is oriented parallel to the CuO_2 planes, the mainly transverse components of the nuclear spins of copper interact, and this results in the exponential decay of the echo signal $A(t)\sim\exp(-2t/T_2)$.

The fluorine ion F^- has the same outer electronic shell $2s^22p^6$ as the oxygen ion O^{2-}, and correspondingly the hyperfine constants of the fluorine and oxygen ions should be close. For this reason, the interactions of the longitudinal and transverse components of the nuclear spins are important for the fluorine nuclei (just as for the oxygen nuclei).

Correspondingly, in this case the decay of the echo amplitude should not be described simply by Gaussian or exponential laws. In Ref. 7 it is shown that for slow flip-flop processes $wt<1$, where w is the spin flip-flop rate, the decay of the amplitude of the first echo is described by expression (1) with $k \geqslant 1.5$. In addition, k should decrease as the rate of the flip-flop processes increases. For this reason, the decrease in k (approach to the exponential law $k=1$) means that the flip-flop processes grow (the growth of the interaction of the transverse components of the nuclear spins) at $T<300$ K (see Fig. 1c).

Examining the temperature dependences of the relaxation rates of the fluorine nuclei (Figs. 1a–c), two temperature ranges separated by a temperature $T' \cong 300$ K where the behavior of the relaxation rates is different can be distinguished. At temperatures $T>T'$ the quantities $(T_1T)^{-1}$, T_2 and k are virtually temperature-independent (see Figs. 1a–c). This means that at high temperatures ($T>T'$), the magnetic correlations in the electronic system of a CuO_2 plane have no effect on the uniform susceptibility $\chi''(0,\omega_n) \approx$ const, i.e., at these temperatures the ordinary Korringa mechanism of nuclear relaxation operates: $(T_1T)^{-1} \cong 1.7$ $(\text{s}\cdot\text{K})^{-1}$. The temperature-independent transverse-relaxation rate T_2^{-1} is determined at these temperatures probably by the dipole–dipole interaction of the fluorine nuclei.

Conversely, at temperatures $T<T'$ the quantity $(T_1T)^{-1}$ is observed to decrease with temperature; this indicates that the imaginary part $\chi''(0,\omega_n)$ of the uniform susceptibility decreases. The decrease in $\chi''(0,\omega_n)$ with decreasing temperature is ordinarily attributed to the appearance of a gap in the spin-excitation spectrum.[5] A kink in the temperature dependence of T_2 attests to the appearance of a new efficient channel at temperatures $T<T'$ for the interaction of fluorine nuclei with one another: indirect interaction via the electronic system of the CuO_2 plane. An increase in the indirect interaction of the fluorine nuclei results in a change in the manner in which the echo amplitude decays — a change in k.

Proceeding from the results of the measurements of the relaxation rates (Korringa slope) on the ^{63}Cu and ^{19}F nuclei in electronic superconductors, we shall estimate the value of the E hyperfine coupling constant of the ^{19}F nuclei with the electronic system of the CuO_2 plane. For the ^{63}Cu nuclei we have[8] $(^{63}T_1T)^{-1} \cong 6.8$ $(\text{s}\cdot\text{K})^{-1} = C(^{63}\gamma)^2(A^2+4B^2)$, where C is related with the susceptibility of the electronic system in the CuO_2 plane, γ is the gyromagnetic ratio of the corresponding nucleus, and A and B are the hyperfine constants of the copper nuclei, which we take to be equal to the corresponding constants of hole superconductors.[5] The Korringa slope for the fluorine nuclei at $T>T'$ equals $(^{19}T_1T)^{-1} \cong 1.7$ $(\text{s}\cdot\text{K})^{-1} = C(^{19}\gamma)^2 4E^2$. Having estimated C from the first formula, proceeding from the Korringa slope for the fluorine nuclei we find $E \cong 6.3$ kOe/μ_B.

We shall now list the main results of this work. At temperature $T' \cong 300$ K sharp changes are observed in the magnetic properties of the CuO_2 planes of the electronic superconductor $Pr_2CuO_{4-x}F_x$. At high temperatures $T>T'$ Korringa relaxation of the fluorine nuclei is observed: $(^{19}T_1T)^{-1} \cong 1.7$ $(\text{s}\cdot\text{K})^{-1}$. The coupling constant of the ^{19}F nuclei with the electronic system of the CuO_2 plane was determined from the Korringa slopes of the relaxation of the copper and fluorine nuclei: $E \cong 6.3$ kOe/μ_B. At temperature T' a kink is observed in the temperature dependences of the longitudinal and transverse relaxation rates of the fluorine nuclei. This is probably attributable to the appear-

ance at $T<T'$ of a gap in the spin-excitation spectrum of the electronic system of a CuO_2 plane and of a new effective channel for the interaction of fluorine nuclei with one another.

In conclusion, using the results of Ref. 4 and the present letter, we shall consider the electronic superconductor $Pr_2CuO_{4-x}F_x$ as a possible system with stripe ordering of the carriers and spins (similar to that observed in some high-T_c superconducting compounds[9]). The formation of stripe ordering of carriers and copper spins, which probably occurs in the electronic superconductor $Pr_2CuO_{4-x}F_x$ at $T'\cong 300$ K, means partial carrier localization (forbiddenness of carrier motion in a direction transverse to the bands). The gap arising at the Fermi surface in this case results in a lower value of $(T_1T)^{-1}$ (see Fig. 1a). The stripe domains of AF-ordered electronic magnetic moments of copper (lying between the carrier stripes) have quite sharp boundaries. A new interaction channel arises for the ^{19}F nuclei located at the boundaries of the domains: via the AF fluctuations of the electronic magnetic moments of copper. The actuation of the new interaction channel for ^{19}F nuclei appears in the form of a kink in the temperature dependences of the transverse-relaxation time T_2 (see Fig. 1b) and the value of k (see Fig. 1c). In Ref. 4 it was shown that a glass phase transition is observed in this compound at temperatures $T^*\cong 100$ K. It can be attributed to the sharp slowing down of the fluctuations (displacement of the entire system of stripes in a transverse direction) with decreasing temperature. The growth in the spectral component of the fluctuations at the resonance frequency of ^{19}F nuclei leads to an increase in the longitudinal relaxation rate T_1^{-1} (see Ref. 4). We note that a similar dynamics of the nonuniform carrier distribution has been well studied for quasi-one-dimensional conductors.[10]

We thank G. B. Teĭtel'baum for his interest in this work and helpful discussions.

[a)]e-mail: mustafin@dionis.kfti.kcn.ru

[b)]In Ref. 4 there is a misprint in a similar plot: The scale along the Y axis should be the same as the scale of the plot in Fig. 1a in the present letter.

[1] T. Moriya and K. Uede, J. Phys. Soc. Jpn. **63**, 1871 (1994); P. Monthoux and D. Pines, Phys. Rev. B **49**, 4261 (1994).
[2] A. C. W. P. James, S. M. Zahurak, and D. W. Murphy, Nature **338**, 240 (1989); A. Krol, Y. L. Soo, Z. H. Ming *et al.*, Phys. Rev. B **46**, 443 (1992).
[3] G. M. Luke, L. P. Le, B. J. Sternlieb *et al.*, Phys. Rev. B **42**, 7981 (1990).
[4] E. F. Kukovitskiĭ, R. G. Mustafin, and G. B. Teĭtel'baum, JETP Lett. **57**, 739 (1993).
[5] A. J. Millis, H. Monien, and D. Pines, Phys. Rev. B **42**, 167 (1991); M. Takigava, A. P. Reyes, P. C. Hammel *et al.*, Phys. Rev. B **43**, 247 (1991).
[6] C. H. Pennington and C. P. Slichter, Phys. Rev. Lett. **66**, 381 (1991).
[7] A. D. Milov, K. M. Salikhov, and Yu. D. Tsvetkov, Zh. Éksp. Teor. Fiz. **63,** 2329 (1972) [Sov. Phys. JETP **36**, 1229 (1973)].
[8] K. Kumagai, M. Abe, and S. Tanaka, Physica B **165–166**, 1297 (1990).
[9] J. M. Tranquada, B. J. Sternlieb, J. D. Axe *et al.*, Nature **375**, 561 (1995); A. Bianconi, M. Missori, N. L. Saini *et al.*, J. Supercond. **8**, 545 (1995); O. N. Bakharev, M. V. Eremin, and M. A. Teplov, JETP Lett. **61**, 515 (1995).
[10] L. Gor'kov and G. Gruner [Eds.], *Charge Density Waves in Solids*, Elsevier Science, Amsterdam (1989).

Translated by M. E. Alferieff

Metal–insulator transition in amorphous $Si_{1-c}Mn_c$ obtained by ion implantation

A. I. Yakimov[a] and A. V. Dvurechenskiĭ
Institute of Physics, Siberian Branch of the Russian Academy of Sciences, 630090 Novosibirsk, Russia

(Submitted 6 January 1997)
Pis'ma Zh. Éksp. Teor. Fiz. **65**, No. 4, 333–337 (25 February 1997)

A metal–insulator transition (MIT) induced by a change in the impurity Mn concentration in a material with topological disorder — amorphous $Si_{1-c}Mn_c$ — is investigated. It is found that near the critical point the localization radius, permittivity, and conductivity vary according to a power law in accordance with the scaling theory of localization. The critical exponents are determined. It is concluded that the basic mechanisms of the MIT in disordered systems do not depend on the type of disorder and are universal. © *1997 American Institute of Physics.* [S0021-3640(97)00804-9]

PACS numbers: 71.23.Cq, 71.30.+h

The metal–insulator transition (MIT) is related with the shift in the Fermi level from the region of distributed electronic states of the main or impurity band into the region of localized states or into the band gap. Two types of MITs are distinguished: the Mott transition, stimulated by intracenter electron-electron interaction, and the Anderson transition, caused by carrier localization at the Fermi level under the influence of a disordering factor. In practice it is often found that in real systems the main features of both types of transitions are combined in the MIT, since interaction and localization effects are present simultaneously.[1] For this reason more detailed investigations, both theoretical and experimental, are required.

The central problem in the theory of the MIT is the behavior of the main physical characteristics of the system near the critical point. The zero-temperature conductivity $\sigma(0)$ is such a characteristic on the metal side. The models currently under development (one-[2] and two-parameter[3] scaling theories of localization, method of extrapolation of quantum corrections into the critical region[4]) describe the behavior of the conductivity near the MIT by a power-law function

$$\sigma(0)=\sigma_M(c/c_{\rm cr}-1)^{\nu_\sigma}, \tag{1}$$

where c is the impurity density, $c_{\rm cr}$ is the impurity density at which the transition occurs, ν_σ is the critical exponent of the conductivity, and

$$\sigma_M=0.03e^2c_{\rm cr}^{1/3}/h \tag{2}$$

is the so-called minimum metallic conductivity. The question of the value of the critical exponent and its universality has not been completely solved. Scaling theory predicts $\nu_\sigma=1$. This value corresponds to the experimental data for most disordered systems, though in uncompensated semiconductors $\nu_\sigma=1/2$ is often observed (see the review Ref.

5 and citations there). The state of the system in the insulator phase of the MIT (for $c<c_{cr}$) is characterized by the carrier localization radius ξ_{loc} and the static permittivity ϵ. According to the scaling theory of localization, the continuous variation of the conductivity near the MIT is related with the power-law divergence of the characteristic length, responsible for the presence of a critical region, $\xi=\xi_0(c/c_{cr}-1)^{-\nu_\xi}$ via the relation $\sigma(0)=Ge^2/h\xi$, where G is a constant. This means that $\nu_\sigma=\nu_\xi$. For $c<c_{cr}$ the parameter ξ_{loc} plays the role of a critical length. Therefore $\xi_{loc}=\xi_0(1-c/c_{cr})^{-\nu_\xi}$. The application of the renormalization-group method[6] to the description of the behavior of the impurity component of the permittivity $\epsilon_i-\epsilon-\epsilon_0$, where ϵ_0 is the permittivity of the matrix, likewise leads to the analogous formula $\epsilon_i=\epsilon^*(1-c/c_{cr})^{-\nu_\epsilon}$. Here[7]

$$\nu_\epsilon=2\nu_\xi=2\nu_\sigma. \tag{3}$$

Most experimental works on this subject are devoted to the study of strongly doped crystalline semiconductors in which disorder is compositional and is associated with randomly distributed charged impurities.[1] In amorphous materials a metallic state can be formed only by introducing metal impurities up to a concentration comparable to that of the matrix atoms. Nonetheless, in this case the disorder is of the topological type, and the magnitude of the random potential is virtually independent of the impurity composition and is determined by the absence of long-range order in the arrangement of the core atoms as a result of the distortion of the bond lengths, valence angles, and dihedral angle. The experimental data on the behavior of amorphous materials near a MIT, being less abundant, refer only to the dependences $\sigma(0,c)$.[1] There are virtually no investigations of the evolution of the localization radius and permittivity in systems with topological disorder. This makes it difficult to check the main scaling relations. As a rule, amorphous mixtures are obtained by melting together silicon or germanium and a doping metal. The drawback of this procedure is the possibility that metallic clusters will form, which can introduce the classical ''two-phase mixture'' effect, which is studied with the aid of a continuous theory of percolation and masks the real Anderson or Mott transition. The ion-implantation method makes it possible to introduce impurities one by one, varying precisely the carrier density near the MIT and avoiding the formation of metallic inclusions.[8,9]

The objective of the present work was to investigate the MIT in the amorphous $Si_{1-c}Mn_c$ obtained by implantation of manganese ions and to determine the entire set of critical exponents.

Implantation was performed either in layers of amorphous silicon predeposited on quartz substrates or in a crystalline silicon film on sapphire with simultaneous amorphization of the films. Sapphire substrates with a high thermal conductivity must be used in the case of high irradiation doses (impurity concentration $c\geqslant 15$ at.%) to prevent heating of the layers during bombardment. The ion current density was equal to 0.5–5 μA/cm^2 and the irradiation dose was equal to 10^{16}–10^{17} cm^{-2}. A uniform distribution of the impurity over the thickness of the *a*-Si layers (0.2–0.3 μm) was achieved by varying the ion energy in the range 20–300 keV. The method for preparing the samples and the structural and electrical properties of the samples are described in detail in Refs. 10 and 11.

1. The permittivity was determined on the basis of measurements of the low-frequency capacitance of Ni/*a*-$Si_{1-c}Mn_c$/Al structures according to a parallel substitution

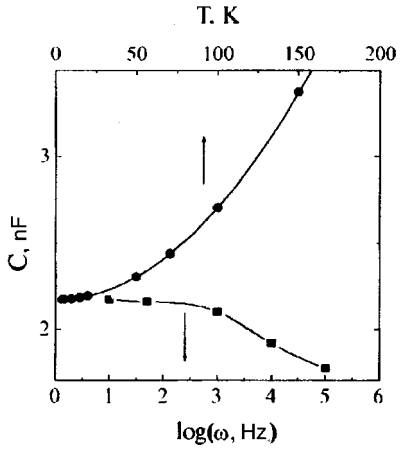

FIG. 1. Capacitance of the structure Ni/a-$Si_{1-c}Mn_c$/Al ($c=7$ at.%) versus the measurement temperature and voltage frequency.

scheme. A 20 nm thick layer of nickel, serving as the bottom plate of a capacitor, was deposited on a quartz substrate immediately prior to the deposition of a-Si. The measurements of the resistance of the Ni layer after irradiation with manganese showed that ion bombardment does not result in a loss of conducting properties of the layer. The area of the top contact (Al) was equal to $1.3\cdot 10^{-2}$ cm^2. Figure 1 shows the temperature and frequency dependences of the capacitance of such a structure ($c=7$ at.%). The value of ϵ can be determined by extrapolating the curves $C(T)$ and $C(\omega)$ to zero values of T and ω. For an undoped a-Si film, this procedure gives $\epsilon_0=11.7\pm 0.4$, which agrees well with the existing data for the dielectric constant of silicon, 11.4.[12]

2. In Refs. 10 and 11 it was discovered that in the Mn concentration range $c<13$ at.% the low-temperature dependence of the conductivity $\sigma(T)$ in a-$Si_{1-c}Mn_c$ layers on quartz is described by the exponential expression $\sigma(T)=\sigma_0\exp[-(T_0/T)^{1/2}]$. This behavior is due to hopping transport along localized states of a parabolic Coulomb gap.[8] In this case

$$T_0=\beta e^2/k\epsilon\xi_{\rm loc}, \tag{4}$$

where k is Boltzmann's constant, β is a numerical parameter, taking on the value 1.4 in the presence of Hubbard correlations in the impurity band[9] (such correlations are present in a-$Si_{1-c}Mn_c$ (Ref. 13)). Using $\epsilon(c)$ and the values of $T_0(c)$ found in Ref. 10, the dependence $\xi_{\rm loc}(c)$ can be determined.

3. An investigation of the conductivity in structures with Mn concentration $c\geqslant 14$ at.%[14] showed that in the temperature range 20–200 K the temperature dependence $\sigma(T)$ is described by the power-law function $\sigma(T)=\sigma(0)+aT^{1/2}+bT$, where the first temperature-dependent term is the result of electron-electron interaction and the second one is a quantum correction to the conductivity due to weak localization. The quantity $\sigma(0)$ can be determined by extrapolating these data to zero temperature.

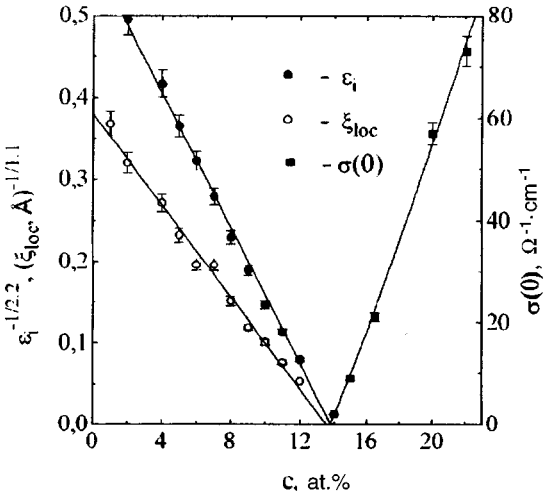

FIG. 2. localization radius $\xi_{\rm loc}$, impurity part of the permittivity ϵ_i, and the conductivity at zero temperature $\sigma(0)$ versus the Mn concentration. The solid lines were obtained by approximating the experimental data by power-law functions (see text). The metal–insulator transition point is $c_{\rm cr} \approx 13.7$ at.%.

The function $\sigma(0,c)$ is shown in Fig. 2. Approximating the experimental points by formula (1) by fitting the three parameters σ_M, $c_{\rm cr}$, and ν_σ gives the values $\sigma_M = 129 \pm 8$ S/cm, $c_{\rm cr} = 13.7 \pm 0.1$ at.%, and $\nu_\sigma = 1.1 \pm 0.1$ (solid line). The minimum metallic conductivity can be estimated independently according to Eq. (2). We obtain $\sigma_M \approx 120$ S/cm. An independent estimate of the critical concentration $c_{\rm cr}$ can be made with the aid of Mott's criterion,[1] which holds well for amorphous materials:[15] $c_{\rm cr}^{1/3} a_H = 0.26$, where a_H is the empirical atomic radius of the impurity. Taking for Mn $a_H = 0.14$ nm,[16] we obtain $c_{\rm cr} \cong 13$ at.%. The closeness of the values of σ_M and $c_{\rm cr}$, predicted theoretically and obtained as a result of the fit, indicates the correctness of the three-parameter approximation procedure.

A similar approximation of the data on $\epsilon_i(c)$ and $\xi_{\rm loc}(c)$, found with the aid of the procedures described in Secs. 1 and 2, gave the following values: $\epsilon^* = 3.3 \pm 0.1$, $c_{\rm cr} = 13.7 \pm 0.1$ at.%, $\nu_\epsilon = 2.2 \pm 0.1$, $\xi_0 = 2.9 \pm 0.5$ Å, $c_{\rm cr} = 13.6 \pm 0.2$ at.%, and $\nu_\xi = 1.1 \pm 0.1$. Figure 2 displays the experimental curves $\epsilon_i^{-1/2.2}(c)$ and $\xi_{\rm loc}^{-1/1.1}(c)$. One can see that the plots of the permittivity and localization radius do indeed rectify well in the chosen coordinates (the solid lines were obtained by a fitting procedure). The fact that the values of the critical concentration determined for three different characteristics of the system and both phases of the MIT are equal to one another attests to the adequacy of the description of the behavior of the localization radius, permittivity, and conductivity in amorphous silicon by analogy to second-order phase transitions in the form of power-law functions of the type (1) of the closeness to the critical point. Furthermore, it is easy to see that the relation (3) between the critical exponents does indeed hold with good accuracy. Therefore the main features of the metal–insulator transition do not depend on the type of disorder in the system and are universal.

This work was supported by the International Association INTAS (Grant 94-4435).

[a)]e-mail: yakimov@isp.nsc.ru

[1] N. F. Mott, *Metal–Insulator Transitions*, Taylor and Francis, London (1990).
[2] E. Abrahams, P. W. Anderson, D. C. Licciardello, and T. V. Ramakrishnan, Phys. Rev. Lett. **42**, 673 (1979).
[3] W. L. McMillan, Phys. Rev. B **24**, 2739 (1981).
[4] N. F. Mott and M. Kaveh, J. Phys. C: Solid State Phys. **15**, L45 (1982).
[5] G. A. Thomas, Philos. Mag. B **52**, 479 (1985).
[6] C. Castellani, C. Di Castro, P. A. Lee, and M. Ma, Phys. Rev. B **30**, 527 (1984).
[7] P. A. Lee and T. V. Ramakrishnan, Rev. Mod. Phys. **57**, 287 (1985).
[8] A. L. Efros and B. I. Shklovskii, J. Phys. C: Solid State Phys. **8**, L49 (1975).
[9] J. H. Davies, J. Phys. C: Solid State Phys. **17**, 3031 (1984).
[10] A. V. Dvurechenskii, V. A. Dravin, and A. I. Yakimov, Phys. Status Solidi A **113**, 519 (1989).
[11] A. V. Dvurechenskiĭ and A. I. Yakimov, Zh. Eksp. Teor. Fiz. **95**, 159 (1989) [Sov. Phys. JETP **68**, 91 (1989)].
[12] H. Hess, K. De Kondo, T. F. Rosenbaum, and G. A. Thomas, Phys. Rev. B **25**, 5578 (1982).
[13] J. C. Slater, *Quantum Theory of Molecules and Solid*, McGraw-Hill, New York (1965), Vol. 2, p. 103.
[14] A. I. Yakimov, A. V. Dvurechenskii, C. J. Adkins, and V. A. Dravin, J. Phys., Condens. Matter. **9**, 499 (1997).
[15] K. Morigaki, Philos. Mag. B **42**, 979 (1980).
[16] A. V. Dvurechenskiĭ, V. A. Dravin, and A. I. Yakimov, Fiz. Tverd. Tela (Leningrad) **30**. 401 (1988) [Sov. Phys. Solid State **30**, 228 (1988)].

Translated by M. E. Alferieff

Investigation of the intrinsic conductivity of Al–Cu–Fe quasicrystals in a zero-gap semiconductor model

A. F. Prekul, A. B. Rol'shchikov, and N. I. Shchegolikhina
Institute of Metal Physics, Russian Academy of Sciences, 620219 Etaterinburg, Russia

(Submitted 8 January 1997)
Pis'ma Zh. Éksp. Teor. Fiz. **65**, No. 4, 338–340 (25 February 1997)

Experimental proofs are obtained for the fact that the intrinsic conductivity of quasicrystals at low temperatures satisfies the $T^{3/2}$ law.
 [S0021-3640(97)00904-3]

PACS numbers: 75.50.Kj, 72.15.Eb

As a result of the exceptionally high sensitivity of the resistive properties of quasicrystals to composition fluctuations, quench conditions, and subsequent heat treatment, the question of what are properties of the quasicrystalline phase itself has been under discussion for several years.[1]

Specifically, the ''semiconductor hypothesis'' of the electronic band structure of quasicrystals has recently been elaborated. Components similar to the intrinsic conductivity of semiconductors due to thermal activation of carriers from the valence band into the conduction band have been discovered in the temperature dependences of the electrical conductivity $\sigma(T)$ of stable aluminum-based quasicrystals.[2,3] In addition, it has been found that in the system Al–Pd–Re the conventional form

$$\sigma(T)=A\ \exp(-E_g/2k_BT), \tag{1}$$

where E_g is the energy gap parameter, k_B is Boltzmann's constant, and $A=$ const, is adequate, signifying that the carrier mobility in the conduction band varies with temperature as $T^{-3/2}$.[4]

The system Al–Cu–Fe behaved differently. The measurements in Ref. 3 showed that in the low-temperature region ($T<300\ K$) the gap, if it is present, is small.[5] Then the simple power law

$$\sigma_{\text{int}}(T)=AT^{3/2} \tag{2}$$

is an adequate approximation. The use of a semiconductor model shows that if the component of the form (2) is the intrinsic conductivity of the quasicrystal, it must remain constant or a weakly-varying part compared with the total conductivity of the system. As is well known, the latter can vary over wide limits on account of the extrinsic conductivity.

We studied the conductivity of five samples of an alloy with the nominal composition $Al_{62}Cu_{25.5}Fe_{12.5}$, whose residual resistivity $\rho_{4.2}$ varies from 3500 to 6300 $\mu\Omega\cdot$cm. All samples have approximately the same dimensions $1\times1\times10$ mm. The resistivity is measured by the standard four-probe method. The accuracy of the measurements is 10^{-5}, and the stability of the temperature at all points in the range 4.2–300 K is not

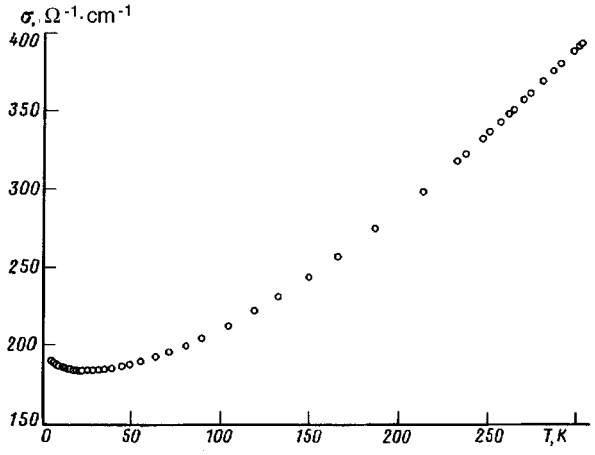

FIG. 1. Temperature dependence of the conductivity of an Al–Cu–Fe quasicrystal.

worse than 10^{-1} K. Graphical illustrations are given for one sample with $\rho_{4.2}=5500$ $\mu\Omega\cdot$cm. A numerical comparison of the results of the analysis is used to draw a general conclusion.

The results of a direct experiment in the form of the temperature dependence $\sigma(T)$ are displayed in Fig. 1. They are typical for the experimental material and differ by the presence of finite conductivity at the lowest temperatures and a minimum at $T\simeq 20$ K. In terms of the semiconductor model, both features are related with the conductivity σ_{ext} of the extrinsic carriers.

Figure 2 displays the results of applying Eq. (2) taking account of the component σ_{ext} in the simplest form of an arbitrary temperature-independent quantity σ_*. This is the only adjustable parameter in linearizing the experiment in the coordinates

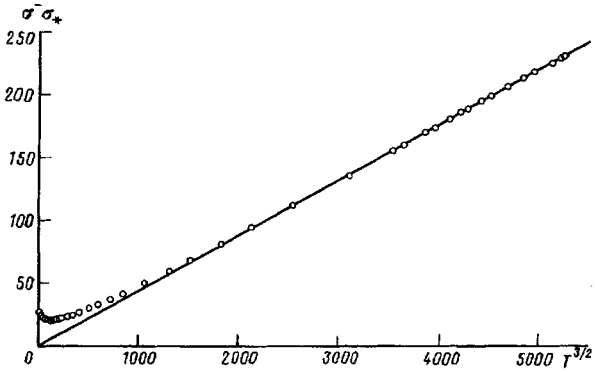

FIG. 2. Description of the temperature dependence of the conductivity by the $T^{3/2}$ law with the extrinsic conductivity of the quasicrystal approximated by a constant σ_*.

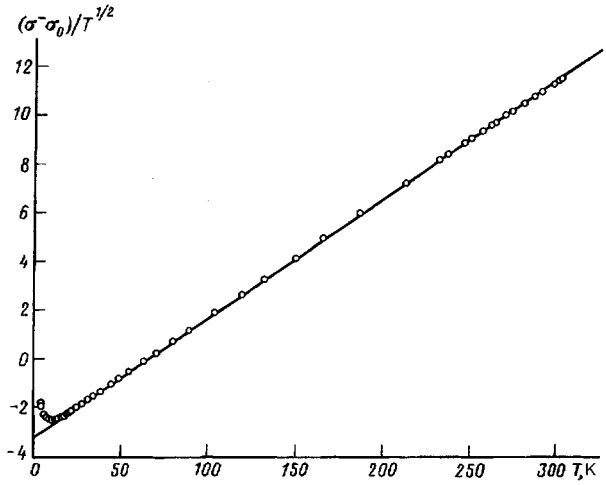

FIG. 3. Description of the temperature dependence of the conductivity by the $T^{3/2}$ law taking account of the extrinsic conductivity of the quasicrystal in the form $\sigma_{\text{ext}}=\sigma_0-BT^{1/2}$.

$[\sigma(T)-\sigma_*]$ versus $T^{3/2}$. Linearity is achieved without any special difficulty. The temperature interval of linearity 100–300 K agrees well with the previously determined interval 80–250 K. This indicates that the zero-gap approximation is indeed a good approximation.

At the same time it is easy to see that the linearity is limited from below by the roughness of the approximation of the extrinsic conductivity as a temperature-independent quantity. We made use of the indications of many investigations of the fact that ''radical'' corrections due to the electron-electron interaction are important in the conductivity of quasicrystals at low temperatures.[6] The existence of a minimum in the curves $\sigma(T)$ suggests an extrinsic conductivity of the form

$$\sigma_{\text{ext}}=\sigma_0-BT^{1/2}, \tag{3}$$

and a total conductivity of the form

$$\sigma(T)=AT^{3/2}+\sigma_0-BT^{1/2}. \tag{4}$$

The possibility of describing an experiment by expression (4) can be conveniently judged in the coordinates $[\sigma(T)-\sigma_0]/T^{1/2}$ versus T. The only adjustable parameter here is σ_0 — the residual conductivity of a system at absolute zero temperature. The final result in Fig. 3 shows that virtually ideal linearity is achieved in the interval 15–300 K.

The general picture of the behavior of the conductivity, shown in Fig. 1–3 for one sample, also holds for all other samples in the range of values of $\rho_{4.2}$ which we studied. It remains to compare the coefficients A in the $T^{3/2}$ law. The maximum value of this coefficient is 0.06, the minimum value is 0.046, and the average value is $A=0.053\pm 13\%$. The variance is obviously less than the difference in the value of σ_0, which on the average equals $224.5\pm 30\%$. Here it is necessary to take account of the fact

that if the variance of σ_0 is determined with the same accuracy as are the geometric dimensions of the samples, which we estimate to be $\pm 5\%$, then the inaccurate knowledge of the temperature dependence of the extrinsic conductivity and possible changes in the basic parameters of the charge carriers, effective mass and mobility, contribute to the variance of the coefficient A, so that the real variance of A apparently does not exceed $\pm 5\%$.

On this basis, our results can be regarded as an experimental proof of the fact that the intrinsic conductivity of quasicrystals in the system Al–Cu–Fe at low temperatures follows the $T^{3/2}$ law.

This work was supported by the Russian Fund for Fundamental Research (Project 96-02-19586).

[1] C. Janot, Phys. Rev. **1**, 81 (1996).
[2] D. N. Basov, F. S. Pierce, P. Volkov *et al.*, Phys. Rev. Lett. **73**, 1865 (1994).
[3] A. F. Prekul, L. V. Nomerovannaya, N. I. Shchegolikhina *et al.*, Fiz. Met. Metalloved. **82**, 5 (1996).
[4] F. J. Blatt, *Theory of Mobility of Electrons in Solids*, Academic Press, New York, 1957.
[5] I. M. Tsidil'kovskiĭ, *Gapless Semiconductors: A New Class of Materials*, VCH Publishers (1988) [Russian original, Nauka, Moscow (1986)].
[6] S. J. Poon, Adv. Phys. **41**, 303 (1992).

Translated by M. E. Alferieff

Effect of magnetic field on the sound velocity of a dilute Kramers-ion glass at low temperature

A. V. Lazuta
St. Petersburg Nuclear Physics Institute, Gatchina, 188350 St. Petersburg, Russia

(Submitted 5 November 1996, resubmitted 10 January 1997)
Pis'ma Zh. Éksp. Teor. Fiz. **65**, No. 4, 341–346 (25 February 1997)

Recent results on the effect of magnetic field on the sound velocity V in aluminosilicate glasses doped with dysprosium are analyzed on the basis of a minimal model for the ground state of Dy^{3+} (Kramers ion with $J=15/2$) described by a wave function $\varphi_{\pm}=\varphi_{\pm J_m}+\eta\varphi_{\pm 1/2}$. The first term represents a state with a large **J** projection on the local crystal field axis and the random parameter η ($\langle\eta\rangle=0$, $\langle\eta^2\rangle\ll 1$) introduces a small admixture of the state $\varphi_{\pm 1/2}$ into the ground state. The relative variation of V due to the resonance interaction of sound waves with this state split by H is determined as a function of H and T. It possesses a universal asymptotic behavior. Our results are in reasonable agreement with the experiment. A possible structure of the crystal fields that can induce this state is discussed [S0021-3640(97)01004-9]

PACS numbers: 75.50.Kj

INTRODUCTION

Acoustic wave propagation, photon echoes, nonlinear magnetic susceptibility, and spin echoes of Kramers-ion-doped (Dy, Gd, Eu) aluminosilicate glasses have recently been studied[1,2] at low T. An effect of magnetic field on the sound velocity V in Dy-doped glasses is one of the typical and important results. Measurements have been performed at $T=10$ mK–6 K, $\nu=100$ MHz, and H up to 50 kG on samples with ion concentrations $n=1.5$–10.0 at. %. Magnetic field was found to modify substantially the temperature variation of V. This did not occur in the glass doped with Ho (a non-Kramers ion).

The interpretation was based on combining the results of the theory of elastic tunneling states (ETS) in glasses and the known properties of Kramers ions with a large spin in amorphous material with a random axis of anisotropy ($\mathscr{H}=-DJ_z^2$, where z is the direction of the local axis of anisotropy, $J=15/2$, $D\simeq 120$ K for Dy^{3+}). The low-temperature properties of these glasses in a magnetic field are determined by the magnetic ions whose axis of anisotropy is almost perpendicular to the local field (magnetic tunneling states (MTS)).[3] Some of these properties are similar to those of the ETS. However the ETS are characterized by two random parameters (potential asymmetry and tunnel integral), whereas the MTS are described by one parameter (the angle between a local axis and a local field). They may show a similar behavior only when there is a single relevant parameter (the energy). A linear T dependence of the specific heat is an example.

In the general case there is no such simple correspondence in behavior of the ETS

and the MTS. The relaxation processes were assumed to give $\Delta V \propto \ln (T/T_0)$ for the MTS, just as for the ETS. This answer arises as a result of averaging a specific expression, describing the interaction of sound waves and the ETS, over two random parameters with a very particular distribution function.[4] Therefore there are no grounds to expect that the MTS relaxation contribution to ΔV can be represented as a product of their density of states and $\ln (T/T_0)$. The second explanation exploits the results of the ETS relaxation by electrons. It requires the existence of fast MTS. But, as the authors pointed out, the relevant relaxation processes are entirely obscure. Furthermore, this assumption seems not to be confirmed experimentally, because a minimum spin–lattice relaxation time $T_1 \simeq 20$ μs was found for Dy magnetic moments in a glass doped with 0.1 at. % Dy at $T=14$ mK,[2] whereas the shortest relaxation time was found to be $\tau_{\min} < 1$ μs for the ETS in a glass with 1.5 at. % Dy at the same T.[1]

Our purpose is to suggest a new explanation for the influence of H on V.

MODEL

The single-ion approximation is used because the effect is proportional to n and exists in a large H (larger than dipolar or exchange interactions). The traditional model mentioned above cannot explain the effect. It leads to extremely weak spin–phonon interaction which depends strongly on H.[3] As a result, the resonance processes cannot be responsible for the smooth H dependence of V observed in Ref. 1. The contribution of the relaxation processes to V is most likely suppressed by virtue of the inequality $\omega T_1 \gg 1$. Available experimental data are consistent with this assumption. There are no other data on T_1 for Kramers ions in insulating glasses besides those mentioned above. A value $T_1 \simeq 10$ μs was found for Ho^{3+} (10 at. %) in the same glass at 3.5 K.[5] Since T_1 is usually shorter for non-Kramers ions ($J=8$ for Ho^{3+}) than for Kramers ions, both these results allow the assumption that for Dy ions $\omega T_1 \gg 1$ at $\nu = 100$ MHz and $T < 3.5$ K.

Let us consider effects of non-axial electric field gradients. The most general model with a quadrupolar Hamiltonian $\mathscr{H} = \alpha J_x^2 + \beta J_y^2 + \gamma J_z^2$ (α, β, and γ are randomly distributed) has been found to be nearly equivalent to the simple model ($\mathscr{H} = -DJ_z^2$) when J is large.[6] Therefore, it is unlikely that a specific Hamiltonian such as $\mathscr{H} = -DJ_z^2 - KJ_x^2$ with fixed $D > K$, which was suggested in Ref. 2, is realized for the Dy^{3+} ion in the aluminosilicate glasses.

Since in vitreous matrices there is no clear information available on the local crystal field acting on a rare-earth ion, we use a simple minimal model for the Dy^{3+} ground state (GS). We shall assume that the GS is described by a wave function $\varphi_{\pm} = \varphi_{\pm J_m} + \eta \varphi_{\pm 1/2}$. The main term $\varphi_{\pm J_m}$ represents the state with a large projection of $\mathbf{J}$ ($\pm J_m$) on the direction of the local axis of anisotropy, i.e., ions occupy sites with a predominant axial component in the crystal field. The random parameter η ($\langle \eta \rangle = 0$, $\langle \eta^2 \rangle \ll 1$) introduces a small admixture of the state $\varphi_{\pm 1/2}$ into the GS. This contribution results from non-axial distortions. Note that the assumption of a slightly and randomly distorted axial symmetry is supported by the spectroscopic data.[5] In a field H, lifting the degeneracy of the GS, the second term is responsible for transitions between two split levels which are produced by phonons in the first order in the spin–phonon interaction due to the change in the g factor with strain. As a result, the effect of H on V

is not suppressed, unlike the situation where $\eta=0$. This H effect does not occur in the glass doped with non-Kramers ions, because electrostatic non-axial distortions lift the degeneracy of the GS which can exist in the case of axial symmetry.

The terms of the form $\varepsilon_n\varphi_{\pm J_n}(3/2\leqslant J_n\leqslant 15/2,\ \varepsilon_n$ are random parameters), which may occur in the GS are unimportant if $\langle\varepsilon_n\rangle=0$ and $\langle\varepsilon_n^2\rangle \ll 1$, since, when **H** is parallel to the local axis, the corresponding splitting is small, $2g\mu J_n\langle\varepsilon_n^2\rangle H\ll 2g\mu J_m H$, if **H** is directed perpendicular to the axis and these terms do not generate a splitting $\propto H$ and do not influence the resonant coupling of a sound wave with the GS.

The effect of the ligandfields is described by the Hamiltonian $\mathscr{H}=\Sigma B_n^m O_n^m$, where O_n^m are spin operators.[7] We assume that the axial part of $\mathscr{H}$ is well defined, i.e., the standard deviations of the $B_n^0(n=2, 4, 6)$ are small in comparison with their mean values. The non-axial coefficients vary considerably and have negligibly small mean values. This part of $\mathscr{H}$ is a weak disturbance. These assumptions are consistent with Ref. 8, where crystal fields were investigated numerically for a random close-packed sphere model in a single-element material. It gives an example of the typical glass local field with the dominant terms of an axial symmetry.

Using the matrix elements of O_n^0 from Ref. 7, it can be found that the axial part generates a GS with a large J_m ($\geqslant 11/2$ for definiteness) over a rather wide region of B_n^0 variations.

Let us consider some important examples. A crystal field of the form $O_4^0+B_6^0O_6^0$ leads to a GS with $J_m=13/2$ when $B_6^0>5/3$. The $B_2^0O_2^0$ term does not change it if $0\geqslant B_2^0>-(26/3+13/3B_6^0)$. The small trigonal components $\eta B_6^6O_6^6$ and $\varepsilon_n B_n^3O_n^3$ $(n=4, 6)$ (reference to this local symmetry can be found in Ref. 5) admix the state $\eta\varphi_{\pm 1/2}$ to the GS and give unessential terms $\varepsilon_n\varphi_{\pm 7/2}$. For $J_m=11/2$ the needed admixture can be generated by a term $O_6^5\propto\{J_+^5J_z+J_zJ_-^5\}_s$. This typical glass term was found to be the dominant non-axial component in the model of Ref. 8. If the O_6^6 term is also important the admixture is characterized by two random parameters: $\eta_1\varphi_{1/2}+\eta_2\varphi_{-1/2}$. In this case V exhibits a stronger T dependence (see below). Finally, for $J_m=15/2$ the component $\varphi_{\pm 1/2}$ comes to the GS in the second order of perturbation theory (typically in the form $\eta_1\eta_2\varphi_{\pm 1/2}$). For this admixture the function $V(T,H)$ is very similar to that of the one-parameter case.

In order to use a minimal number of free parameters, the coefficients B_n^m of the non-axial distortions were assumed above to be real quantities. It means that a local environment of the ion possesses a symmetry plane containing the local axis.

$V,(T,H)$ for the GS in Eq. (1). The splitting, which depends on the angle ϑ between the local axis and **H**, is given by

$$\Delta E(\vartheta,\eta)=2g\mu Hf(\vartheta,\eta), f(\vartheta,\eta)=(p_\parallel^2(\eta)\cos^2\vartheta+p_\perp^2(\eta)\sin^2\vartheta)^{1/2}, \tag{1}$$

$$p_\parallel(\eta)=(J_m+1/2\,\eta^2)(1+\eta^2)^{-1}, p_\perp(\eta)=(J+1/2)\,\eta^2(2(1+\eta^2))^{-1}. \tag{2}$$

The interaction of a sound wave with the ions due to the change of g factor with strain can be written[9]

$$H' = \frac{1}{2} g\mu \sum_{i,k} t_{ik}(H_i J_k + H_k J_i), t_{ik} = \sum_{l,m} F_{iklm} e_{lm},$$

where $\hat{F}$ is the spin–phonon coupling tensor, $\hat{e}$ is the strain tensor, and $e_{lm} = (V_l V_m / V^2) e_0$ (e_0 is the strain amplitude) for the longitudinal waves used in Ref. (1). It is expected that in glasses there will be no relations among the components of $\hat{F}$ imposed by the local symmetry and that they can be treated as random variables independent of the orientation of the anisotropy axis.[3] To calculate transitions between the states (1) split by H we chose a coordinate system with $\mathbf{H} \| \hat{z}$, in which the transition operator is $t_{zx} J_x + t_{zy} J_y$. For the local axis in the (z,x) plane, we have $|\langle \psi_1 | J_x | \psi_2 \rangle| = p_\| p_\perp / f \equiv w_\|$ and $|\langle \psi_1 | J_y | \psi_2 \rangle| = p_\perp$ ($\psi_{1,2}$ are the wave functions of the states).[7] Integrating the transition probability, obtained for arbitrary orientation of the axis, over the angle φ in the (x,y) plane at fixed ϑ yields an expression proportional to $(w_\|^2 + p_\perp^2)(t_{zx}^2 + t_{zy}^2)/2$. Averaging over the distribution of F_{iklm} leads to an effective dimensionless spin–phonon coupling constant $\lambda^2 = \langle t_{zx}^2 + t_{zy}^2 \rangle / (2e_0^2)$. It may depend markedly on the mutual orientation of **H** and **V**.

Using the expression[10] for the variation of V induced by resonant interaction of a sound wave with a two-level system at small ω and averaging it over ϑ as well as the η distribution, we finally get

$$\delta V(T,H) = \frac{\Delta V}{V} = -\lambda^2 \frac{n}{\rho V^2} \int_0^{\pi/2} \sin\vartheta \, d\vartheta \int P(\eta) d\eta \, \frac{M^2(\vartheta,\eta)}{2\Delta E(\vartheta,\eta)} \times \left(1 - 2 \frac{e^{-\beta \Delta E(\vartheta,\eta)}}{1 + e^{-\beta \Delta E(\vartheta,\eta)}} \right), \tag{3}$$

$$M^2(\vartheta,\eta) = (g\mu H)^2 (w_\|^2(\vartheta,\eta) + p_\perp^2(\eta)), \quad w_\|(\vartheta,\eta) = p_\|(\eta) p_\perp(\eta) (f(\vartheta,\eta))^{-1}, \tag{4}$$

where ρ is the bulk density and $P(\eta)$ is the distribution function. These expressions give δV for a two-level system with a specific form of the splitting and the transition probability M^2 between levels determined by two random parameters.

To determine the low-T variation of δV for $\Delta E_0 / T \gg 1$ ($\Delta E_0 = 2g\mu H J_m$ is the splitting at $\vartheta = \eta = 0$) it is convenient to write $\delta V(T,H) = \delta V_0(H) + \delta \tilde{V}(T,H)$, where the part $\delta V_0 \propto -H$ is given by the first term of Eq. (3) and the second part leads to positive T dependence of δV.

We assume that $\langle \eta^2 \rangle \ll 1$. Hence, one can set $p_\| \approx J_m$ and $p_\perp(\eta) \approx (J + 1/2)\eta^2/2$ (see Eq. (3)). Then in the new variables $\cos\vartheta = r\cos\phi$, $\eta^2 = (2J_m/(J+1/2)) r \sin\phi$, we get $\Delta E(r,\phi) = r\Delta E_0 \{1 - ((1/2) r \sin 2\phi)^2\}^{1/2}$. The principal contribution to the integral over r in Eq. (3) comes from $r \sim T/\Delta E_0$ when $\Delta E_0 / T \gg 1$. One can therefore keep only the terms of the lowest order in r in the exponential ($\Delta E \approx r\Delta E_0$) and pre-exponential ($M \approx g\mu H w_\| \approx g\mu H J_m \sin\phi$) factors. The distribution $P(\eta)$ is assumed to be a function of one parameter: $\tilde{P}(\eta/a) a^{-1}$, where a is the scale of the η distribution and $a^2 \ll 1$ corresponds to small uniaxial distortions. Since $\eta/a = (r \sin\phi)^{1/2}/a_0$ ($a_0 = a((J$

$+1/2)/2J_m)^{1/2}$), there are two regimes of $\delta\tilde{V}$ behavior. If $\Delta E_0 a_0^2/T \gg 1$, one can set $P(\eta) \approx P(0)$ in evaluating the integral over r, since $(\eta/a)^2 = r \sin\phi/a_0^2 \leqslant T/\Delta E_0 a_0^2 \ll 1$ for $r \sim T/\Delta E_0$. As a result,

$$\delta\tilde{V}(T,H) = C\lambda^2 \frac{n}{\rho V^2} \frac{P(0)}{[(J+1/2)/2J_m]^{1/2}} (T\Delta E_0)^{1/2},$$
$$C = \frac{1}{4}\int_0^\infty \frac{dx}{x^{1/2}} \frac{e^{-x}}{1+e^{-x}} \int_0^{\pi/2} (\sin\phi)^{3/2} d\phi \simeq 0.23. \tag{5}$$

A dependence $\Delta\tilde{V} \propto (TH)^{1/2}$ arises from the part of the ions determined by $P(0)$, for which $\Delta E \sim T$. If the low-spin component of the GS as the form $\eta_1\eta_2\varphi_{\pm 1/2}$ a similar method gives the former result, whereas for $\eta_1\varphi_{1/2} + \eta_2\varphi_{-1/2}$, one finds $\delta\tilde{V} \propto T$ because the second random parameter introduces a new degree of freedom into the GS.

In regime $\Delta E_0/T \gg 1$ but $\Delta E_0 a_0^2/T \ll 1$ a similar procedure gives $\delta\tilde{V}(H) = (\lambda^2/8\rho V^2)\Delta E_0$. Here $\delta\tilde{V} \propto H$ is determined by the ions whose ΔE is much less than T, and $\delta\tilde{V}$ becomes independent of T. From Eqs. (8) and (9) one can see that the T dependence of $\delta\tilde{V}$ exhibits crossover at $T \sim \Delta E_0 a_0^2$. In the limiting cases $\delta\tilde{V}$ shows universal behavior which is sensitive to the form of $P(\eta)$ in the crossover region only.

COMPARISON WITH EXPERIMENTAL DATA

Since $V(T)$ was measured relative to reference point $T_0 \simeq 30$ mK, the T-independent background $\delta V_0(H)$ in Eq. (3) is assumed to be unimportant, and we take $\delta V(T,H) = \delta\tilde{V}(T,H)$ at $T \geqslant T_0$. The effect of H on V is given by the difference between experimental values: $\delta V_{ex}(T,H) - \delta V_{ex}(T,0) = \delta\tilde{V}(T,H)$. We compare our results with the measured variation of V in 10 at. % dysprosium doped glass. An extremely simple steplike $P(\eta)$ $(P(\eta) = (1/2)a,\ -a \leqslant \eta \leqslant a)$ and $J_m = 13/2$ (for definiteness) are used. It is seen from Fig. 1 that the T dependence of $\delta\tilde{V}(T,H)$ at $H = 30$ kG and 50 kG are in a reasonable agreement with the data. The magnitudes of λ and a can be easily obtained because λ^2/a is the only unknown factor in the coefficient in the initial variation of $\delta V \propto T^{1/2}$ (0.1 K $\leqslant T \leqslant$ 1 K) and the parameter a determines the crossover temperature to the behavior $\delta\tilde{V} \propto H$. As a result, using the ion value $g = 4/3$, we find $a \approx 0.3$, $\langle\eta^2\rangle = (1/3)a^2 \approx 0.03$, and $\lambda \approx 20$. The small $\langle\eta^2\rangle$ is the essential evidence in favor of the model. A rough estimate of λ is $e^2 Z\langle r^2\rangle/R^3\Delta$ (Ref. 9); $Z = 3$ is the ion charge, r is ion radius, R is the ion–ligand distance, and Δ is the energy of the first excited level of Dy^{3+}. Taking the O–Si distance as $R = 1.6$ Å and using $\Delta = 3400$ cm^{-1} and $r = 0.95$ Å, we find $\lambda \sim 5$, which is not far from $\lambda \approx 20$.

In the crossover region the calculated T variation of $\delta\tilde{V}$ deviates somewhat from the experiment. Since this region is sensitive to changes in $P(\eta)$, agreement can be improved by testing various $P(\eta)$ distributions.

Note that this two-level system possesses a wide distribution of one-phonon spin–lattice relaxation times. At fixed ΔE, T_1 varies from $T_{1\,\min}$ to infinity. In particular, we find $T_{1\,\min} \sim 10$ μs at $H = 50$ kG for ions with $\Delta E \approx T \approx 1$ K.

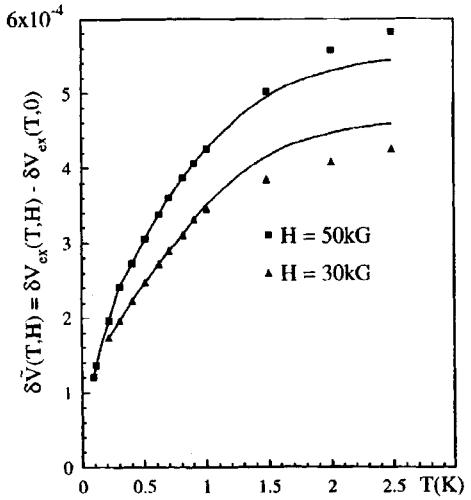

FIG. 1. Relative velocity variation of acoustic waves as a function of T in magnetic fields of 30 kG and 50 kG in an aluminosilicate glass containing 10.1 at. % Dy. The points are experimental data.[1] The solid curves show a fit of the results by Eqs. (5) and (7).

At $H \leqslant 10$ kG, the $\delta\widetilde{V}(T)$ dependence deviates from the expression for isolated ions; this can be attributed to dipolar or exchange interactions between them.

We did not try to explain the change of $V(T)$ behavior for $H=0$ which occurs when nonmagnetic rare-earth La ions are replaced by magnetic ions in this glass. This effect has been attributed to the magnetic degrees of freedom.[1] The difference of ionic radii seems to be also or even more important.[11] According to the traditional arguments concerning the structure of glasses, ions with equal charges are expected to substitute isostructurally only if they have nearly the same ionic radii. Since the ionic radius of La^{3+} is 1.216 Å, whereas, for example, it is 0.95 Å for Dy^{3+}, glasses doped with these ions may possess different microstructure, including essential variations in their ETS parameters and, as a result, show different $T(V)$ behavior.

The author thanks Professor F. Shwabl for a discussion and Professor G. Belessa for some remarks.

[1] N. Vernier and G. Belessa, Europhys. Lett. **14**, 249 (1991); Phys. Rev. B **48**, 12842 (1993).
[2] N. Vernier, G. Belessa, and D. A. Parshin, Phys. Rev. Lett. **74**, 3459 (1995).
[3] I. Ya. Korenblit and E. F. Shender, Zh. Éksp. Teor. Fiz. **75**, 1862 (1978) [Sov. Phys. JETP **48**, 937 (1978)].
[4] P. Doussineau, P. Frencois, R. G. Leisure, *et al.*, J. Phys. (Paris) **41**, 1193 (1980).
[5] N. Bontemps and J. C. Rivol, J. Phys. C **15**, 1301 (1982).
[6] A. Fert and I. A. Campbell, J. Phys. F **8**, L57 (1978).
[7] A. Abragam and B. Bleaney, *EPR of Transition Ions*, Oxford: Clarendon, 1970.
[8] M. I. Darby and G. R. Evans Phys. Status Solidi B **85**, K63 (1978).
[9] S. A. Al'tshuler and B. M. Kozyrev, EPR, Halsted Press, Wiley, 1975.
[10] H. Koizumi, T. Suzuki, K. Kimura, and S. Takeuchi J. Phys. Soc. Jpn. **60**, 1173 (1991).
[11] J. T. Kohli and J. E. Shelby Phys. Chem. Glasses **32**, 67 (1991).

Published in English in the original Russian journal. Edited by Steve Torstveit.

Resistance of superconductor–normal-metal–superconductor (SNS) junctions

F. Zhou and B. Spivak
Physics Department, University of Washington, Seattle, WA 98195, USA

(Submitted 13 January 1997; resubmitted 31 January 1997)
Pis'ma Zh. Éksp. Teor. Fiz. **65**, No. 4, 347–352 (25 February 1997)

It is shown that the conductance of a superconductor–normal-metal–superconductor (SNS) junction can exhibit a significant dependence on the phase of the superconducting order parameter in the situation where the size of the normal region of the junction is much larger than the normal-metal coherence length, so that the critical current of the junction is exponentially small. The period of the conductance oscillations as a function of the phase can be equal to π or 2π, depending on the parameters of the system. © *1997 American Institute of Physics.* [S0021-3640(97)01104-3]

PACS numbers: 05.20.−y, 82.20.−w

The critical current of a superconductor–normal-metal–superconductor (SNS) junction $I_c = I_{c0}\exp(-L/L_T)$ decays exponentially and can be neglected when $L \gg L_T$ (see, for example, Ref. 1). Here L is the length of the normal-metal region of the junction shown in Fig. 1, $L_T = \sqrt{D/T}$ is the coherence length in the normal metal, T is the temperature, $D = lv_F^2/3$ is the electron diffusion coefficient, v_F is the Fermi velocity, and l is the electron elastic mean free path. On the other hand, the χ-dependent part of the conductance $\delta G(\chi)$ of the SNS junction can survive even in the case $L_T \ll L \ll L_{\rm in}$. Here $\chi = \chi_1 - \chi_2$, where $\chi_{1,2}$ are the phases of the order parameters in the superconductors of the junction, and $L_{\rm in} = \sqrt{D\tau_{\rm in}}$ and $\tau_{\rm in}$ are the inelastic diffusion length and inelastic mean free time, respectively. The χ dependence of δG originates from the fact that the amplitude of the Andreev reflection of an electron into a hole at the superconductor–normal-metal (SN) boundary acquires an additional phase factor $\exp(i\chi_{1,2})$, while the amplitude of the reflection of a hole into an electron acquires a phase factor $\exp(-i\chi_{1,2})$. The weak-localization contribution $\delta G_1(\chi)$ to $\delta G(\chi)$ was analyzed long ago.[2] It arises in the first-order approximation in the parameter $\hbar/p_F l \ll 1$ and is due to the interference of electrons traveling clockwise and counterclockwise along diffusive paths with closed loops which contain Andreev reflections. Here p_F is the Fermi momentum. The value of δG_1 is insensitive to the ratio of L to L_T, and the characteristic energy interval which gives the main contribution to δG_1 is $\epsilon \sim T$. The period of $\delta G_1(\chi)$ as a function of χ is π (Ref. 2).

In this paper we consider two other contributions to δG, viz., δG_2 and δG_3, and show that the period of the oscillations of δG as a function of χ can be either π or 2π depending on the parameters of the system and the way in which the conductance is measured. The contribution δG_2 can be associated with the spatial coherence between electrons and holes arising due to Andreev reflection from the SN boundary.[3] It arises in

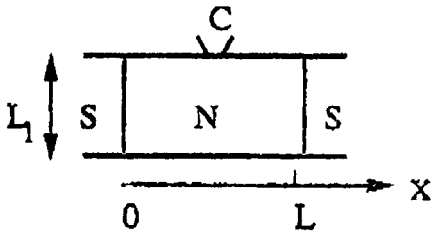

FIG. 1.

the zeroth-order approximation in the parameter $\hbar/p_F l \ll 1$. The contribution from this mechanism to the resistance of an SN junction was considered in Refs. 4–11. It has been pointed out[10] that the electron–hole coherence in the metal extends over a distance of order $L_\epsilon = \sqrt{D/\epsilon}$. Therefore, it is clear that the main contribution to δG_2 comes from the relatively small energy interval $\epsilon \sim E_c = D/L^2 \ll T$, and for $L_T \ll L \ll L_{\text{in}}$, the correction δG_2 decreases with L only as L^{-2}. The period of $\delta G_2(\chi)$ as a function of χ is 2π. The sum $\delta G_1 + \delta G_2$ gives the main contribution to δG, provided that the voltage drop V between the two superconductors of the junction is zero, so that χ does not change with time. In this case $\delta G(\chi)$ can be measured with the help of an additional lead ''C'' shown in Fig. 1, while the phase difference χ across the junction can be determined by means of an additional Josephson junction. In the case where the resistance of the SNS junction is measured by applying a voltage V between the superconductors, there is a third contribution, δG_3, to δG. The origin of δG_3 is similar to the Debye relaxation mechanism of microwave absorption in dielectrics. In this case, due to the Josephson relation, χ and, hence, the quasiparticle density of states in the metal $\nu(\epsilon,x)$ are functions of time. In other words, at small V the quasiparticle energy levels move slowly. The electron populations of the energy levels follow adiabatically the motion of the levels themselves, and, as a result, the electron distribution becomes nonequilibrium. Relaxation of the nonequilibrium distribution due to inelastic processes leads to entropy production, to the absorption of energy from the external field, and therefore contributes to δG.

We start with the calculation of δG_2. In the zeroth-order approximation in the parameter $\hbar/p_F l$ the most adequate theoretical description of the system is provided in the framework of the Keldysh Green's function technique elaborated for superconductivity in Refs. 12–14. In the diffusive approximation and in the absence of electron–electron interaction in the normal-metal region of the junction, the linear response to the external electric field is described by the following set of equations:

$$j_n = eD\nu_0 \int_{-\infty}^{+\infty} \cosh^2\theta_2(\epsilon,x)\,\partial_x f_1(\epsilon,x)\,d\epsilon, \tag{1}$$

$$\frac{D}{2}\partial_x^2\theta(\epsilon,x) + \left(i\epsilon - \frac{1}{\tau_{\text{in}}}\right)\sin\theta(\epsilon,x) - \frac{1}{2}(\partial_x\chi(\epsilon,x))^2 \sin 2\theta(\epsilon,x) = 0,$$

$$\partial_x(\sin^2(\theta(\epsilon,x)\partial_x\chi(\epsilon,x)) = 0, \tag{2}$$

$$D\partial_x\{\cosh^2\theta_2(\epsilon,x)\partial_x f_1(\epsilon,x)\} = 0. \tag{3}$$

Here j_n is the normal current density across the junction, ν_0 is the density of states in the bulk normal metal, Eqs. (2) are the Usadel equations for the retarded normal $g^R(\epsilon,x)=\cos\theta(\epsilon,x)$ and anomalous $F^R(\epsilon,x)=-i\exp(i\chi(\epsilon,x))\sin\theta(\epsilon,x)$ Green's functions [$\theta(\epsilon,x)=\theta_1(\epsilon,x)+i\theta_2(\epsilon,x)$ is a complex variable], and Eq. (3) is the diffusion equation for the distribution function of quasiparticles f_1, which describes the imbalance of the populations of the electron and hole branches of the spectrum in the metal. Inside the superconductor $\theta_1=\pi/2$ and $\theta_2=0$. The boundary conditions for Eqs. (2) and (3) have the form[15]

$$
\begin{aligned}
&D\partial_x\theta(\epsilon,x)=t\ \cos(\theta(\epsilon,0^+))\cos\left(\frac{\chi}{2}-\frac{\chi(\epsilon,0^+)}{2}\right),\\
&D\ \sin(\theta(\epsilon,0^+))\partial_x\chi(\epsilon,x=0^+)=t\ \sin\left(\frac{\chi}{2}-\frac{\chi(\epsilon,0^+)}{2}\right),\\
&D\ \cosh\ \theta_2(\epsilon,0^+)\partial_x f_1(\epsilon,0^+)\\
&\quad=t\{f_1(\epsilon,0^+)-f_1(\epsilon,0^-)\}\sin(\theta_1(\epsilon,0^+))\cos^{-1}\left(\frac{\chi}{2}-\frac{\chi(\epsilon,0^+)}{2}\right),
\end{aligned}
\tag{4}
$$

$$
f_1(\epsilon,x=0^-)=0,\quad f_1(\epsilon,x=L^+)=-eV\partial_\epsilon\tanh\frac{\epsilon}{2kT}. \tag{5}
$$

Here 0^+ ($0^-,L^+$) represents the normal-metal (superconductor) side of the SN boundary, $t=t_0v_F$, where t_0 is the dimensionless transmission coefficient through the SN boundary, and V is the voltage drop across the junction.

Using Eqs. (1)–(5), we get the following expression for the resistance of SNS junction:

$$
G_{\mathrm{SNS}}=G_NL\int_{-\infty}^{+\infty}d\epsilon\partial_\epsilon\left(\tanh\frac{\epsilon}{kT}\right)\left\{\frac{L_t}{\cosh\ \theta_2(\epsilon,0^+)\sin\theta_1(\epsilon,0^+)\cos\left(\frac{\chi}{2}-\frac{\chi(\epsilon,0^+)}{2}\right)}+\int_0^x\frac{1}{\cosh^2\theta_2(\epsilon,x')}dx'\right\}^{-1}. \tag{6}
$$

Here $G_N=\sigma_D(S/L)$, $\sigma_D=e^2D\nu_0$ and $S=L_1L_2$ are the conductance of the normal-metal part of the junction, the Drude conductivity, and the area of the junction, respectively. The first and second terms in Eq. (6) can be associated with the resistance of the SN boundary and the resistance of the normal region of the junction, respectively. There are two major effects in the metal due to the proximity of the superconductor: 1) The effective diffusion coefficient in Eq. (3) is renormalized on account of Andreev reflection and is governed by the parameter θ_2. The correction to the local conductivity of the metal from this effect leads to the second term in Eq. (6). 2) The local density of states $\nu(\epsilon,x)=\nu_0\ \mathrm{Re}\ g^R(\epsilon,x)=\nu_0\cos\theta_1(\epsilon,x)\cosh\theta_2(\epsilon,x)$ in the metal at small ϵ is suppressed by

Andreev reflection and is governed by the parameter θ_1. The contribution to the conductance of the SN boundary from this effect corresponds to the first term in Eq. (6). The χ dependence of G_{SNS} originates from the corresponding χ dependence of θ_1 and θ_2. It follows from Eqs. (2) and (4) that near the SN boundary at small ϵ the value of $\theta(\epsilon,x)$ should be close to its value in the superconductor $\theta_S(\epsilon<\Delta)=\pi/2$. It approaches its metallic value $\theta_M=0$ only after a distance L_ϵ. The main contribution to Eq. (6) comes from the energy interval $\epsilon\sim E_c\ll T$. As a result,

$$\delta G_2=\alpha G_N\frac{E_c}{T}g(\chi). \tag{7}$$

Here $g(\chi)$ is a universal function of χ with period 2π; $\alpha\sim 1$ at $L\gg L_t=D/t$ and $\alpha\sim(L/L_t)^2$ at $L\ll L_t$.

Let us now discuss the contribution of the Debye relaxation mechanism which arises when a voltage V is applied between the superconductors in Fig. 1, so that χ changes in time: $d\chi/dt=(2e/\hbar)V$. Generally speaking, in this case one has to solve a nonstationary version of Eqs. (2) and (3). However, in the case when $eV\ll E_c$ one can use the adiabatic approximation, in which case the time dependence of $\theta(\epsilon,x,\chi(t))$ and of the local density of states $\nu(\epsilon,x,\chi(t))$ originates from the corresponding time dependence of $\chi(t)$. The standard expression for the power absorption due to Debye relaxation has the form (see, for example, Ref. 16)

$$Q=v\nu_0^{-1}\int d\epsilon\left\langle\left(\int_{-\infty}^{\epsilon}\frac{d\overline{\nu(\epsilon',\chi(t))}}{dt}d\epsilon'\right)^2\right\rangle\frac{\tau_{\mathrm{in}}(\epsilon)}{1+(\omega\tau_{\mathrm{in}}(\epsilon))^2}\partial_\epsilon f_0(\epsilon), \tag{8}$$

where $\overline{\nu(\epsilon,\chi(t))}$ is the local density of states averaged over the volume $v=LL_1L_2$ of the normal-metal region, and the brackets $\langle\ldots\rangle$ denote averaging over the period of the oscillations, $\hbar/eV$. Using Eqs. (2) and (4), one can prove that in the absence of an insulator barrier $\overline{\nu(\epsilon,\chi)}=\nu_0\Pi_1(\epsilon/E_c,\chi)$. When $L\ll L_t$, one has $\overline{\nu(\epsilon,\chi)}=\nu_0(L^2/L_t^2)\Pi_2(\epsilon/E_c,\chi)$. Here $\Pi_{1,2}(\mu,\chi)$ are universal dimensionless functions, with $\Pi_1(\mu\gg 1,\chi)\sim\Pi_2(\mu\gg 1,\chi)=\cos\chi\exp(-\sqrt{\mu})$. Furthermore, at $E_c\ll T$ one can neglect the ϵ-dependence of $\tau_{\mathrm{in}}(\epsilon)$. The main contribution to Eq. (8) comes from the interval of energies $\epsilon\sim E_c$, where the quasiparticle density of states is significantly suppressed compared with ν_0 in the absence of an insulator at the boundary. As a result, we have the following expression for the contribution of this mechanism to the dc conductance of the junction ($Q=V^2\delta G_3$):

$$\delta G_3=\alpha^2 G_N\frac{E_c^2\tau_{\mathrm{in}}}{T\hbar}, \tag{9}$$

which can be even larger than G_N. Equation (9) is valid when $eV\tau_{\mathrm{in}}/\hbar\ll 1$. In this limit one can introduce $\delta G_3(\chi(t))$, which is given in order of magnitude by Eq. (9) and has a period of 2π. In the opposite limit $eV(\tau_{\mathrm{in}}/\hbar)\gg 1$, the function Q saturates, which means that δG_3 decays as $(\hbar/eV\tau_{\mathrm{in}})^2$.

We would like to mention that the contribution of the Debye mechanism to the dc resistance of a closed sample with the Aharonov–Bohm geometry has been discussed in Ref. 17. In that case the time dependence of the electronic density of states was induced by a change in the magnetic flux Φ through the ring. The important difference is that the

average density of states in the normal metal is flux-independent (and, consequently, time-independent). Therefore, the Debye absorption is nonzero only on account of mesoscopic fluctuations of the density of states, whereas in the case of an SNS junction the average density of states can be time-dependent. Using results obtained in Ref. 17 in the case when $\hbar/\tau_{\rm in} \gg \delta_0$, $L_t \gg L$, $L_{\rm in} \gg L, L_1, L_2$ we can estimate the contribution to δG due to the mesoscopic part of the Debye relaxation mechanism as $\delta G_3^m \sim \alpha_1 (e^2/\hbar^3) E_c \delta_0 \tau_{\rm in}^2$. Here δ_0 is the mean spacing between energy levels in the normal metal, and $\alpha_1 \sim 1$ for $L_t \ll L_{\rm in}$ and $\alpha_1 \sim (L_{\rm in}/L_t)^4$ for $L_t \gg L_{\rm in}$. We will neglect this contribution because, as we shall see below, $\delta G_3^m \ll \delta G_1$.

Another contribution to δG which arises in the first-order approximation in the parameter $\hbar/p_F l$ is the aforementioned weak-localization correction δG_1. It reflects the fact that in the course of each Andreev reflection the amplitudes of the electron diffusion paths acquire the aforementioned additional phases $\pm\chi_{1,2}$, but they do not take into account the spatial coherence between the electron and the hole which arises due to Andreev reflection. This is correct if $L_T \ll L$ or $E_c \ll T$. As a result,[2]

$$\delta G_1 = -\alpha_1 \frac{e^2}{\hbar} g_3(\chi) \begin{cases} E_c \tau_{\rm in} & \text{for the } 0D \text{ case} \\ \dfrac{L_{\rm in} L_1}{L^2} & \text{for the } 1D \text{ case} \\ \ln\left(\dfrac{L_{\rm in}}{l}\right) \dfrac{L_1 L_2}{L^2} & \text{for the } 2D \text{ case.} \end{cases} \tag{10}$$

Here $g_3(\chi)$ is a periodic function with period π, the $0D$ case corresponds to $L, L_1, L_2 \ll L_{\rm in}$, the $1D$ case corresponds to $L_1 \gg L_{\rm in} \gg L_2, L$, and the $2D$ case corresponds to $L_1, L_2 \gg L_{\rm in} \gg L$.

The ratios between the three contributions to δG considered above depend on the parameters and the dimensionality of the system. For example, in the $0D$ case at $0 < eV\tau_{\rm in}/\hbar \ll 1$ we have

$$\frac{\delta G_1}{\delta G_2} \approx \frac{\alpha_1}{\alpha} \frac{e^2}{\hbar G_N} T\tau_{\rm in}; \quad \frac{\delta G_1}{\delta G_3} \approx \frac{\alpha_1}{\alpha^2} \frac{e^2}{\hbar G_N} \frac{T}{E_c}. \tag{11}$$

At large enough $eV \gg \sqrt{(\hbar/\tau_{\rm in}) E_c \alpha}$ (but still smaller than E_c), δG_3 becomes much smaller than δG_2. In this case the χ-dependent part of the resistance is determined by the sum $(\delta G_1 + \delta G_2)$. For example, in the $0D$ case the ratio of δG_1 (with period π) to δG_2 (with period 2π) is of the order of

$$\frac{\delta G_1}{\delta G_2} \approx \frac{\alpha_1}{\alpha} \frac{T}{V} \frac{e^2}{\hbar G_N}. \tag{12}$$

If $V = 0$ and the conductance is measured with the help of contact ''C'' in Fig. 1, δG will be the sum of δG_1 and δG_2, the ratio of which is determined by the correponding terms in Eqs. (11) and (12). These ratios can be larger or smaller than unity, and so the period of the oscillations of $\delta G(\chi)$ can be either π or 2π. This can explain why some experiments[18,19] demonstrate π periodicity of δG, while others[20,21] show a period of

2π. The reason why δG_1, which arises only in the first-order approximation in the small parameter $\hbar/p_F l$, can be comparable with δG_2 is that δG_2 arises from the small energy interval $\epsilon \sim E_c \ll T$, while δG_1 arises from $\epsilon \sim T$.

We acknowledge helpful discussions with B. Altshuler, H. Courtois, M. Devoret, D. Esteve, B. Pannetier, M. Sanquer, and B. V. Wees. This work was supported by the Division of Material Sciences, U.S. National Science Foundation under Contract DMR-9205144.

[1] L. Aslomasov, A. I. Larkin, and Y. N. Ovchinnikov, Zh. Éksp. Teor. Fiz. **55**, 323 (1968) [Sov. Phys. JETP **28**, 171 (1969)].
[2] B. Z. Spivak, D. E. Khmelnitskii, JETP Lett. **35**, 412 (1982).
[3] A. F. Andreev, Zh. Éksp. Teor. Fiz. **46**, 1832 (1964) [Sov. Phys. JETP **19**, 1228 (1964)].
[4] A. Shelankov, unpublished (1981).
[5] A. F. Volkov and T. M. Kapwijk, Phys. Lett. A **168**, 217 (1992); A. F. Volkov, A. Zaitsev, and T. M. Klapwijk, Physica C **210**, 21 (1993).
[6] C. W. J. Beenakker, Phys. Rev. B **46**, 12841 (1992).
[7] F. W. J. Hekking, Yu. V. Nasarov, Phys. Rev. Lett. **71**, 1625 (1993).
[8] A. F. Volkov, Physica B **203**, 267 (1994).
[9] A. V. Zaitsev, Phys. Lett. A **194**, 315 (1994).
[10] F. Zhou and B. Spivak, Phys. Rev. B **52**, 4467 (1995).
[11] Y. V. Nazarov and T. H. Stoof, Phys. Rev. Lett. **76**, 823 (1996).
[12] V. Galaiko and V. Shumeiko, Zh. Éksp. Teor. Fiz. **71**, 671, (1976) [Sov. Phys. JETP **44**, 353 (1976)].
[13] A. I. Larkin and Yu. N. Ovchinnikov, Zh. Éksp. Teor. Fiz. **73**, 299 (1977) [Sov. Phys. JETP **41**, 960 (1977)].
[14] A. Schmidt and O. Schon, J. Low Temp. Phys. **20**, 207 (1975).
[15] M. Yu. Kuprianov and V. F. Lukichev, Zh. Éksp. Theor. Fiz. **94**(6), 139 (1988) [Sov. Phys. JETP **67**, 1163 (1988)].
[16] B. Spivak, F. Zhou, and T. M. Beal, Phys. Rev. B **51**, 13226 (1995).
[17] A. Kamenev, B. Reulet, H. Bouchiat, and Y. Gefen, Europhys. Lett. **28**, 391 (1993).
[18] V. T. Petrashov, V. N. Antonov, P. Delsing, and R. Claeson, Phys. Rev. Lett. **70**, 347 (1993).
[19] P. G. N. de Vegvar, T. A. Fulton, W. H. Mallison, and R. E. Miller, Phys. Rev. Lett. **73**, 1416 (1994).
[20] H. Pothier, S. Gueron, D. Esteve, and M. H. Devoret, Phys. Rev. Lett. **73**, 2488 (1994).
[21] A. Dimoullas, J. P. Heida, B. J. V. Wees, T. M. Klapwijk, W. V. D. Graaf, and B. Borghs, Phys. Rev. Lett. **74**, 602 (1995).

Published in English in the original Russian journal. Edited by Steve Torstveit.

Local magnetic states and hyperfine interactions in Fe/Ti magnetic superlattices

P. M. Stetsenko, S. D. Antipov, G. V. Smirnitskaya, and A. L. Kolumbaev
M. V. Lomonosov Moscow State University, 119899 Moscow, Russia

G. E. Goryunov
Institute of Physical Chemistry, Russian Academy of Sciences, 117334 Moscow, Russia

(Submitted 14 January 1997)
Pis'ma Zh. Éksp. Teor. Fiz. **65**, No. 4, 353–357 (25 February 1997)

Multilayer Fe/Ti films are synthesized by deposition in a Penning discharge. Measurements are made of thhe static hysteresis loops and Mössbauer spectra on Fe^{57} nuclei. The hyperfine magnetic field distribution functions are calculated. It is established that the spontaneous magnetization of Fe/Ti magnetic superlattices undergoes very strong oscillations as a function of the Ti layer thickness. Three groups of peaks are noted in the hyperfine field distribution functions, corresponding to three nonequivalent states of the Fe ions, in one of which these ions do not have a characteristic magnetic moment. These results also agree with measurements of the temperature dependence of the magnetization in weak magnetic fields. For some Ti interlayer thicknesses the saturation magnetization scaled to the Fe content is much higher than the saturation magnetization of bulk Fe. © *1997 American Institute of Physics.* [S0021-3640(97)01204-8]

PACS numbers: 75.70.Cn, 75.60.Ej, 76.80.+y, 31.30.Gs

1. Multilayer magnetic films and magnetic superlattices (MSLs) synthesized on the basis of such films make it possible to investigate experimentally a number of fundamental problems in the modern physics of magnetic phenomena, such as the question of whether magnetic ordering can exist in two-dimensional systems, the characteristic features of the formation of the local atomic magnetic moments in surface layers and interphase regions, the mechanisms of indirect interactions between magnetic layers, and others. The kinetic properties of MSLs are also distinguished by remarkable features, the primary one being the giant magnetic resistance observed in these systems.

Many important magnetic parameters of MSLs, such as the spontaneous magnetization, the magnetic resistance, the Curie temperature, the magnetic-anisotropy constant, and others, exhibit oscillatory behavior as a function of the nonmagnetic interlayer thicknesses.[1,2] This is apparently due to the spatial oscillations of the spin density of delocalized electrons in nonmagnetic layers, which is responsible for the indirect exchange interaction between the magnetically ordered layers. The mechanism of this interaction can be described either in terms of the RKKY approximation or Friedel's model.[3] Interpretations of the oscillatory character of a number of magnetic parameters in MSLs in terms of interference effects with partial reflection of electron waves from

interfaces in the periodic MSL structures have been elaborated in recent years.[4]

Magnetic superlattices are essentially composite materials and are highly nonuniform systems, as a result of which the investigation of their integral parameters is not always sufficiently informative and experimental methods yielding information about local magnetic states must be used. They include one or another of the methods for observing hyperfine interactions (HFIs) and, specifically, the Mössbauer (ME), nuclear magnetic resonance, $\gamma-\gamma$ angular correlation, μSR spectroscopy, and others.

2. The multilayer magnetic films for the present investigation were synthesized by the method of cathodic sputtering in a Penning discharge in an atmosphere of purified Kr. The residual-gas pressure was equal to 10^{-7}–10^{-8} torr and the pressure of the inert working gas was equal to 10^{-5} torr. The Kr content in synthesized films did not exceed 0.15 at.%. Two series of Fe/Ti MSLs were synthesized. In one series the thickness of the Fe layers was equal to ~ 6 Å and was maintained constant and the thickness of the Ti layers was varied from 8.4 to 83 Å. In the second series the thickness of the Fe layers was varied from 6 to 32.4 Å with constant Ti interlayer thickness ~ 40 Å. The number of Fe and Ti layers reached 580. X-ray analysis of the MSLs showed that they have a highly textured bcc structure.

The magnetization curves were measured in a static regime with the aid of a completely computerized vibrational magnetometer in external fields of up to ± 15 kOe. The sensitivity of the magnetometer was equal to 10^{-7} emu. The magnetometric measurements were performed in weak variable fields with the aid of an induction magnetometer.

The Fe^{57} Mössbauer spectra were measured at room temperature in a transmission arrangement on a spectrometer with constant acceleration. The nonlinearity of the motion of the electrodynamic vibrator did not exceed 0.3% and Co^{57} in Rh served as the γ-ray source. A novel mathematical program,[5] in which the desired functional is represented in an analytic form as a sum of a definite number of Lorentzians followed by an efficient minimization program, was used for mathematical analysis of the Mössbauer and for reconstructing the probability distributions of the hyperfine magnetic field H_{hf} at the Fe^{57} nuclei.

3. Hysteresis loops for the MSL [Fe(7 Å)/Ti(8.4 Å)]$\cdot$400 with the external magnetic field oriented in the plane of the film are displayed in Fig. 1. Figure 1a shows the comlete loops in the maximum field of ± 15 kOe. The characteristic features are the small values of the susceptibility of the paraprocess and the high degree of squareness of the loops. The central part of these same loops in a field up to ± 300 Oe is shown in Fig. 1b for two mutually perpendicular directions. The difficult direction of magnetization is also the direction of the external magnetic field during deposition of the film. A high degree of in-plane magnetic anisotropy, due to the presence of an external magnetic field during deposition of the films, and also the anomalous ''stretched'' shape of the loop for the easy direction of magnetization, which could be due to the characteristic features of the domain structure of the film associated with the above-noted anisotropy and with the characteristic features of the indirect exchange interactions between the magnetic layers, are characteristic.

The dependence of the values of the spontaneous magnetization and coercive force of the MSL, calculated from these curves, on the thickness of the Ti layers is presented

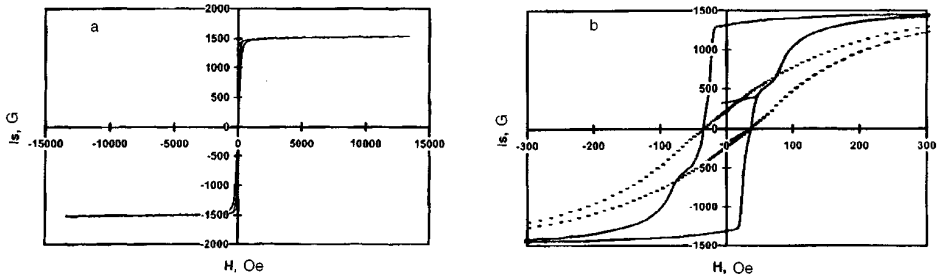

FIG. 1. Hysteresis loops for the MSL [Fe(7 Å)/Ti(8.4 Å)]·400 for an in-plane external field orientation: a) Hysteresis loops in a maximum field; b) central sections of the same loops. Dots — the external magnetic field during the measurements is oriented in the same direction as the external magnetic field during film deposition; solid curves — the external field during the measurements is perpendicular to the preceding orientation.

in Fig. 2. As one can see from the figure, the main feature of this curve is its pronounced oscillatory character. The increase in the spontaneous magnetization from minimum to maximum value is greater than two orders of magnitude! The coercive force also varies similarly as a function of the thickness of the Ti interlayers. Such sharp changes in the magnetic parameters with increasing thickness of the Ti layers attests to sharp boundaries between the Fe and Ti layers.

As is well known, such oscillations of the magnetic parameters are apparently due to changes in the sign of the indirect exchange interaction between the magnetically ordered layers, which occurs by means of the polarization of the spin density of the delocalized electrons in the nonmagnetic interlayers.

These interactions are most often interpreted either on the basis of the RKKY approximation or in terms of Friedel oscillations, though there are great difficulties in explaining the experimentally observed periods of the oscillations. The fact that in our case the values of the resulting spontaneous magnetization for some Ti layer thicknesses are very small attests to the almost complete compensation of the magnetization of individual layers and therefore a 180° orientation of the magnetization of neighboring Fe layers.

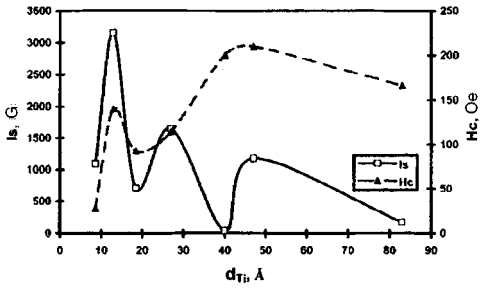

FIG. 2. Spontaneous magnetization I_S (□) and coercive force H_c (△) of a Fe/Ti MSL versus Ti layer thickness. Fe layer thickness ~6 Å.

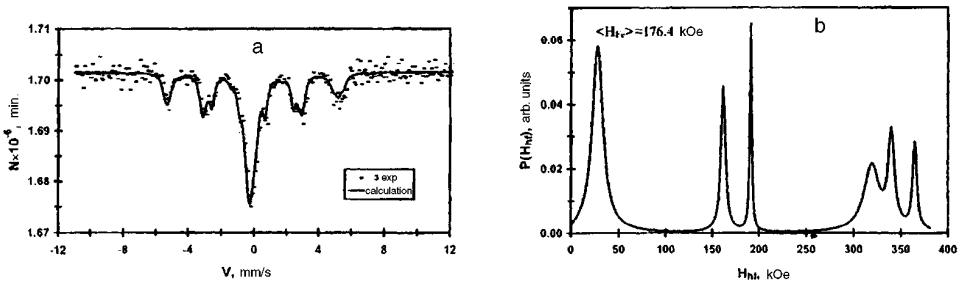

FIG. 3. a) Mössbauer spectrum of the MSL [Fe(5.2 Å)/Ti(47 Å)]·550; b) probability distribution function of H_{hf} for the same MSL.

It should be noted that for some Ti layer thicknesses the values of the spontaneous magnetization of the MSLs scaled to the Fe content are much higher than the values characteristic for Fe ions in pure Fe. The possibility of such an increase was shown theoretically in Ref. 6 and confirmed experimentally in Ref. 7. The very high values of the average atomic magnetic moment μ_{Fe} at room temperature $-\mu_{\mathrm{Fe}}=3.5\ \mu_B$ were measured in single-crystal $Fe_{16}N_2$ films with the aid of a vibrating sample magnetometer and Rutherford backscattering.[8] An important factor here is the decrease in the coordination numbers for the Fe ions located at the surface; this results in a narrowing of the *d* band and an increase in the atomic moments as well as additional contributions from the orbital moments associated with the changes in the local symmetry of the environment of the Fe ions and contributions from the polarized spin density of nonlocalized electrons, participating in indirect-exchange processes, in nonmagnetic layers.

The Fe^{57} Mössbauer spectrum for the MSL [Fe(5.2 Å)/Ti(47 Å)]·550 is displayed in Fig. 3a, and the probability distribution at these nuclei which is reconstructed from this spectrum is presented in Fig. 3b. As follows from the form of the distribution function, the maxima of the probability fall into three groups, corresponding to the three nonequivalent local states of the Fe ions. For one of these groups $H_{hf}=30$ kOe, which indicates that the Fe ions in these local states do not have an intrinsic magnetic moment and H_{hf} is due to the polarization of the electronic spin density at the nuclei by ions from the environment. These local states can correspond to definite positions of the Fe ions in the interphase regions. The group of peaks that corresponds to the maximum values of H_{hf} (up to 380 kOe) is apparently due to Fe ions with high atomic magnetic moments and located in the surface layers.

These conjectures agree with the measurements, presented in Fig. 4, of the temperature dependence of the magnetization in weak magnetic fields. The anomalies observed in this dependence could be due to the magnetic transitions of Fe ions in corresponding local states. The maximum near 750°C is apparently due to the Hopkins effect in the high-temperature magnetic phase.

The measurements of the spontaneous magnetization of the Fe/Ti MSL as a function of the Fe layer thickness were performed on a series where the Ti layer thickness was maintained constant near the value 40 Å and the Fe layer thickness was varied from 6 to

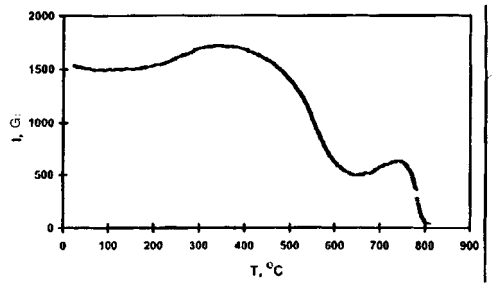

FIG. 4. Temperature dependence of the magnetization I of the MSL [Fe(6.2 Å)/Ti (8.6 Å)]·580 in weak alternating fields.

32.2 Å. The 40 Å thickness of the Ti layers corresponded to the minimum value of the spontaneous magnetization in the series with a constant Fe layer thickness. The dependences of the spontaneous magnetization and coercive force of the MSL from this series on the Fe layer thickness are presented in Fig. 5. As one can see from the figure, in this case the indicated parameters do not undergo oscillatory variations.

4. Measurements of the magnetic properties and hyperfine magnetic fields at the Fe^{57} nuclei as a function of the Ti and Fe layer thicknesses were perfomed on Fe/Ti MSLs synthesized by cathodic sputtering in a Penning discharge. An oscillatory dependence of the spontaneous magnetization and coercive force of the MSL on the Ti layer thickness was found. The magnitude of the spontaneous magnetization varies by more than two orders of magnitude. For some values of the Ti layer thickness the spontaneous magnetization of the MSL is much greater than the corresponding value for pure Fe. The distribution function for H_{hf} at the Fe^{57} nuclei in Fe/Ti MSLs, reconstructed from the experimental Mössbauer spectra, contains three groups of peaks which correspond to the three types of nonequivalent local magnetic states of the Fe ions. For the states which correspond to the minimum values of H_{hf} (25–50 kOe) the Fe ions apparently have no intrinsic magnetic moments. These conjectures agree with the measurements of the temperature dependence of the magnetization in weak alternating fields.

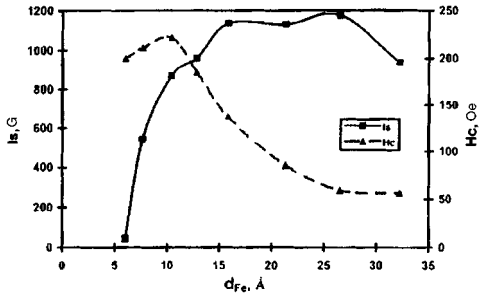

FIG. 5. Spontaneous magnetization I_S (□) and coercive force H_c (△) of a Fe/Ti MSL as a function of the Fe layer thickness. Ti layer thickness ~40 Å.

In the cases when the Ti layer thickness in Fe/Ti MSLs remained constant and the Fe layer thickness was varied, the values of the spontaneous magnetization and coercive force did not undergo oscillatory variations.

This work was supported by the Russian Fund for Fundamental Research (Grant 96-02-18141).

[1] S. S. P. Parkin, N. Moore, and K. P. Roche, Phys. Rev. Lett. **64**, 2304 (1990).
[2] G. Bayreuther, F. Bensch, and V. Kottler, J. Appl. Phys. **79**, 4509 (1996).
[3] L. Nordström and D. J. Singh, J. Appl. Phys. **79**, 4515 (1996).
[4] P. Bruno, Phys. Rev. B **52**, 411 (1995).
[5] S. D. Antipov, G. E. Gorjunov, P. N. Stetsenko *et al.*, Hyperfine Interact. **78**, 391 (1993).
[6] A. J. Freeman and C. L. Fu, J. Appl. Phys. **61**, 3356 (1987).
[7] J. A. C. Bland, C. Dabbo, B. Heinrich *et al.*, J. Magn. Magn. Mater. **148**, 85 (1995).
[8] J. Sugita, H. Takahashi, M. Komuro *et al.*, J. Appl. Phys. **79**, 5576 (1996).

Translated by M. E. Alferieff